LUT University
School of Energy Systems
Trilateral Master's Degree Programme in Energy Technology

Andrei Wallin

Simulation study of a semi-deep ground source heat pump system for a new residential building

Examiners: Teemu Turunen-Saaresti, Professor, D.Sc. (Tech)
Jari Shemeikka, Research Team Leader, M.Sc (Tech)
Supervisor: Jari Shemeikka, Research Team Leader, M.Sc (Tech)

ABSTRACT

Lappeenranta-Lahti University of Technology LUT
LUT School of Energy Systems
Trilateral Master's Degree Programme in Energy Technology

Andrei Wallin

Simulation study of a semi-deep ground source heat pump system for a new residential building

Master's Thesis

2020

95 pages, 39 figures, 14 tables, 37 equations, 4 appendices

Examiners: Professor Teemu Turunen-Saaresti, Research Team Leader Jari Shemeikka

Supervisor: Research Team Leader Jari Shemeikka

Keywords: GSHP, geoenergy, coaxial borehole heat exchanger, regeneration.

Semi-deep (~800 m) ground source heat pump systems have potential for application in dense urban areas, where the lack of space renders the typical shallow systems (~300 m) unprofitable. The aim of this thesis was to perform initial evaluation of the technical potential of such system covering the heating and cooling demand of a new residential building. In the process building load profiles were generated with IDA-ICE, and a previously developed numerical coaxial borehole heat exchanger model implemented in Apros was validated. System operation was simulated with the Apros heat exchanger model coupled with a heat pump model.

800 m deep borehole heat exchangers were found to sustain a specific heat load of 32-35 W/m, depending on grout heat transfer coefficient, without mean heat carrier fluid temperature dropping below 0 °C during 50 years of operation. In practice four 800 m boreholes could then sustainably supply building heating demand at heat pump coverage of 66 % power and 99 % energy. However, thermal interaction between boreholes may increase the required number of boreholes unless it is mitigated by adequate safety distances and/or ground regeneration.

Covering the building's cooling load exclusively by free cooling using the heat carrier fluid circulating in the boreholes was deemed unfeasible, since the heat carrier temperatures during summer exceed those likely required by the cooling system. Partial free cooling coverage is possible, but the potential electricity savings are relatively low due to low cooling energy consumption of the building. Utilization of free cooling is also in conflict with possible ground regeneration, which further increases heat carrier temperatures during summer.

Introducing regenerative heat during summer was found to increase ground temperatures pronouncedly at higher levels (0-200 m), possibly due to the chosen flow direction in the heat exchanger. Further study regarding the effect of flow direction should be conducted.

The coaxial borehole heat exchanger simulation model was found to have potential for both short-term and long-term simulations of undisturbed boreholes, but further development is required to more accurately account for the effect of groundwater natural convection on heat transfer, as well as to thermal interaction between boreholes, among other things.

TIIVISTELMÄ

Lappeenrannan-Lahden teknillinen yliopisto LUT
LUT School of Energy Systems
Trilateral Master's Degree Programme in Energy Technology

Andrei Wallin

Simulaatiotutkimus uuden asuinkerrostalon keskisyvästä maalämpöjärjestelmästä

Diplomityö

2020

95 sivua, 39 kuvaa, 14 taulukkoa, 37 yhtälöä, 4 liitettä

Tarkastaja: Teemu Turunen-Saaresti, Professori, TkT, Jari Shemeikka, Research Team Leader, DI

Ohjaaja: Jari Shemeikka, Research Team Leader, DI

Hakusanat: maalämpö, maalämmönvaihdin, vapaajäähdytys, regeneraatio

Keskisyvää (~800 m) maalämpöä voidaan potentiaalisesti hyödyntää tiheään rakennetussa kaupunkiympäristössä, jossa tyypilliset matalat (~300 m) lämpökaivot ovat kannattamattomia. Tässä diplomityössä kartoitettiin keskisyvän maalämpöjärjestelmän potentiaalia kattaa uuden kerrostalon lämmitys- ja jäähdytysenergiantarve. Rakennuksen kulutusprofiilit laskettiin IDA-ICE-ohjelmistolla, ja aiemmin kehitetty Apros-ohjelmassa toteutettu koaksiaalimaalämmönvaihdinmalli validoitiin. Järjestelmän toimintaa simuloitiin lämpökaivomalliin kytketyllä lämpöpumppumallilla.

800 metriä syvien lämpökaivojen todettiin toimivan noin 32-35 W/m huipputeholla, riippuen porareiän täyttömateriaalin lämmönsiirtokertoimesta, ilman että maapiirin nesteen keskilämpötila putoaa alle 0 °C:n 50 vuoden kuluessa. Siten neljän 800 m lämpökaivon voitiin todeta riittävän kattamaan rakennuksen lämmönkulutus kestävästi, kun lämpöpumppu oli mitoitettu 99 % energiankulutusta vastaavalle 66 % osateholle. Käytännössä neljä lämpökaivoa on kuitenkin optimistinen arvio, mikäli kaivojen lämpövaikutusta toisiinsa ei saada minimoitua riittävillä etäisyyksillä tai maaperän regeneraatiolla.

Rakennuksen koko jäähdytystarvetta ei kyetä kattamaan vapaajäähdytyksellä maapiiriä hyödyntäen, sillä kesäisin kiertonesteen lämpötila kohoaa ajoittain liian korkeaksi jäähdytysjärjestelmän vaatimaan lämpötilaan nähden. Osavapaajäähdytyksellä voi saavuttaa säästöjä kylmäkoneen sähkönkulutuksessa. mutta potentiaalisesti saavutettu säästö on pieni johtuen rakennuksen suhteellisen pienestä jäähdytysenergian tarpeesta. Lisäksi on huomionarvoista, että vapaajäähdytyksen käyttö ja maaperän lämmön regenerointi ovat ristiriidassa, sillä regeneraatio nostaa maapiirin nesteen lämpötilaa kesäisin.

Ilmanvaihdon ulostuloilmasta voidaan kesäisin ottaa lämpöä maaperän regenerointiin korkeammassa lämpötilassa kuin ulkoilmasta. Esimerkkisimulaatiossa regeneraation havaittiin nostavan maaperän lämpöjä enemmän ylemmissä osissa, johtuen suuremmasta lämpötilaerosta kiertonesteen ja maaperän ylempien osien välillä, sekä mahdollisesti kiertonesteen virtaussuunnasta.

ACKNOWLEDGEMENTS

This thesis was written at VTT's Urban Energy Systems research team during the latter half of 2020. Working on the thesis has been very educational, not only regarding the technical aspects involved and the process of writing a thesis, but also since it has highlighted many of my own strengths and weaknesses. Many thanks to my supervisor Jari Shemeikka for enabling me to work on this important topic, and assisting in the process. I'm also grateful to Rinat Abdurafikov for helping me get started with Apros and the CBHE model.

I'd also like to thank Muovitech CTO Adib Kalantar for providing borehole heat exchanger technical data, as well as practical information about the topic and inspiring discussions.

Finally I'd like to thank Teemu Turunen-Saaresti for reviewing the thesis at quite a short notice.

TABLE OF CONTENTS

1 INTRODUCTION 9
1.1 Background 9
1.2 Objectives 10
1.3 Outline 11
2 BUILDING ENERGY DEMAND 13
2.1 Residential building energy end use 13
2.2 Building energy efficiency 16
3 GROUND SOURCE HEAT PUMPS 19
3.1 Vapor compression cycle 19
3.2 Coefficient of performance 20
3.3 Heat pump modelling 21
3.4 Power coverage factor 22
4 BOREHOLE HEAT EXCHANGERS 23
4.1 Geothermal heat 23
4.2 Ground heat exchangers 24
4.3 BHE construction 25
4.4 Heat transfer 27
4.4.1 Heat transfer within the BHE 28
4.4.2 Tube flow convective heat transfer 30
4.4.3 Pressure drop 31
4.4.4 Natural convection 32
4.4.5 Heat transfer within the ground 34
4.4.6 Unbalanced loads 36
4.4.7 Regeneration 37
4.4.8 BHE modelling 38
4.5 Coaxial BHE design 39
5 BUILDING LOAD PROFILE 43
5.1 Case building 43
5.2 IDA-ICE 44
5.3 Model configuration 45
5.4 Energy efficiency parameters 46
5.4.1 Parameter analysis 47
5.5 Heat pump coverage factor 51
5.6 Heat pump model 53

6 BHE MODEL & VALIDATION 54
6.1 Model description 54
6.2 Model validation 56
6.2.1 Validation against DTRT measurement data 56
6.2.2 Validation against EED simulation results 58
6.3 Model configuration 59
7 SIMULATION STUDY METHODOLOGY 62
7.1 Objectives 62
7.1.1 Borehole resistance 62
7.2 Scenarios 64
7.2.1 Minimum number of BHE's 64
7.2.2 Diameter & conductivity analysis 64
7.2.3 Free cooling analysis 64
7.2.4 Regeneration analysis 65
7.3 Model inputs 67
8 RESULTS 70
8.1 Minimum number of BHE's 70
8.2 Diameter & conductivity 73
8.3 Utilization of free cooling 74
8.4 Regeneration 75
9 DISCUSSION 80
9.1 Minimum number of BHE's 80
9.2 Borehole diameter and grout conductivity 82
9.3 Free cooling 83
9.4 Regeneration 83
9.5 Further study 84
9.5.1 Technical model improvements 84
9.5.2 Further studies of relevance 85
10 CONCLUSIONS 87
REFERENCES 90
APPENDIX

SYMBOLS AND ABBREVIATIONS

Roman alphabet

A	area	m^2
c_p	specific heat capacity	J/kgK
D	diameter	m
f_D	friction factor	
h	convective heat transfer coefficient	W/m^2K
K	radius ratio	-
k	conductive heat transfer coefficient	W/mK
L	length	m
n	air change rate	1/h
P	power	W
p	pressure, specific power	Pa, W/m^2
Q	heat energy	J, Wh
q	heat flow	W
q_m	mass flow rate	kg/s
q_v	volumetric flow rate	m^3/s
R	heat transfer resistance	m^2K/W
r	radius	m
T	temperature	°C, K
t	time	s
U	overall heat transfer coefficient	W/m^2K
W	work	J
w	velocity	m/s
x	length scale	m
z	depth	m

Greek alphabet

α	thermal diffusivity	m^2/s
β	heat expansion coefficient	1/K
Δ	change	-
η	efficiency	-
ρ	density	kg/m^3
μ	dynamic viscosity	kg/ms

Subscripts

b	borehole
c	condenser
comp	compressor
e	evaporator
eq	equivalent
gw	groundwater
hc	heat carrier

Dimensionless numbers

C	Courant number
Gr	Grashouf number
Nu	Nusselt number
Pr	Prandtl number
Ra	Rayleigh number
Re	Reynolds number

Abbreviations

BHE	borehole heat exchanger
CBHE	coaxial borehole heat exchanger
DHW	domestic hot water
EED	Earth Energy Designer
EER	energy efficiency ratio
FC	free cooling
GSHP	ground source heat pump
HX	heat exchanger
MFT	mean fluid temperature
SCL	Simantics Constraint Language
SFP	specific fan power
SPF	seasonal performance factor
TRT	thermal response test
WWHR	wastewater heat recovery

1 INTRODUCTION

1.1 Background

Activities concerning buildings consume a major fraction of the energy produced from primary sources worldwide, around 36 %. This includes energy end use during the operational phase - heating, cooling, lighting and appliances - as well as construction and decommissioning phases of the buildings. The energy consumption is reflected in the amount of GHG emissions; IEA reports building sector as responsible for 28 % of energy related CO_2 emissions in 2019, with an overall increasing trend. (IEA, 2020)

The need as well as high potential for emissions reduction within the sector is broadly acknowledged. Commonly the means of reducing emissions of building operational phase are presented as a two-stage process: reducing building energy losses to the minimum technologically and economically feasible level, and providing the remaining energy from renewable, preferably local energy sources, such as solar, wind and geothermal (European Parliament, 2010).

Most visions of sustainable building sector include widespread adoption of heat pumps, a heating/cooling technology which has quickly gained popularity during the 21st century. Because they utilize ambient or waste heat, heat pumps typically output 3-5 times the amount of heat energy with the same primary energy input as traditional heating methods employing fuel combustion or electrical resistors. Further, if the electricity used by the heat pumps is generated from non-fossil primary resources, the CO2e impact of heat pumps is very small. In particular heat pumps utilizing ground ambient heat (ground source heat pumps, GSHP) enable high performance throughout the year, independent of climate conditions, and they also offer a possibility for energy storage. In a comparison made in 2020, GSHPs were found to have the lowest CO2e impact of any heating method in Finland (Oksanen, 2020, p. 59).

In Finland the use of GSHP's in heating has been growing rapidly in 2000s, following the development of technology and the market: in new single-family houses GSHPs have been the most popular heating system since around 2013 (Rouhiainen, 2018). Adoption of GSHPs in large buildings has been slower due to aspects such as the construction business's tendency toward traditional solutions, lack of skilled designers and capital, but the amount of large installations has also increased in recent years, especially in areas not covered by district

heating networks (Lauttamäki 2018, p.168). Large installations may actually constitute a majority of GSHP installations in the future, due to increasing competition from air to water heat pumps in single family houses (Lauttamäki, 2018, p.221).

Apartment buildings are usually situated in urban areas with an existing district heating network. This, as well as limited space for borehole fields of sufficient size, has limited the technical and economical suitability of GSHPs in the application. However, recently utility companies have also shown interest in ground-source heat as a source for district heating grids, following the trend of a more distributed mix of energy sources, as coal is being phased out and biofuels are a limited and environmentally controversial substitute for combustion of similar scale. (Lehtinen, 2020). For example in city of Helsinki, which is struggling to find alternatives for its coal heat plants about to be decommissioned in 2029, the local utility company Helen has expressed its interest in GSHPs both for individual buildings and blocks, as well as within the larger district heating grid. (Helen, 2020).

In order to improve the feasibility of GSHPs in urban areas by reaching higher ground temperatures and larger landmasses, the development trend is toward deeper boreholes. In Finland the typical borehole depth has increased from 150 m to 300 m since the start of the millennium, 300 m being currently the standard maximum depth for GSHPs (Lauttamäki, 2018, p.185). Large-scale implementation of deep GSHP systems requires development in many aspects, such as drilling, ground heat exchangers, geological measurements and simulation models.

Smart Otaniemi is an innovation ecosystem for piloting different technologies and business models related to the ongoing systemic change of the energy system (Smart Otaniemi, 2020). As a part of the phase 3 of the innovation ecosystem, an under-design apartment building in Kalasatama, Helsinki will employ a GSHP system with 800 m deep boreholes, serving as a test ground for different technologies involved in deep GSHP. The end goal of the project is a holistic solution for semi-deep GSHPs, that can be replicated for large-scale production.

1.2 Objectives

Designing a geoenergy system is more involved than that of most alternative heating systems, due to ground thermal response: dimensions of the ground heat exchanger should be such that heat extraction can be sustained for the planned lifetime of the system without excessive ground cooling, which can lead to groundwater freezing and possible damage to the collector tubes.

The aim of this thesis is to perform initial evaluation of the technical potential of a deep GSHP system covering the heating and cooling demand of the mentioned building.

Three specific objectives were devised to guide the study, the first being concerned with the sustainability of heat extraction; the objective is to find out the amount of 800 m boreholes required to sustainably supply the heat energy for the case building for a time period of 50 years, using a reference design for the coaxial borehole heat exchanger.

The second objective is related to cooling. Ground heat exchangers can potentially be used for free cooling of buildings during summer; meaning that no refrigerator operation is necessary. This brings about electricity savings, as no compressor operation is required. However, deeper boreholes reach to higher ground temperatures, which may lead to heat carrier fluid temperatures which are excessively high to be used. This thesis will aim to answer whether free cooling is feasible using 800 m boreholes using the same heat exchanger design as for the previous objective.

Excess heat from various sources, mostly during summer, can be used to heat up the heat carrier fluid circulating in the ground heat exchanger, and subsequently increase ground temperatures to improve GSHP performance and/or increase system lifetime. As a third objective this thesis will investigate the technical potential of heat energy available from ventilation outlet air during summer. The long-term effect of the regeneration on heat carrier fluid temperature and ground thermal response will be studied.

IDA Indoor Climate and Energy (IDA-ICE) will be used to calculate annual heating and cooling load profiles for the building. The effect of individual building-level energy efficiency improvements to the loads is scrutinized in the process. The load profiles will be used as an input for a previously developed numerical dynamic coaxial borehole heat exchanger (CBHE) model implemented in Apros. Prior to use, the CBHE model will be validated against measurement data and a BHE field dimensioning software EED. In addition to the objectives stated above, the thesis will attempt to highlight further topics of study regarding operation of the geoenergy system as well as the CBHE model used.

1.3 Outline

Sections 2-4 are concerned with the theoretical background of the study, with section 2 introducing residential building energy demand, section 3 heat pumps, and section 4 borehole heat exchangers. Section 5 describes the process of generating the building load profiles.

Section 6 introduces the CBHE model, including its validation, and configuration used. Section 7 describes the procedure for performing the system simulations, and section 8 contains the results of the simulations. Section 9 contains result analysis and discussion, and section 10 concludes the thesis.

2 BUILDING ENERGY DEMAND

This section gives an overview of residential buildings' energy end use, with the focus on the climate conditions in Finland.

2.1 Residential building energy end use

The distribution of residential building energy end uses in Finland is presented in the figure below. (Statistics Finland, 2018).

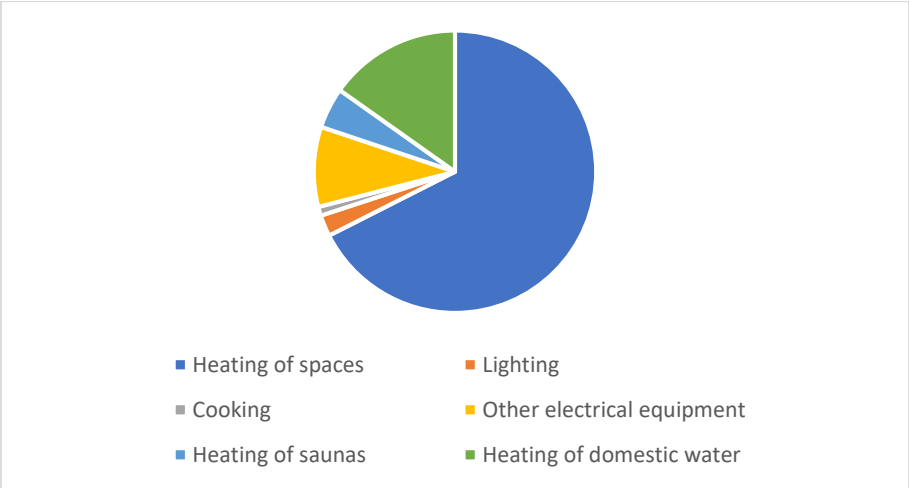

Figure 1. Distribution of residential energy consumption by end use.

While all the major energy end uses are present in the figure, the more exact distribution of end energy use depends on building type and age; for example apartment buildings have higher indoor volume compared to envelope area, and new buildings of each type have smaller portion of space heating due to relatively large improvements in insulation and ventilation heat recovery in recent decades. On the other hand the portion of DHW (domestic hot water) is considerably higher in new buildings due to lack of development in conservation and heat recovery methods (Meggers, Leibundgut, 2011, p. 879). The figure also doesn't display space cooling energy demand, which is higher in new and renovated buildings due to increased insulation level and resident preferences, but still low compared to space heating (Airaksinen et al, 2015).

In the perspective of an energy system designer, DHW and space heating and cooling are the loads taken care of by a centralized system, for which the energy source(s) must be selected. Electricity end use within the building also manifests as internal heat load, which needs to be considered in dimensioning the energy system, as it affects the annual heating and cooling demand. Simulation tools such as IDA-ICE used in this thesis can be used to calculate the

detailed hourly profile of each load. The different types of energy end use are introduced in more detail below.

Space heating and cooling

Space heating and cooling systems keep the spaces at the desired temperature. In apartment buildings this is done by a centralized heating system combined with a water circulation system delivering the heat/cool to local units within the apartments. Buildings with mechanical inlet ventilation (practically all new apartment buildings) also incorporate a ventilation heating/cooling unit which sets inlet air temperature to a specific level. The centralized plant supplying the heat can be a district heating heat exchanger, a heat pump or an electrical or combustion boiler.

In new apartment buildings heating energy is typically distributed both to ventilation inlet air, and to local space heating units situated within the rooms. The space heating units are usually radiators placed near walls, or radiant emitters under the surfaces of the rooms (e.g. floor heating). Radiant emitters can operate on lower heating temperatures (typically maximum of 35 - 40 °C) compared to traditional radiators (maximum 70-80 °C), due to their larger heat transfer area. In turn radiant emitters also operate on higher cooling temperatures. In buildings with heat pumps radiant emitters are the preferred method, since lowering heating circuit temperature improves heat pump performance, as will be seen in section 3. Regardless of the heater type, heating circuit inlet temperature is usually controlled as a function of ambient (outdoor) temperature, e.g. with a scheme similar to one shown in figure 2.

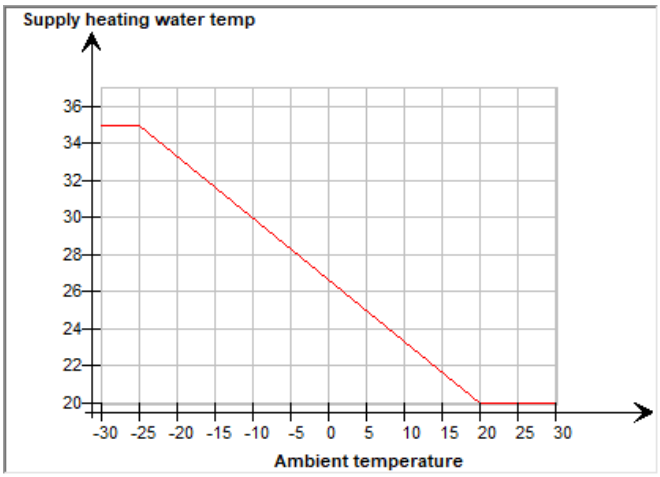

Figure 2. Space heating temperature control (screenshot from IDA-ICE).

Space heating in Finland is very seasonal, with the highest loads occurring in January and February, and no heating load during summer months. During summer there may be instead be need for cooling, which can be distributed in a similar fashion to inlet air or to spaces directly.

Domestic hot water

DHW systems are concerned with delivering hot water to resident's end use points such as kitchen and toilet taps. In new apartment buildings with good insulation and ventilation heat recovery, DHW energy consumption is of similar magnitude as that of space heating (Yrjölä, Laaksonen, 2015, 8). In new buildings utilizing heat pumps the energy portion of DHW is further increased due the fact that it is heated to higher temperature (58-62 °C) than space heating circuit, reducing heat pump efficiency, as will be seen in section 3.

DHW consumption is relatively constant throughout the year compared to space heating, meaning that during summer it is the only heating load in a building. In an hourly level, however, it is typically less constant than the space heating profile, since it depends more on resident schedules. Typically there are pronounced peaks in DHW consumption in the morning and evening (Johansson, 2019, p. 8). During nighttime (when very little tap water is used), heating is mainly required to compensate for pipe heat losses (recirculation heating) (Yrjölä, Laaksonen, 2015, p. 8). Figure 3 presents the DHW load profile used for simulation in this thesis.

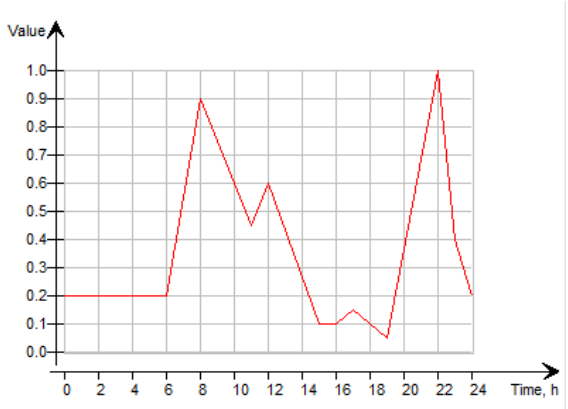

Figure 3. Example of the daily DHW consumption profile, scaled (screenshot from IDA-ICE).

Internal loads

Internal heat loads constitute the residents themselves, electricity end use by building services such as lighting and ventilation and residents' devices within the building. Electricity converted to heat during the heating season is not "waste heat", in that it reduces the space heating load. However, new apartment buildings employ heating sources more efficient than direct electrical

heating, and during summer months internal loads increase space cooling load. In addition minimizing electricity use of the end use devices is an end in itself, to reduce the demand for non-renewable primary energy. This incentivizes e.g. implementing more energy efficient devices and demand-tailored control where possible.

Load peaks

Heating and cooling load profiles can be to an extent manipulated, for example shifting the timing of peak loads, or spreading the energy use from peaks to a longer period of time (peak shaving). Typical motivation for this is to achieve savings by reducing the dimensioning peak power of grid connection or an on-site energy supply system (Hellström 1991, p. 1). An example of peak shaving is the use of thermal storages which are charged during periods of low load (e.g. higher ambient temperature) and discharged during periods of high load (lower ambient temperatures). The building envelope in itself is a heat energy storage, since it exhibits high heat capacity and responds slowly to changes in ambient temperature. Other commonly used heat storages are hot or cold water storage tanks situated within the building. Ground can also be used as a short-term or seasonal heat storage, as will be discussed in section 4.

2.2 Building energy efficiency

Within a long time period the heat input to a building by different end uses will exit the building by some method of heat transfer. This heat loss from the building interior happens mainly by conduction through the envelope, sensible and latent heat of ventilation outlet air and with wastewater into the sewer (Vihola et al, 2015, p. 603).

Building form

The energy efficiency level of a building is to an extent defined already during the architectural planning: one notable factor affecting heat consumption is the building form factor (envelope area divided by indoor volume). Form factor is increased by complicated envelope shapes. The form and position of rooms and windows also affects passive heating by sunlight, which is desirable during heating season. During summer excess sunlight can be blocked by external or internal window shadings. Windows can also be equipped by coatings that reflect specific wavelengths of solar radiation. Solar heating through a window is expressed by window g-value, which includes the effect of direct heating (radiation transmittance through the glass into the building) and indirect heating (radiation absorptance to the glass and frames) (Equa

Simulation AB, 2020). G-value of a window is between 0 and 1; value of 0 would indicate no solar heating through windows.

Insulation and thermal bridges

Adding insulation to the building envelope (and in some cases internal walls) reduces conduction losses through the envelope. The amount of conduction heat transfer through a layer is quantified by a heat transfer coefficient, U-value [W/m^{2}K]. Window glazings and frames are notably the part of the envelope with the highest U-value.

Good insulation practices also take into account thermal bridges, which are pathways of more conductive materials through insulation layers, usually appearing due to structural reasons, such as for balconies. In addition to energy losses, thermal bridges can lead to moisture problems within the structure. Heat losses through thermal bridges can be minimized by using structures specifically designed for the purpose. (Seppänen, Seppänen, 1996, p. 69)

Airtightness

Airtightness refers to the amount of leakage air through the envelope, for example through seams at windows and doors. In buildings with mechanical inlet and outlet ventilation (most new apartment buildings), leakage air manifests in increased space heating energy, since it doesn't pass through the ventilation heat recovery unit. (Tommerup, Svendsen 2005, p. 620).

Heat recovery

Heat stored into flows of ventilation outlet air and wastewater can be partially recovered to inlet flows of air and water by heat exchangers. Ventilation heat recovery (VHR) is established technology by now, and used in practically all new apartment buildings. One definition for heat recovery efficiency, assuming balanced inlet and outlet mass flows, is:

$$\eta = \frac{q}{q_{\max}} = \frac{T_2 - T_1}{T_3 - T_1}, \quad (1)$$

where T_1 is cold air inlet temperature (to heat recovery heat exchanger) [K],

T_2 is cold air outlet temperature [K], and

T_3 is hot air inlet temperature [K].

In practice the values of efficiency range from 50 % to 90 %, depending on heat exchanger type. (Schild, 2004)

Unlike ventilation heat recovery, wastewater heat recovery (WWHR) is not widely in use. It is, however, becoming an increasingly attractive option for improving building energy efficiency especially in modern apartment buildings, where DHW is often the largest energy consumer. A common solution is to exclude blackwater (wastewater from the toilet seat) from the heat exchanger; this alleviates the problem of heat surface fouling and increases the temperature of the recovered heat (Johansson, 2019, p. 3). However it leads to additional complexity of the sewage system in countries such as Finland, where blackwater is not usually separated from greywater. The performance of WWHR is more dependent on resident habits than VHR, and issues reported from existing systems include the over-estimation of DHW usage (Arvola, 2017, p. 18). Therefore the demand profile of the buildings should be considered when planning to implement a WWHR system.

National standard for building energy efficiency

Standardized levels for building energy efficiency and indoor environment exist, depending on building type (use profile). Current national regulations in Finland state a limit for net heating energy requirement per area and an e-value which new buildings must not exceed. The net heating energy requirement must not exceed a standardized level which is calculated by reference U-values for each element of construction, and standardized equations for the heating load presented by ventilation, DHW and leakage air. E-value takes into account all annual energy use in the building; different primary energy sources used are weighed with factors which reflect the emissions impact of the energy source. (Ympäristöministeriö, 2017, p. 3).

3 GROUND SOURCE HEAT PUMPS

This section will provide some basic information about ground source heat pumps (GSHP), necessary for understanding the content of the thesis. This includes the working principle and the most important operating parameters.

Heat pumps

Heat pump is a device that upgrades heat from low temperature source to higher temperature, by utilizing a closed loop thermodynamic cycle. Because they utilize ambient or waste heat, heat pumps typically output 3-4 times the amount of heat energy with the same primary energy input as traditional heating methods employing fuel combustion or electrical resistors.

3.1 Vapor compression cycle

The reverse heat flow from lower to higher temperature is made possible by phase change of the circulating fluid; phase changes in desired temperatures are made possible by manipulating fluid pressure using a compressor and an expansion valve. Therefore the cycle used in practical heat pump applications, vapor compression cycle, involves a circulating fluid undergoing vaporization, compression, condensing and expansion. Figure 4 illustrates the working principle of the cycle.

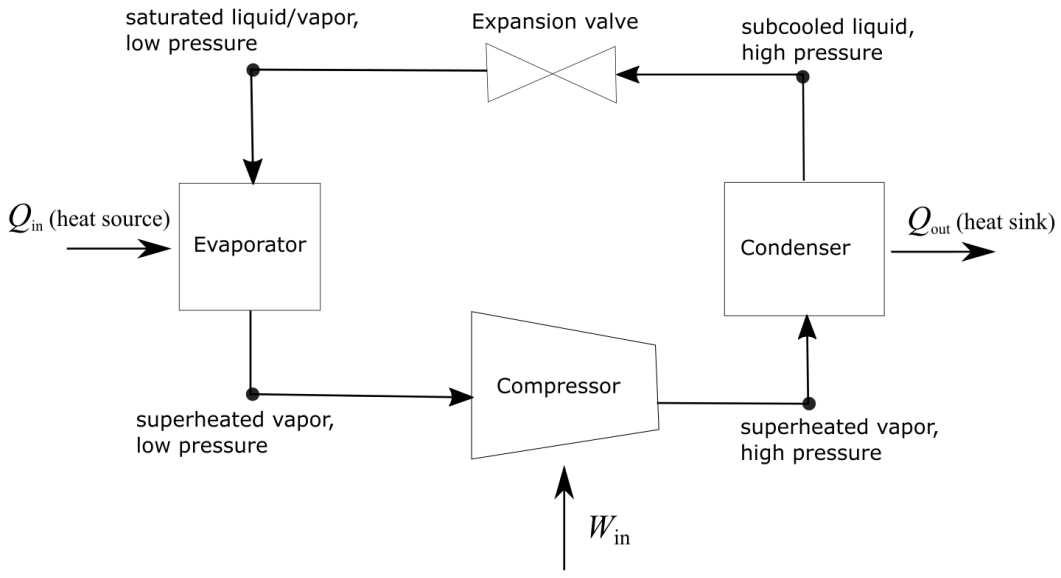

Figure 4. Vapor compression cycle working principle.

A reader more interested in the working principle of heat pumps is advised to consult any basic level thermodynamics textbook.

If the vapor compression cycle is used instead for the primary purpose of transferring heat away from a space, the device is instead called a refrigerator, and household refrigerators are indeed the most common application for it. A single device can be made to perform either purposes by a simple switch configuration; many domestic heat pumps can be used for space cooling as well as heating.

3.2 Coefficient of performance

The main parameter describing heat pump performance is the coefficient of performance (COP).

$$\mathrm{COP} = \frac{Q_{\mathrm{out}}}{W_{\mathrm{in}}}, \tag{2}$$

where Q_{out} is heat output [J], and
W_{in} is work input [J].

COP describes how many units of heat energy the heat pump will output per one unit of input high grade energy (typically electrical) driving the compressor. Therefore a COP as high as possible is desirable for any application, to minimize electricity consumption. The input energy term can be defined to also include auxiliary equipment, such as heat carrier fluid (the fluid in the ground loop) pumps, to better reflect system level efficiency.

For refrigerator operation the desired outcome is instead cooling; therefore a different indicator is used to describe performance:

$$\mathrm{EER} = \frac{Q_{\mathrm{in}}}{W_{\mathrm{in}}}, \tag{3}$$

where Q_{in} is heat input [J].

For an ideal heat pump cycle (reversed Carnot cycle) the COP only depends on the ratio of input and output temperature:

$$\mathrm{COP}_{\mathrm{carnot}} = \frac{1}{1 - T_{\mathrm{L}}/T_{\mathrm{H}}} \tag{4}$$

In practice, then, COP increases with higher evaporator temperatures and lower condenser temperature. Real heat pumps follow the above shown relation in principle, but their COP is lower due to irreversibilities, mainly taking place in the compressor. Manufacturers report the COP of their devices as measured under standardized rating temperatures. For example for GSHPs typical rating conditions are 0/35 °C (low temperature) and 0/55 °C (medium

temperature), where the first number is evaporator input temperature and the latter is condenser output temperature. (SFS EN 14511-2:2018). Heat output capacity of a heat pump also depends on the temperature levels.

Seasonal performance factor

In real applications the temperature level on either side is likely to change as a function of ambient temperature and heat requirement; for example the space heating circuit supply temperature typically changes according to a control curve similar to the one displayed in section 2. SPF (seasonal performance factor) is a commonly used indicator for annual performance of a heat pump, and it is calculated by annual energy values:

$$\mathrm{SPF} = \frac{Q_a}{W_a} \tag{5}$$

3.3 Heat pump modelling

During operation evaporator and condenser temperature levels can differ from the standardized ones, therefore mathematical models are used to predict HP performance for detailed hourly calculations. The complexity and accuracy of used models varies depending on the specific modelling needs.

Distinction can be made between so-called equation fit models and deterministic models (Fisher, Rees, 2005, p. 313). The former are a kind of a black box, fitting a polynomial function into a performance map based on manufacturer's data. The latter is based on modelling the actual physical phenomena within the components of the heat pump, using thermodynamic balance equations.

The equation fit model typically utilizes two polynomial equations for condenser heat and compressor power, respectively, with both functions having evaporator inlet and condenser outlet temperatures as variables. The polynomials can be of varying degree. For example in (Carbonell et al, 2014, p. 2), a second degree polynomial is used:

$$q_\mathrm{c} = a_0 + a_1 T_\mathrm{e,in} + a_2 T_\mathrm{c,out} + a_3 T_\mathrm{e,in} T_\mathrm{c,out} + a_4 T_\mathrm{e,in}^2 + a_5 T_\mathrm{c,out}^2, \tag{6}$$

$$P_\mathrm{comp} = b_0 + b_1 T_\mathrm{e,in} + b_2 T_\mathrm{c,out} + b_3 T_\mathrm{e,in} T_\mathrm{c,out} + b_4 T_\mathrm{e,in}^2 + b_5 T_\mathrm{c,out}^2, \tag{7}$$

where *a* and *b* are heat pump-specific coefficients obtained by curve fitting,
$T_\mathrm{e,in}$ is evaporator inlet temperature [K],
and $T_\mathrm{c,out}$ is condenser outlet temperature [K].

For inverter driven (variable speed) compressors, frequency can be included in the polynomials as a third variable. COP at any specific moment can then be calculated using eq. (2).

3.4 Power coverage factor

Heat pump power coverage signifies the portion of heating energy provided by the heat pump in peak load (dimensioning outdoor temperature) situation. The remaining portion of heat is provided by an auxiliary heating system, typically electric resistance, which is often included in commercial heat pumps. A typical power coverage is 70 %, in which case the energy coverage is usually over 95 %. However, the exact relation between power and energy percentage depends on the shape of the building load profile. The load profile can also be manipulated by dividing the energy demands across a longer time span, by energy storages or load flexibility. (Mazzotti et al 2018, p. 3).

Economically the choice of power coverage factor comes down to finding the balance between energy costs and system investment cost. In GSHPs not only the increased capacity of the heat pump must be considered, but the BHE heat extraction capacity and available heat energy in the ground must also conform to the requirements of the heat pump. In practice increasing coverage factor can require an increase total BHE length or introduction of some means of ground regeneration. If the available energy in the ground doesn’t allow for high enough coverage factor, the system will not be profitable, as has been reported for example in studies of potential of shallow (300 m) geoenergy in Northern Pasila (Helsingin maalämpötyöryhmä, 2019, p. 15).

4 BOREHOLE HEAT EXCHANGERS

This section will deal with borehole heat exchangers (BHE), with the emphasis on coaxial BHE's (CBHE) and deep boreholes. Different definitions for "deep" borehole exist; in some sources a depth of more than 300-350 m has been suggested for the context of GSHP's (Morcio, Fossa, 2019, p. 1), (Helsingin maalämpötyöryhmä, 2019, p. 7). BHE heat transfer, construction and typical modelling approaches will be presented. The section will concentrate on heating (heat extraction) application of BHE's, but the same theory and design aspects mostly apply to cooling (heat injection).

4.1 Geothermal heat

The main attraction of using ground as a heat source or sink for heat pumps is the stability of ground temperature. Below the surface level (~20 m) ground temperature is practically constant throughout the year, increasing with depth due to geothermal heat flux from the Earth's center towards surface (GTK, 2019, p. 51). The stable temperature allows for maintaining high COP also during the coldest months of the year. Similarly during summer months the ground is (at least in moderate depths) cooler than ambient air, which allows for more efficient cooling. Figure 5 is a visualization of the temperature profile within the ground.

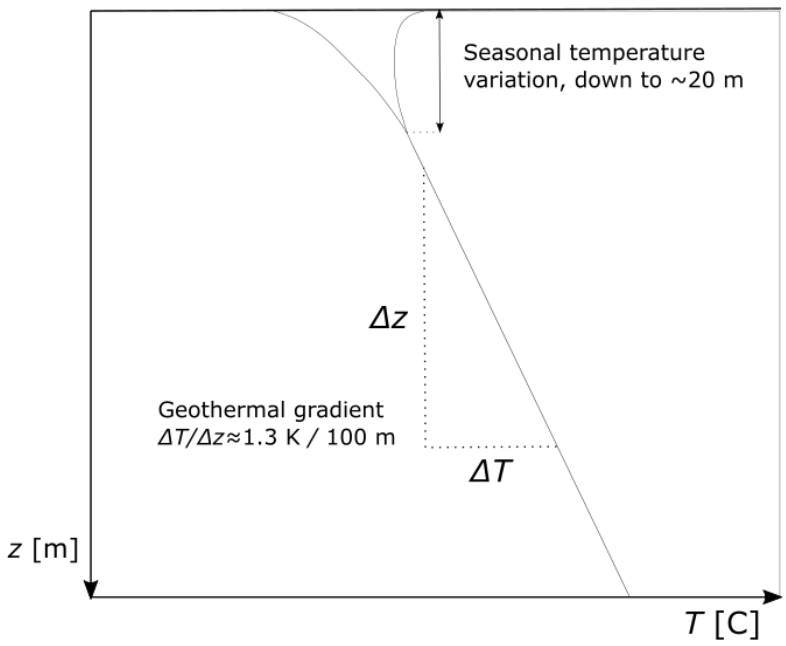

Figure 5. Visualization of ground heat fluxes and geothermal gradient.

Human activity can also have a limited effect on local geothermal gradient; in urban areas the heat transfer from building floors to ground during decades has been found to increase ground temperature, notable as an inverted temperature gradient up to 100 m (Gehlin et al, 2016). This

has a positive effect on the output of GSHP systems situated in such areas. The impact of GSHP systems themselves on ground temperature will be covered further below. The next subsection introduces the aspects of heat transfer from ground to a GSHP.

4.2 Ground heat exchangers

The system transferring heat from the ground to the heat carrier is called a ground heat exchanger (GHE). Only closed loop heat exchangers will be discussed here. In closed loop ground heat exchangers the heat carrier, usually a mix of water and ethanol, is circulating contained within collector tubes. The collector tubes can be installed either horizontally within the soil or vertically within the bedrock. Horizontal collectors can only be used where horizontal space is plenty, but their installation cost is lower since there is no drilling involved. Vertical collectors are placed in drilled boreholes. In 2018 vertical collectors (borehole heat exchangers, BHE) constituted around 90 % of new installations in Finland (Lauttamäki, 2018, p. 174).

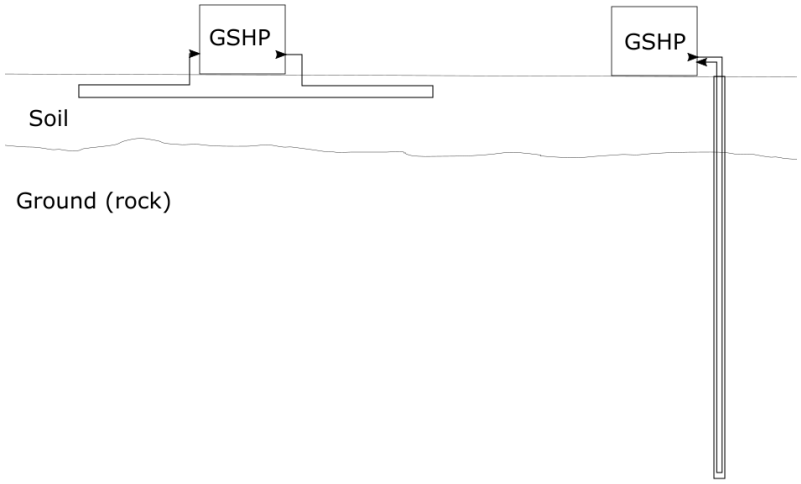

Figure 6. Horizontal and vertical GHE's.

As can be inferred from the ground temperature figure 5, vertical collectors reach seasonally more stable, and higher ground temperatures than horizontal installations, resulting in higher COP for heating. For mainly cooling-purpose applications the higher temperatures at deeper levels are on the contrary detrimental.

For applications with high energy and/or heat power requirement, such as that of an apartment building, a borehole field with multiple BHEs is usually required. BHEs can be connected in series or parallel, or a combination of both, depending on application-specific needs. In a series connection the same heat carrier fluid goes through every BHE, and in parallel connection the

total mass flow rate is the sum of heat carrier flow rates in all the BHEs. In practice parallel connection is more common (Holmberg 2016, p.46).

4.3 BHE construction

A borehole heat exchanger consists of the borehole, collector tubes placed in the borehole and filling material which transfers heat from the borehole wall to the collector tubes. The collector tubes form a closed loop, through which heat carrier fluid travels, absorbing or rejecting heat in the process. Borehole filling practices differ by location; for example in North America and Central Europe specific solid grouting materials with high conductivity are used, but in Nordic countries the practice is to let the boreholes fill with groundwater by themselves. Groundwater is a cheaper option, and although it is a poor heat conductant, the vertical temperature differences within the borehole cause natural convection, which significantly improves the heat transfer (Holmberg 2016).

Figure 7 is a more detailed side view of a BHE.

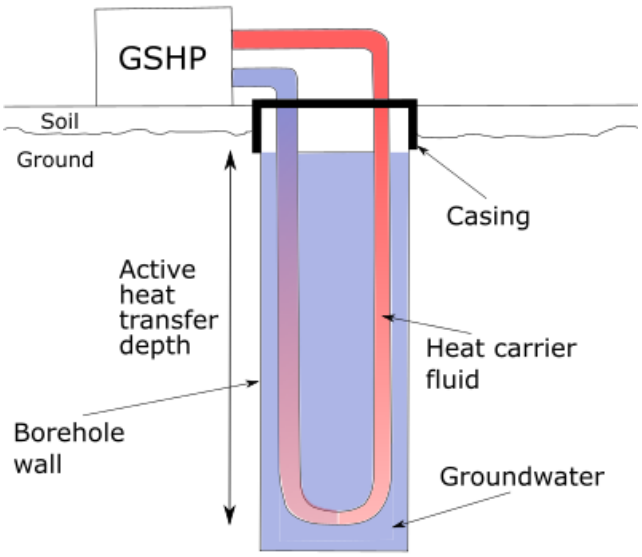

Figure 7. Side view of a borehole heat exchanger, not in scale.

The effective heat transfer depth (active depth) is from the groundwater surface level downwards. The top part (1-5 m) of the borehole usually penetrates soil layer, which is composed of small solid particles of organic matter and minerals. This part of the borehole is covered with a casing to prevent soil matter from falling into the borehole, and to protect the collector tubes from twisting or wearing.

Collector tube arrangement within a BHE affects heat transfer resistance between the ground and the heat carrier, and therefore the required borehole length. There are different options for

the tube arrangement, the most common being u-tube and coaxial (tube-in-tube) collectors. Side views and cross-sections of these tube arrangements are presented in figures 8 and 9.

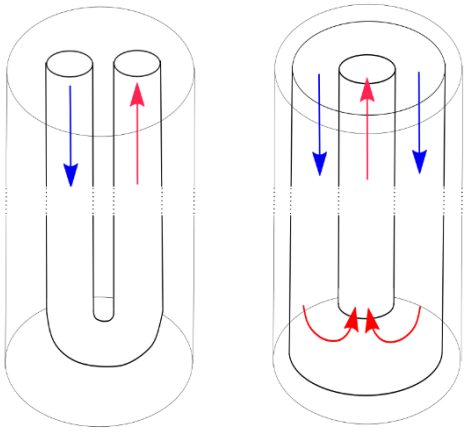

Figure 8. Side views of u-tube BHE and CBHE.

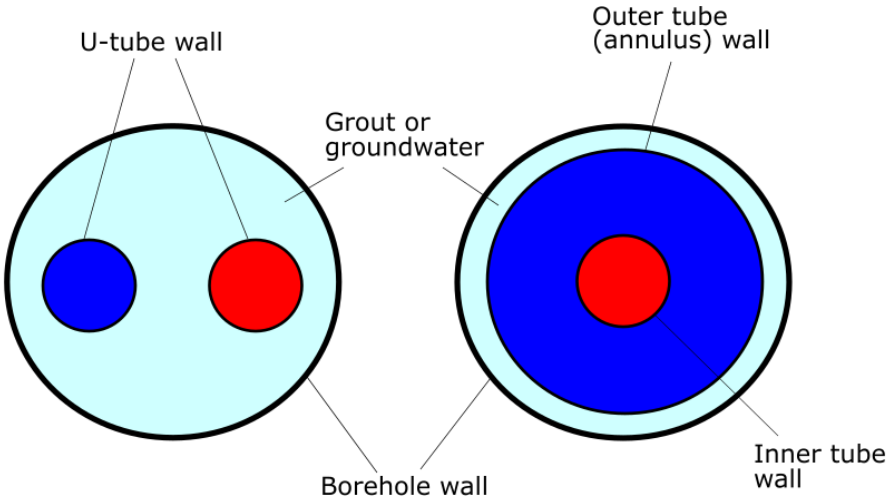

Figure 9. Cross-sections of a u-tube BHE and CBHE.

In a u-tube BHE the downward and upward tubes are joined at the bottom, forming a u-shape. BHEs with multiple u-tubes also exist, exhibiting better thermal performance. The coaxial tube consists of concentric tubes. Studies have been made involving more complicated coaxial designs with multiple tubes, but they will not be discussed in this thesis. In both of the presented variants the heat carrier travels down in a straight path, changes direction at the bottom and returns up.

No generally applicable conclusion has been made from comparisons between thermal performance of U-tubes and coaxial tubes, due to differences in other BHE design aspects, such as borehole depth, tube materials, diameters and mass flow rate, between studies (Aresti et al, 2018, pp. 760-761). However, as can be seen in figure 9, coaxial tube utilizes the available

borehole cross-section space more efficiently, allowing for higher flow rate given a borehole of similar diameter. Deep boreholes inherently require higher flow rates to minimize thermal shunt (heat transfer between the collector tubes), which is why coaxial tubes are considered to be a more practical option for them (Holmberg et al, 2016, p. 65).

4.4 Heat transfer

Both external (ground) and internal (within the BHE) heat transfer needs to be considered. Heat transfer within the ground is mainly conductive, although convective heat transfer is also present in areas with groundwater flows. Heat transfer within the borehole is convective (within groundwater filling and heat carrier fluid) and conductive (through tube walls, and in case of grout filling).

Bulk heat flow from ground into the heat carrier can be described by a fundamental thermal energy balance equation:

$$q = q_{\mathrm{m}} \cdot c_{\mathrm{p}} \cdot (T_{\mathrm{out}} - T_{\mathrm{in}}), \qquad (8)$$

where q is heat flow from ground to heat carrier [W]
q_{m} is heat carrier mass flow [kg/s],
c_{p} is heat carrier specific heat capacity [J/kgK],
T_{out} is heat carrier temperature at borehole outlet [K],
T_{in} is heat carrier temperature at borehole inlet [K].

From equation (8) the rate of useful heat transfer can be calculated at any given time, when the operating parameters (heat carrier flow rate and temperature difference) are known. Alternatively the possible combinations of heat carrier flow rate and temperature difference can be calculated when the heat demand profile is known. However, Q must also be related to the heat transfer properties of the BHE and the ground.

Effective borehole resistance

In applications of heat transfer, thermal resistance R or its reciprocal heat transfer coefficient U are used to quantify the effectiveness of heat transfer in an application. For BHE's it is common practice to quantify the entire heat transfer process with a parameter for effective borehole thermal resistance, R_{b}^{*} (Mazzotti et al, 2018, p. 4). Using R_{b}^{*}, the heat flow between borehole wall and heat carrier can be written as:

$$\bar{q} = \frac{\bar{T}_\mathrm{f} - \bar{T}_\mathrm{b}}{R_\mathrm{b}^*}, \tag{9}$$

where $\bar{q}$ is depth-averaged heat flux [W/m],

$\bar{T}_\mathrm{f}$ is average heat carrier temperature [K],

$\bar{T}_\mathrm{b}$ is average borehole wall temperature [K],

R_b^* is effective borehole resistance [mK/W].

When used in design, equation (9) can be used for crude calculation of total required borehole length. Notably the term R_b^* depends only the specifications of the BHE (tube diameters, conductivities, flow rate etc.). The effect of ground heat transfer, on the other hand will manifest in the term $\bar{T}_b$, which changes over time as heat is extracted from the ground. Heat transfer in the ground and within the BHE are usually studied separately, and in mathematical models they are also often modelled with different methods that are coupled at the borehole wall, due to differences in heat transfer mechanisms and timescales involved. In this theoretical section we follow a similar approach, with the next section concentrating on the BHE, and ground heat transfer discussed after that.

4.4.1 Heat transfer within the BHE

While R_b^* describes the performance of the BHE as a whole, the involved heat transfer mechanisms can be studied in more detailed form by a thermal resistance network corresponding to BHE geometry. In a coaxial BHE with a single annulus and inner tube the resistance network can at its simplest by divided to two parts; resistance R_{12} resisting the heat flux between annulus flow and inner tube flow and resistance R_{b1} resisting the heat flux between borehole wall and annulus flow.

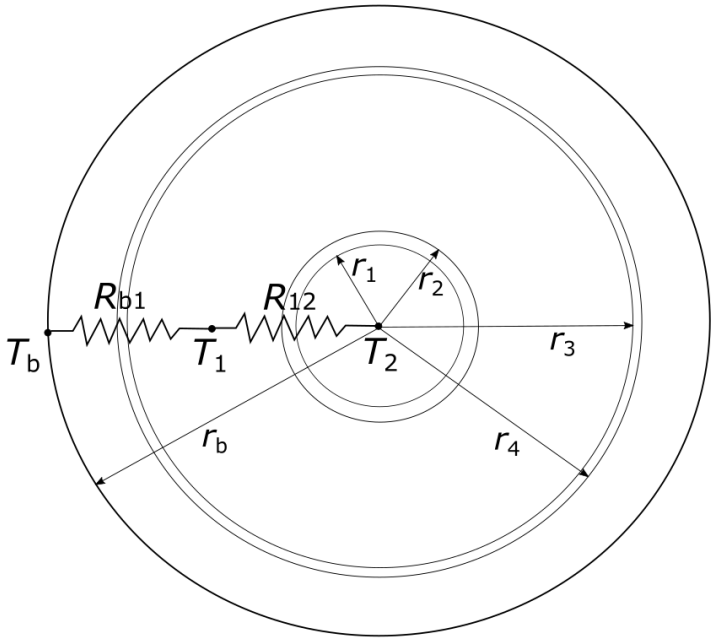

Figure 10. Heat transfer resistance network of a CBHE.

Resistance R_{12} consists of two convective parts (for flow in the inner tube and annulus) and one conductive part (for inner tube wall). (Holmberg et al, 2016, p. 68):

$$R_{12} = \frac{1}{2\pi r_1 h_1} + \frac{\ln\left(\frac{r_2}{r_1}\right)}{2\pi k_c} + \frac{1}{2\pi r_2 h_2} \tag{10}$$

where h_1 is convective heat transfer coefficient at inner tube inner wall [W/m^{2}K],
h_2 is convective heat transfer coefficient at inner tube outer wall [W/m^{2}K],
k_i is conductive heat transfer coefficient of the inner tube wall [W/mK].

Resistance R_{b1} consists of one convective part (flow in the annulus) and two conductive parts (annulus wall, groundwater between annulus and borehole wall) (Holmberg et al, 2016, p. 68):

$$R_{b1} = \frac{1}{2\pi r_3 h_3} + \frac{\ln\left(\frac{r_4}{r_3}\right)}{2\pi k_a} + \frac{\ln\left(\frac{r_b}{r_4}\right)}{2\pi k_{gw}}, \tag{11}$$

where h_3 is convective heat transfer coefficient at inner tube inner wall [W/m^{2}K],
k_a is conductive heat transfer coefficient of the annulus tube wall [W/mK],
k_{gw} is conductive heat transfer coefficient of groundwater [W/mK],

The components of R_{b1} should portray the construction of the BHE; in case the outer tube is very close to or in contact with the borehole wall, the convection heat transfer in the groundwater between the annulus wall and borehole wall may be negligible, in which case it

can be instead be modelled as conduction, as in the equation above, or simply as a contact resistance term. The same applies if a solid grouting material is used. If, instead, the amount of groundwater between annulus wall and borehole wall is more considerable (as it is in u-tube BHEs), the effect of natural convection on heat transfer also needs to be taken into account. Natural convection will be discussed further below.

While R_{b1} should obviously be minimized to maximize heat transfer, R_{12} should instead be as high as possible to minimize so-called thermal short-circuit, or heat transfer from upward-travelling hot fluid to cold fluid travelling downward in the borehole.

From equations (10) and (11) we can infer that the resistances can be manipulated by changing tube diameters or heat transfer coefficients *k* and *h*. While conduction coefficient *k* is a material property, convection coefficient *h* depends not only on the heat carrier fluid, but on the fluid flow. Therefore *h* cannot be arbitrarily chosen without changing flow variables, such as velocity. The following subsection will briefly go through the basics of convective tube flow heat transfer.

4.4.2 Tube flow convective heat transfer

Convective heat transfer on fluid-solid interface includes both the effect of conduction (which would constitute the heat transfer in the case of completely stationary fluid), as well as the transport effect due fluid flow. Heat is therefore transported faster than in the case of mere conduction. The ratio of convective, or "actual", heat transfer coefficient to conductive heat transfer coefficient is quantified with a dimensionless parameter, Nusselt number.

$$\mathrm{Nu} = \frac{hD}{k} \tag{12}$$

where Nu is the Nusselt number [-]
D is tube diameter (characteristic length scale) [m],
k is conductive heat transfer coefficient [W/m].

Turbulence

General analytically derived expressions for Nu as a function of flow conditions do not exist (as is typical for fluid mechanics); instead experimentally derived correlations, for different boundary conditions, are used to predict Nu accurately enough for practical purposes. The value of Nu is influenced by both fluid material and flow properties. A major influence on Nu

is the amount of turbulence: eddy motions of fluid particles, or vortexes, within the flow. High turbulence improves flow mixing, leading to higher convective heat transfer. Turbulence is quantified by flow Reynolds number, which can be interpreted as the ratio of inertial forces to viscous forces within the flow:

$$\mathrm{Re} = \frac{\rho w D}{\mu} \tag{13}$$

where ρ is fluid density [kg/m^3],
w is fluid velocity [m/s],
μ is fluid viscosity [kg/ms].

A so-called critical value of Reynolds number marks transition from laminar to turbulent flow. The critical value depends on flow channel geometry; for tube flow Reynolds number of 2300 is typically used. In laminar flow the fluid particles mostly follow straight streamlines; therefore fluid mixing in radial direction is minimal and radial heat transfer within the fluid is mostly conduction. In practice this results in lower Nu - and h - for laminar flows; due to this laminar flows are unwanted in most heat transfer applications.

In addition to Re, Nu depends on Prandtl number, which is a material property describing the ratio of heat and momentum diffusion:

$$\mathrm{Pr} = \frac{\mu}{\rho \alpha}. \tag{14}$$

The value of Pr for a specific material can vary as a function of pressure and temperature.

Correlations

Due to highly different fluid behavior in laminar and turbulent flows, different correlations for Nusselt number in each case exist. Typically the correlations are given a range of Reynolds number for which they are applicable. In the context of BHE's, Hellström (1996) notes that ideally it should be ensured that any correlations used are applicable to the specific circumstances present in BHE collector tubes, namely low flow temperature, long and vertical tubes, and the direction of heat transfer.

4.4.3 Pressure drop

As seen in the definition of Reynolds number, turbulence (and consequently convective heat transfer) can be increased by increasing flow velocity. However, this has an adverse effect of

increasing the pressure drop within the tubes. The same is true for improving heat transfer by increasing surface roughness. Pressure drop in a tube flow follows the equation below:

$$\Delta p = f_{\mathrm{D}} \frac{L}{d} \rho \frac{w^2}{2} \tag{15}$$

where f_{D} is Darcy's friction factor [-].

Darcy's friction factor f_D is a dimensionless quantity, which depends on flow Reynolds number and tube surface roughness. Pressure drop within the tubes manifests in required pumping power, which depends on both pressure drop and flow rate:

$$P = \frac{\Delta p q_v}{\eta} = \frac{f_D L d \rho \pi}{8\eta} w^3 \tag{16}$$

where η is pump efficiency [-],

and q_{v} is volumetric flow rate [m^3/s]

Therefore the choice of flow velocity requires optimization between heat transfer and pumping power.

4.4.4 Natural convection

In the space between outer tube wall and borehole wall there is (usually) no mechanically driven flow, yet the temperature differences and consequent density differences present in the groundwater cause buoyancy-driven flow, also called natural convection. Grashof number is a dimensionless number describing flow driven by density differences:

$$\mathrm{Gr} = \frac{\rho^2 \beta \Delta T L^3 g}{\mu^2}, \tag{17}$$

where β is thermal expansion coefficient [1/K],

L is a length scale [m],

ΔT is the temperature difference across the length scale [K].

Similarly to Reynolds number (eq. 13), the value of Gr with respect to the critical value indicates whether the flow in question is laminar or turbulent. Below the critical value buoyancy forces are too small compared to viscous forces to cause bulk movement. Also similarly to Re, the critical value depends on flow channel geometry.

When applying eq. (17) to narrow enclosures, the length scale L is usually the distance between adjacent surfaces, which applied to CBHE's is the distance between outer tube wall and borehole wall. While this distance depends on the design (and installation) of the collector

tubes, ΔT depends on ground temperature and heat load. Water density depends on the local temperature of the groundwater. As an important note, β for water reaches a value of zero at around 4 C; therefore natural convection is non-existent at this temperature, and consequently heat transfer resistance between the ground and heat carrier will be highest around this groundwater temperature (Holmberg, 2016, p. 33).

Figure 11 presents the buoyancy-induced laminar flow patterns of groundwater during heat extraction. With increasing Grashof number, the circulating patterns develop into smaller patterns and eventually into turbulent flow regime where no pattern is discernible. (Holmberg, 2016, p. 37).

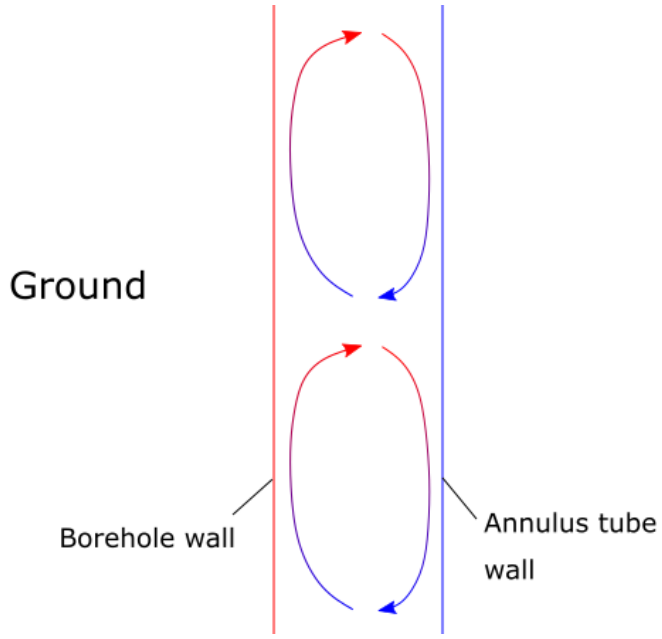

Figure 11. Groundwater movement by natural convection.

Correlations

For natural convection the correlations for Nusselt number are presented as a function of Grashof number and Prandtl number, similarly to how Re and Pr are used in the case of forced convection. Gr and Pr are usually reduced to a single dimensionless number, Rayleigh number.

$$\mathrm{Ra} = \mathrm{Gr} \cdot \mathrm{Pr} \tag{18}$$

$$\mathrm{Nu} = f(\mathrm{Gr}, \mathrm{Pr}) = f(\mathrm{Ra}) \tag{19}$$

Holmberg (2016) presents a correlation for Nusselt number, specifically to account for groundwater natural convection in a BHE's. The correlation is based on previous studies of natural convection in enclosures with high aspect ratio, simplified for application to BHE's:

$$\mathrm{Nu} = 0.1743\ \mathrm{Ra}^{*0.233-0.009\,K} K^{0.442}, \quad (20)$$

where Ra^{*} is modified Ra, using hydraulic diameter as a length scale,

and K is radius ratio [-], defined as

$$K = r_o/(r_o - (r_o - r_1)), \quad (21)$$

where r_o is annulus outer radius [m], and
r_i is annulus inner radius [m].

(Spitler et al, 2016) instead used an experimental approach of using temperature measurements in a reference u-tube BHE, and presented novel correlations for Nu at u-tube outer wall, borehole wall and borehole annular space. The correlation for the annular space is of the form:

$$\mathrm{Nu} = 0.14(\mathrm{Ra}^{*})^{0.25}, \quad (22)$$

However, as the correlation is explicitly based on the u-tube geometry, it is unlikely that it could be applied to CBHE's with any accuracy. While the correlation proposed by Holmberg (2016) is also applied to a u-tube BHE model in the article, the correlation should be equally if not better applicable for CBHE's, since the original studies that the article refers to were performed for annular channels, corresponding to the geometry of CBHE's.

Looking at the geometry alone, in CBHE's r_o (outer tube outer radius) is likely to be larger with respect to r_i (borehole radius) when compared to u-tubes, leading to lower K, and subsequently lower Nu for CBHE's. If assuming other factors, such as temperature level, similar, this would suggest less heat transfer by natural convection in CBHE's compared to u-tube BHE's. The phenomena should be studied in detail, however, to also account for characteristics of deep CBHE's, such as possibly variable borehole diameter and large difference in heat flux between upper and lower parts.

4.4.5 Heat transfer within the ground

Heat transfer in the ground mostly occurs by conduction. Groundwater flows around BHE's improve the heat transfer and also increase the heat energy available (as they import energy from more distant ground) wherever present. They are difficult to predict and model, and as their effect is merely positive, they are typically ignored in models.

Heat conduction is described by Fourier's law. Considering the application at hand, the heat transfer takes place in a cylindrical volume around the BHE, so cylindrical coordinates (radius *r*, angle Φ, elevation z) are typically used:

$$\bar{q}'' = -k\nabla T = -k(i\frac{\partial T}{\partial r} + j\frac{1}{r}\frac{\partial T}{\partial \Phi} + k\frac{\partial T}{\partial z}) \quad (23)$$

Heat flux within the ground is then determined by the temperature gradient and conduction coefficient *k*. All mathematical models describing heat conduction within the ground are based on Fourier's law (Aresti et al 2018).

Ground thermal response

The ground will undergo a change of temperature as heat is extracted from or injected to the borehole. The relation between heat flux and ground temperature change is described by heat diffusion equation. For a cylindrical control volume the heat diffusion equation can be written as (Bergman, Lavine 2017):

$$\frac{1}{r}\frac{\partial}{\partial r}\left(kr\frac{\partial T}{\partial r}\right) + \frac{1}{r^2}\frac{\partial}{\partial \Phi}\left(kr\frac{\partial T}{\partial \Phi}\right) + \frac{\partial}{\partial z}\left(k\frac{\partial T}{\partial z}\right) + \dot{q} = \rho c_\mathrm{p}\frac{\partial T}{\partial t}, \quad (24)$$

The right side of the equation effectively describes the energy storage capability of the ground. Density and heat capacity are assumed constant in the equation. There is heat generation present in the ground due to radioactive decay, but the term is usually negligibly small and therefore omitted. If a further assumption of constant conduction coefficient *k* is made (as can often be done, at least locally), the equation is further simplified:

$$\frac{1}{r}\frac{\partial}{\partial r}\left(r\frac{\partial T}{\partial r}\right) + \frac{1}{r^2}\left(\frac{\partial^2 T}{\partial \Phi^2}\right) + \frac{\partial^2 T}{\partial z^2} = \frac{\rho c_\mathrm{p}}{k}\frac{\partial T}{\partial t} \quad (25)$$

It is common to assume heat transfer only in radial direction (Holmberg 2016). By implementing this further simplification and rearranging, we can arrive in the following 1D form:

$$\frac{\partial T}{\partial t} = \frac{k}{\rho c_\mathrm{p}}\frac{1}{r}\frac{\partial}{\partial r}\left(r\frac{\partial T}{\partial r}\right) = \alpha\frac{1}{r}\frac{\partial}{\partial r}\left(r\frac{\partial T}{\partial r}\right), \quad (26)$$

where α is thermal diffusivity [m^2/s]

Present in equation 26, thermal conductivity *k* describes the ground's ability to conduct heat from further locations to the BHE site, while ρc_p quantifies the heat energy stored in volume

of ground. For long-term heat extraction purposes, ideally both parameters should be high: ground with low k requires larger temperature gradients for the same heat flux as ground with high k - this will manifest in lower heat carrier temperatures - and ground with low ρc_p will experience decreased temperature sooner than with high ρc_p - this will also manifest in lower heat carrier temperatures. Thermal diffusivity α includes these most relevant ground thermal properties within one parameter, representing the rate of heat diffusion within the ground.

Along with the thermal properties mentioned above, it should be noted that the ground also exhibits macroscopic properties which can cause the actual heat transfer differ from ideal (e.g. properties inferred by laboratory experiments on rock specimen from test drillings). Namely, anisotropic structure of the rock can cause bias in the value of k depending on heat transfer direction, and rock porousness can affect both k and ρc_p (GTK, 2019, p. 48).

Thermal response test

Thermal response test (TRT) is the most commonly utilized method for determining ground thermal properties at the BHE site (Aresti et al, 2018, p. 762). In TRT's a constant heat flow is injected to ground over the course of a specific period, usually a couple of days. The evolution of the heat carrier temperatures during the test can be used in conjunction with a mathematical model of choice to estimate ground thermal conductivity k, as well as the actual R^*_b (which can differ from the theoretically calculated resistance due to borehole wall anomalies, tube positions etc.). TRT's are typically conducted only at larger sites, where the benefit of more exact dimensioning of the BHE field outweighs the cost of the test itself.

A more developed version of TRT, called DTRT (distributed thermal response test) utilizes temperature measurements along the length of the borehole to display the actual temperature profile of the heat carrier fluid (Acuna 2013, p. 22). Temperature measurements from a DTRT will be used validation of the used CBHE model in section 6.

4.4.6 Unbalanced loads

If the heat load in a BHE is annually unbalanced toward heating, the ground temperatures in the vicinity of the BHE will exhibit a corresponding long-term trend. Theoretically one could continue extracting heat from the borehole indefinitely at a constant heat rate, by allowing mean fluid temperature to decrease on a similar rate as the local ground temperature (borehole wall temperature) continues to decrease (recall eq. 23). Eventually the temperature gradient in the ground will reach a static state where heat transferred from the surroundings is equal to the

extracted heat. However, in practice there is a limit under which the borehole temperature is not allowed to decrease; this is to prevent groundwater freezing and possible resulting damage to the BHE. This limit can be enforced by setting a lower limit (e.g. -5 C) for the heat carrier fluid within the BHE. In addition heat pump COP is affected by heat carrier temperature: at very low temperatures the operation might become economically unviable.

For borehole fields the effect of an unbalanced load is especially critical; with many adjacent boreholes sharing the same ground mass, ground temperature change caused by each individual BHE is superposed, and the replenishing heat conducting to an individual borehole is less than for a single BHE (Holmberg 2016 p.20). As an extreme example, GTK used a numerical model to compare the performance of an infinite borehole field with boreholes 20 m apart to that of a single borehole: the single lone borehole was found to sustainably provide roughly three times more energy than a single borehole within the infinite field, during the same period of time (GTK, 2019, pp. 77-78).

The BHE or BHE field must be designed such that heat carrier temperature stays within acceptable limits for the planned lifetime of the system, for example 50 years. This can be achieved by limiting the extracted heat per borehole to a sustainable level, distributing the boreholes to a larger area, drilling deeper boreholes, or introducing regenerating heat loads from available sources. It should be noted that while the design of BHE collector tubes determines required temperature difference between heat carrier and borehole wall for a specific heat load (see eq. 9), it has no effect on the long-term sustainability of the BHE, which is determined by ground properties and net heat balance.

4.4.7 Regeneration

In case both cooling and heating loads are available at the same site, the ground can act as a seasonal energy storage: during winter heat is withdrawn from the ground, lowering ground temperature. During summer surplus heat from the building is ejected into the ground, raising ground temperature. In a scenario where heating and cooling loads are equal in during the year, the GSHP system could operate indefinitely without a long-term change in ground temperature (a balanced system). However, in warm and cold climates the loads profiles of apartment buildings tend to be unbalanced toward excess heating or cooling.

In the absence or inadequacy of actual cooling loads, any surplus heat source can be used for heating the ground, storing the heat for use during winter. For example Ranta-Korpi (2018) studied the profitability of ground regeneration of shallow borehole fields using air source and

solar heat, finding both options non-profitable for an apartment building, but the former less non-profitable due to lower investment costs involved. In the study it was also deemed slightly more profitable to transfer heat into the heat carrier fluid before, rather than after the GSHP, due to resulting increase in heat pump COP.

There are losses involved due to heat conduction away from the BHEs, and the efficiency of the ground storage depends on the size of the BHE field. Simulation study by GTK suggests that around 80 % of heat stored in the ground near a single BHE during summer can be utilized during the following winter (GTK, 2019, p. 80). Borehole fields are more efficient for storage-focused applications than single boreholes for the same reason they are relatively worse for long-term unbalanced loads: as multiple boreholes thermally interact with a shared groundmass, the storage volume exterior area is lower relative to the heat injected, and therefore conduction losses to the surroundings are relatively smaller (Hellström 1991, p. 3).

If successfully employed, regeneration can be used to bring about either an increase in BHE lifespan, increase in available energy or reduced BHE length requirement for an application. GTK (2019) studied the effect of borehole recharging to system lifespan for boreholes of different lengths and different amounts of recharge energy, by a numerical simulation. As an example, when recharging a 300 m BHE with an energy amount corresponding to 10 % of the annual extracted energy, the lifespan was estimated to increase by 5 years, or 10 %. (GTK, 2019, p. 81).

4.4.8 BHE modelling

The importance of mathematical modelling of BHE operation stems from the difficulty of conducting experiments to accurately study the performance of a BHE with varying geometry and ground properties, including long timescale of several years or decades. The use of modelling in design is especially important for large borehole fields with unbalanced load, due to the importance of ground response and interaction between BHE's. In large borehole fields the costs of over/underdimensioning the system are also higher. In addition to predicting the operating performance of a BHE or a BHE field in a specific location and formation, models can be used in product development, e.g. computational fluid dynamics models can be used to study the flow within the collector tubes in high detail.

The methods used in the modelling can be divided to numerical and analytical models (Aresti et al, 2018, p. 765). Analytical methods obtain exact solutions (of ground temperature field) by symbolically manipulating the governing differential equations (recall eq. (16) for heat

diffusion) to predict the heat transfer in the relevant geometry, but assumptions such as constant heat flux along borehole length are typically required. Numerical methods are a “brute force” method compared to analytical methods: rather than obtaining an exact solution for the geometry under specific boundary conditions, in numerical methods the relation presented by the governing equation is used as-is: the infinitesimal differences are converted to finite differences of arbitrary size, and calculated for a discontinuous grid of calculation points, representing the geometry. This allows for complex geometries and more realistic and diverse boundary conditions, at the cost of longer computational times and the requirement of setting up the calculation grid. The calculation grid can represent the BHE geometry completely in full 3D, or alternatively in 2D, utilizing axisymmetry.

(Javed et al, 2009) conducted a review of analytical and hybrid (with analytical and numerical elements) BHE models, and made a division into long- and short-term response models. In the article models under “long-term response” ignore the heat capacity (of grouting and heat carrier) within the BHE, and therefore cannot predict the transient behavior in short time scales, such as in an hourly timescale. These models are typically used when only the long-term ground response is of interest, and the results should be generated quickly. The article notes that the short-term response is important in studies such as those involving GSHP system behavior in hourly or sub-hourly timescale. The same is of course true for detailed flow dynamics studies, in which the solution is in turn limited to a very short period, or even steady state, due to long computation times, as seen in e.g. (Gimenez, 2020, p. 50).

4.5 Coaxial BHE design

The parameters of BHE design dictate the internal thermal resistance, as well as the pressure loss. This section briefly introduces the relevant design parameters of a coaxial BHE. Practical concerns about mechanical endurance etc. are largely omitted here.

Flow direction

In CBHE’s the downward and upward flow paths in a coaxial tube have different geometry; therefore the thermal performance is different depending on flow direction. According to many studies of deep CBHEs, for maximum heat transfer in heat extraction mode (heating application) heat carrier should enter from the annulus tube; this way the heat carrier fluid loses minimum amount of heat on the way up and retains as high a temperature as possible. For injection mode (cooling application) the opposite direction is recommended. (Holmberg et al, 2016, p. 75).

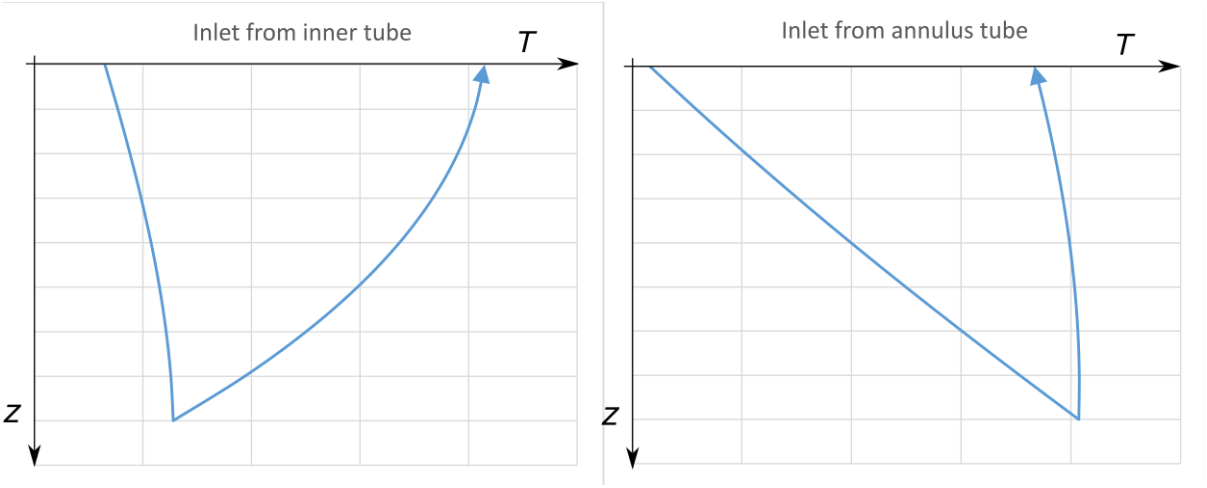

Figure 12. Heat carrier temperature profile shapes with inlet from inner tube and annulus.

Flow rate

Flow rate dictates heat carrier residence time in the CBHE, and therefore also the temperature change that the heat carrier experiences between the inlet and outlet; ideally (with an adiabatic inner tube) by increasing the residence time the heat carrier would exit the CBHE in higher temperature, assuming that the temperature difference between the heat carrier and the ground is high enough. Heat pumps benefit from higher evaporator inlet temperatures, and therefore in this perspective low flow rate would be desirable. However, lowering the flow rate also has adverse effects: firstly the flow velocity in annulus should remain at turbulent region, or convective heat transfer will be severely weakened. Secondly, the total heat extractable from the heat carrier is dependent on flow rate, as seen in eq. 8. Therefore, even if heat pump COP could be improved by the increase in outlet temperature, the total heat flow may decrease. Since the drilling of deep boreholes is expensive, the heat output per borehole will need to be high enough to be economical. Thirdly, at lower flow rates the ratio of shunt heat transfer to useful heat transfer (output heat) tends to get higher, as shown e.g. by (Mazzotti et al, 2018). On the other hand, at higher values the increase of flow rate is countered by flow pressure loss, which, as shown previously in eq. 15, will increase very rapidly with increasing flow rate. It can be concluded that flow rate is an important subject of optimization in CBHE's.

Tube materials

The most common material for u-tube collectors is high density polyethylene (HDPE). It has heat conductivity of 0.46 W/mK, and it is relatively cheap and durable (Mendrinos et al, 2016, p. 1). Although it is not optimal as either heat conductant (for outer tube) or insulator (for inner tube), its performance is reasonably good for shallow applications. Alternative solutions have

been suggested for both the outer and inner tubes. The optimal tube solution usually depends on borehole depth: deeper boreholes entail higher ground temperature, which makes investments in improved tube materials more profitable.

In an implementation described in e.g. (Holmberg et al, 2016, p. 68), the outer tube wall is a flexible liner situated very close or partially in contact with the borehole wall. This has the effect of maximizing cross-sectional flow area, as well as minimizing the thickness of the groundwater layer (and therefore thermal resistance) between tube wall and borehole wall. The outer tube can also be completely omitted, resulting in an open loop. This kind of implementation is the most optimal from the perspective of heat transfer, as the heat carrier will be in direct contact with borehole wall. On the flipside anti-freeze fluids cannot be used, possibly restricting heat extraction rates, and possible heat transfer surface fouling needs to be addressed.

Contrary to the outer tube wall, the inner tube should be designed to have maximum resistance to heat transfer; ideally it would be adiabatic. The inner tube wall is especially critical for deep boreholes, where the temperature difference between downward and upward flows is high. As an extremely performant option for high-temperature BHEs a vacuum-insulated steel wall has also been proposed for the inner tube (e.g. Lund, 2019, p. 19).

Tube diameters

Tube diameters need to be considered both in fluid mechanical and heat transfer point of view. For a given flow rate, tube diameters dictate flow velocity, which in turn affects convective heat transfer coefficient as well as pressure loss. The outer tube diameter also dictates the heat transfer area between fluid flows and the ground.

Holmberg et al (2016, p. 69) note that in theory achieving turbulent flow in the annulus and laminar flow in the inner tube would be an optimal solution from the perspective of heat transfer, but that it is difficult to achieve, as usually annulus tube flow area is much larger than that of the inner tube. By increasing inner tube diameter, Reynolds number of inner tube flow would decrease. However, simultaneously heat transfer area between the inner tube and annulus is increased. Results by Pan et al (2020, p. 12) indicate that when inner tube flow is in turbulent region, shunt heat transfer area is more significant than inner tube flow convection coefficient. This in turn promotes large outer tube and small inner tube diameters. However, in hopes of minimizing shunt heat transfer area the inner tube diameter cannot be made arbitrarily small either, since at smaller diameters the pressure loss will be increased.

Aside from the technical aspects, the design needs to be economically optimized: wider boreholes are more expensive to drill. Borehole diameters in Finland typically range from 100 to 150 mm, with 115 mm being the most common diameter (JH-Lämpö). Optimally there should be minimal space between annulus outer wall and borehole wall to minimize the resistance of the groundwater/grouting layer, but having some clearance is required for the installation of the BHE.

5 BUILDING LOAD PROFILE

This subsection will cover the used building model, inputs and resulting load profile. The generated load profile will be used as input for the GSHP system model in section 7.

5.1 Case building

The case building is a residential building with a small amount of commercial space on the ground floor. The site is situated in Kalasatama, Helsinki, in a previously industrial area now being planned for residential use. The building consists of two parts of different height (5 and 13 floors), as seen in figure 13.

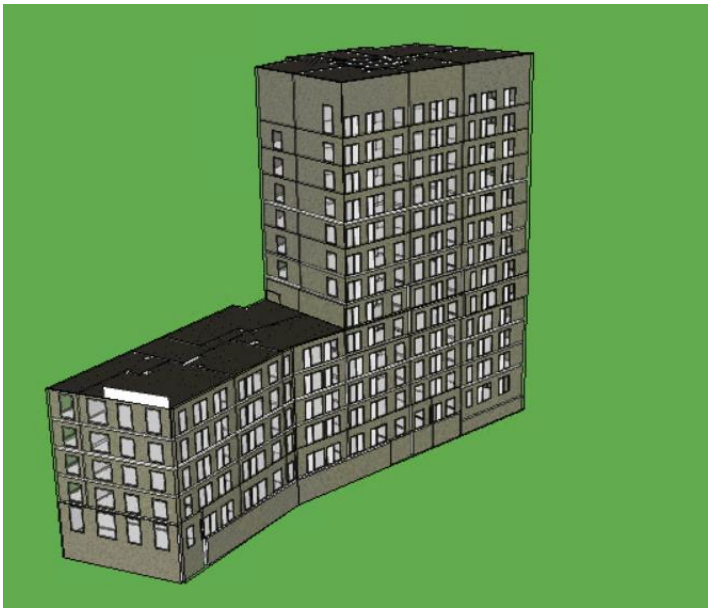

Figure 13. 3D model of the case building in IDA-ICE, viewed from the north.

Along with the architecture, the broad lines of the energy system of the building have been preliminarily decided: the building is to satisfy its heat demand by ground source heat pumps coupled with deep borehole heat exchangers. For peak heat demand an electric auxiliary boiler will likely be installed, but no district heating connection. Cooling during summer months should be done by free cooling if possible.

The building parcel is displayed in figure 14. The case building is situated on the right side.

Figure 14. Building parcel, with some dimensions displayed.

The total parcel area is owned by the builder/promoter of both buildings. From the figure one can immediately note that the available land area is small compared to the footprint of the buildings. The building on the left will also employ a GSHP system, further limiting the land area available for boreholes.

5.2 IDA-ICE

IDA Indoor Climate and Energy (IDA-ICE) is a building performance simulation (BPS) software by Equa Simulations AB, commonly used for modelling energy systems of planned and existing buildings. IDA-ICE is capable of dynamic simulation, meaning the simulation of building energy system response to weather, and internal loads in arbitrary time step, typically one hour. (Equa Simulation AB, 2020)

Output of a simulation is the energy (electricity, heating and cooling) demand profile for the simulated time period. The outputs can be customized to divide the energy consumption output profiles according to preference, by defining the different consumption sources under separate energy meters. For example, in this work separate energy meters were used for ventilation heating, space heating and DHW, since they were assumed to operate at different temperature levels, which affects heat pump COP and maximum output.

In the practical user perspective the indoor volume, separated from the ambient air by the building envelope, is divided into zones (which can be e.g. rooms or apartments, depending on the purpose of simulating and desired accuracy). The properties of each zone can be individually configured, and the program calculates energy balances individually for each zone, while taking into account the heat and mass flows between zones. Building geometry in IDA can be sketched within the software or imported in CAD or IFC formats.

5.3 Model configuration

Constructing the building model from ground up was not included in the scope of this thesis, and a ready model of the case building was provided. Used model inputs are described below.

Climate, load and occupancy profiles

Climate profile is the most important boundary condition for the simulation: it determines the ambient temperature, insolation and wind profile. The climate file used now is for Helsinki-Vantaa in the year 2012 (test reference year by Finnish Meteorological Institute), found by default in IDA-ICE Finnish localization set. Climate profile, temperature & ventilation set points and heat losses together dictate the space heating and cooling load profile. For DHW consumption the profile displayed in figure 3 in section 1 was used.

The model also needs profiles for internal loads for the simulation period, to match the loads to the intended purpose of the building. Standardized profiles for different types of buildings, such as residential buildings, offices or schools, have been defined in regulations (Ympäristöministeriö, 2017, p. 7), and they are also included in the Finnish localization of IDA-ICE.

Temperature levels

This thesis is not concerned with the dimensioning of the room heating and cooling units. Therefore all local and ventilation heating & cooling elements are now modelled as ideal, meaning that in the simulation they automatically supply the correct amount of heat/cold to meet the space temperature requirement. Because of this the heater inlet temperature control curve has no effect on the heating energy required within the building, but it will affect the heat pump COP calculation. Temperature levels assumed for the heating systems are presented in table 1.

Table 1. Heating system temperature levels.

Space heating	20 - 35 °C
Ventilation heating	20 - 45 °C
DHW	58 °C

Ventilation heating temperature level was assumed slightly higher than space heating temperature, due to a conservative assumption that the ventilation heat exchanger heat transfer area is more limited requiring higher temperature differences. Ventilation and space heating temperatures follow a control curve similar to that displayed in section 2.

DHW profile smoothing

The synthetic DHW consumption data used in IDA-ICE (figure 3) was defined on an hourly level. In a real scenario a buffer tank will be implemented, smoothing the demand across a longer time period and reducing consumption peaks. IDA-ICE has an option for including buffer tanks, but in this case the effect of buffer tank was simulated afterwards by smoothing the consumption profile using a 3 hour sliding average.

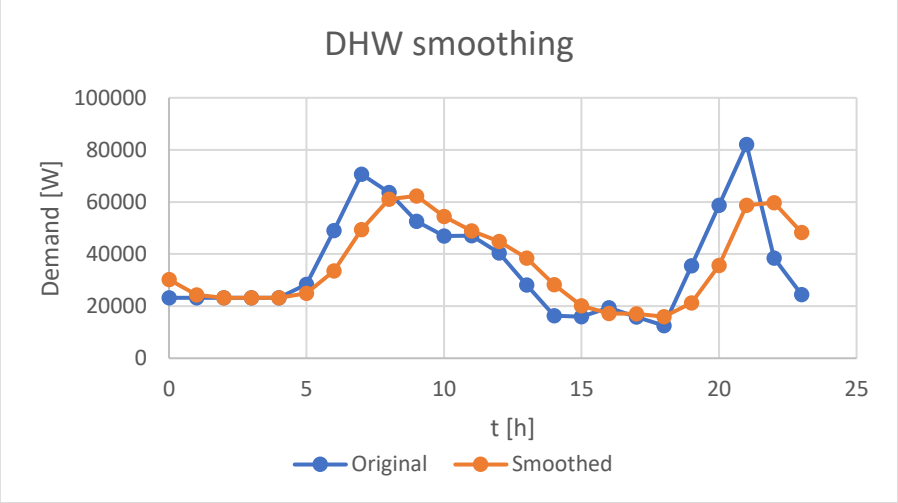

Figure 15. Smoothing of the daily DHW demand profile.

The peaks in the load profiles for space heating and ventilation heating are less transient by their nature (Yrjölä, Laaksonen, 2015, p. 8), and therefore introducing buffer tanks has less effect on their peak demand. Therefore similar smoothing was not used for them.

5.4 Energy efficiency parameters

The technical specifications of the default case are corresponding to the standard building energy efficiency level used in (Reda, Fatima, 2019, p. 602), and they roughly correspond to the Finnish minimum regulations for new apartment buildings. Element U-values, temperature

setpoints and other aspects affecting the energy consumption of the simulated cases were gathered in table 2.

Table 2. Case building default energy efficiency parameters.

External walls *U* [W/m^{2}K]	0.17
Roof *U* [W/m^{2}K]	0.09
Ground floor *U* [W/m^{2}K]	0.1775
Window *U* [W/m^{2}K]	0.8
Window g-factor	0.6
Window shading (g multiplier)	0.33
Air tightness *n* [1/h]	0.07
Ventilation inlet *T* setpoint [°C]	16-19
Cooling - heating setpoint [°C]	21-27
DHW supply setpoint [°C]	55
Cold water temperature [°C]	5
Space heating supply max. temp [°C]	35
Ventilation heating supply max. temp [°C]	45
Space cooling supply temperature [°C]	15
Ventilation control	Constant air volume
VHR efficiency [%]	60
Ventilation SFP [kWh/m^3]	2
Heating system accessory energy [kWh/m^{2}a]	2.5
Lighting specific power [W/m^2]	4.4

5.4.1 Parameter analysis

A few specific energy efficiency improvements were selected for analysis, to gain perspective on their individual effect on building energy consumption, particularly to the primary energy sources of net ground heat and electricity.

The improvements were chosen according to the “passive building” scenario also presented in (Reda, Fatima, 2019, p. 602), except for envelope insulation, for which the “efficient building” scenario specifications were used instead, and WWHR efficiency, for which a more conservative value of 15 % (rather than 47 % of the original study) was chosen.

Table 3. Studied energy efficiency improvements.

Improved envelope insulation	Outer wall *U* 0.17 -> 0.1 W/m^{2}K, roof *U* 0.09 -> 0.07 W/m^{2}K, -> Ground floor *U* 0.16 -> 0.11 W/m^{2}K

Improved airtightness	*n 0.13* -> 0.04 1/h
Improved window insulation	*U* 0.86 -> 0.61 W/m^{2}K
Lower window solar gain	*g* 0.6 -> 0.5
Higher VHR efficiency	η 0.6 -> 0.8
Lower ventilation SFP	SFP 2 -> 1.5 kW/(m^3/s)
Lower lighting specific power	*p* 4.4 -> 3.74 W/m^2
Implement WWHR	η = 0.15

The changes were implemented in IDA-ICE, except for WWHR, the effect of which was simulated as a simple multiplier in a separate Excel tool. An energy simulation was ran for the test reference year. Changes in some key indicators are listed in the table below. Ground net heat and heat pump electricity consumption were calculated using SPF's of 2.4, 4.9 and 5.5 for DHW, ventilation heating and space heating, respectively. Cooling load was assumed to be done by free cooling. For the heat loads heat pump coverage ratio of 100 % was assumed. Table 4 the effects of changes to relevant parameters. Below the table a brief explanation for each case is given.

Table 4. Effect of changing building energy efficiency parameters.

	Total heating demand [MWh]	**Peak heating demand [kW]**	**Total cooling demand [MWh]**	**Peak cooling demand [kW]**	**Ground net heat [MWh]**	**Heat pump electricity consumption [MWh]**	**Total electricity consumption [MWh]**
Default	722	261	27	125	470	225	492
Increased envelope insulation	693 [-4 %]	253 [-3 %]	28 [+4 %]	126 [+1 %]	445 [-5 %]	220 [-2 %]	487 [-1 %]
Increased airtightness	638 [-12 %]	226 [-13 %]	32 [+19 %]	129 [+3 %]	396 [-16 %]	210 [-7 %]	477 [-3 %]
Increased window insulation	688 [-5 %]	248 [-5 %]	29 [+7 %]	128 [+2 %]	440 [-6 %]	219 [-3 %]	486 [-1 %]
Lower window solar gain	735 [+2 %]	263 [+1 %]	21 [-22 %]	111 [-11 %]	487 [+4 %]	227 [+1 %]	495 [+1 %]
Higher VHR efficiency	630 [-13 %]	261 [0 %]	27 [0 %]	124 [-1 %]	396 [-16 %]	207 [-8 %]	474 [-4 %]

Lower ventilation SFP	728 [+1 %]	261 [0 %]	26 [-4 %]	123 [-2 %]	477 [+1 %]	226 [0 %]	476 [-3 %]
Lower lighting specific power	725 [0 %]	262 [0 %]	26 [-4 %]	124 [-1 %]	473 [+1 %]	225 [0 %]	489 [-1 %]
WWHR	666 [-8 %]	251 [-4 %]	27 [0 %]	125 [0 %]	438 [-7 %]	201 [-11 %]	469 [-5 %]

Envelope

Increasing envelope insulation shows decreased heating load due to decreased heat losses, and a slightly increased cooling load due to the same reason.

Window insulation

Increasing window insulation has similar effect as the previous point.

Window solar gain

Reducing window solar gains notably reduces cooling loads during cooling season, but increases heating load during heating season.

Ventilation heat recovery efficiency

Increasing VHR efficiency decreases heating load, since more energy is captured from ventilation exhaust air. Cooling load is unaffected since the heat recovery concerns mostly heating. Notably the maximum peak load is unaffected, since during the highest peaks the temperature of the outlet air falls to zero even at the default 60 % heat recovery efficiency, and therefore the recovered heat cannot be further increased. IDA-ICE uses 0 °C as the minimum allowed temperature to avoid frosting of air moisture.

Ventilation specific fan power

Improving ventilation specific fan power (SFP) manifests in lower internal loads. Heating load is increased and cooling load decreased. Electricity consumption is lowered due to lower fan power consumption.

Lighting specific power

Reduced internal heat load from lighting increases heating load and decreases cooling load. The change in electricity consumption is due to reduction in the devices own consumption.

Wastewater heat recovery

WWHR affects practically only the heating load and electricity consumption. The electricity savings are considerable due to low SPF of DHW heating.

Efficient version

Based on the results of the analysis, an efficient version of the default case was decided and simulated. Improved envelope insulation was not included in the efficient case, since its implementation calls for more comprehensive changes in building construction, and the energy savings are relatively small. Lower window solar gains were also not included due to their adverse effect on heating demand.

Table 5. Annual load numbers of the default building and an efficient version.

	Default building	**Efficient building**
Total heating demand [MWh]	722	469
DHW heating demand [MWh]	373	317
Ventilation heating demand [MWh]	175	75
Space heating demand [MWh]	175	76
Total cooling demand [MWh]	27	34
Peak heating demand [kW]	261	204
Peak cooling demand [kW]	125	128
Net ground heat demand [MWh]	470	271
HP electricity demand [MWh]	225	164
Total electricity demand [MWh]	492	410

Figure 17 gives visual perspective to the scale and timing of annual heating and cooling loads.

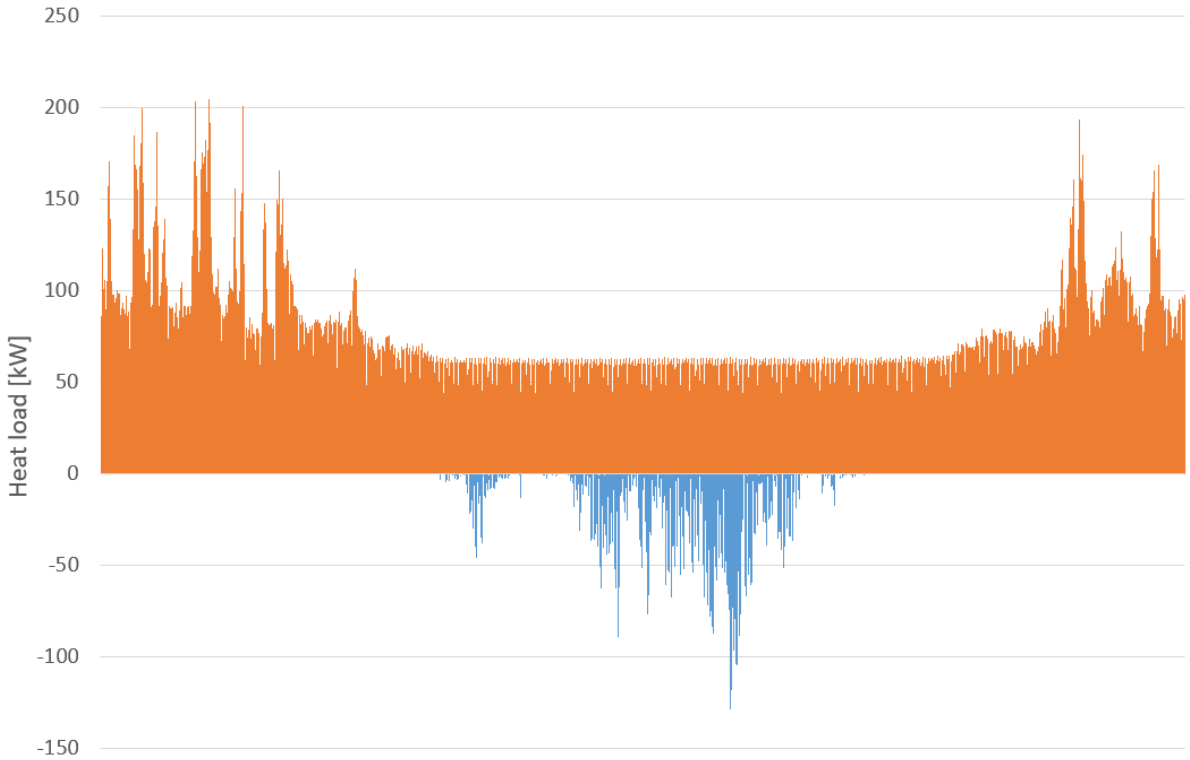

Figure 16. Annual heating & cooling demand.

5.5 Heat pump coverage factor

Heat pump coverage factor dictates the maximum ground extraction load, and therefore needs to be decided in design calculations. In practice the effect of the coverage factor on the load profiles was simulated in a separate Excel tool by setting a constraint for maximum delivered heat pump power, as a percentage of the peak power during the simulated year.

Table 6 and figure 18 illuminate the relation between power and energy coverage in the system.

Table 6. Coverage ratio results.

HP power coverage [%]	HP max. capacity [kW]	HP energy coverage [%]
40	106	90.1
50	133	95.9
60	160	98.6
70	186	99.6
80	213	99.9

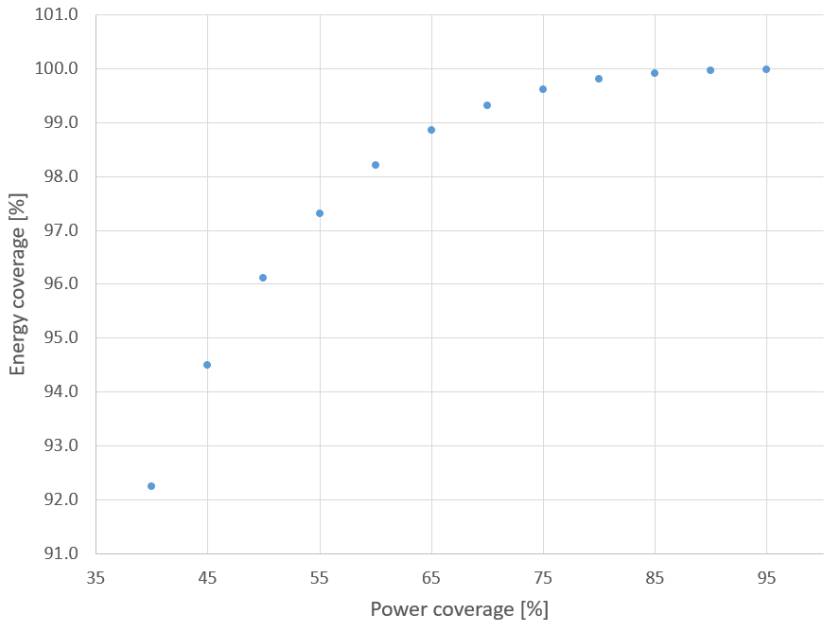

Figure 17. Annual energy coverage as a function of peak power coverage.

Choice of coverage factor

For e.g. an air source heat pump the optimal coverage factor could be defined with the available data, by comparing the investment costs related to the heat pump system with the cost of electricity. In this case economical assessments will not be conducted, since our interest lies instead in the effect of the coverage factor to the operation and dimensions of BHE's. Value of 66 % power coverage was now chosen, corresponding to 99 % energy coverage.

As a sidenote it should be noted that the coverage factors used in different sources may not be directly comparable, since the peak heating demand can be defined differently in different countries and regions. In official procedure of energy system dimensioning, the peak heating demand is based on a "dimensioning outdoor temperature", which is -26 in Southern Finland (Ympäristöministeriö, 2017, p. 17). In this case the dimensioning temperature simulation was not run, and the coverage factor is instead based on the peak heating demand present in the energy simulation of the reference year, to give a more realistic view of a typical year.

Initial estimate of BHE count

As a result of some initial static calculation in Excel, a peak heat carrier flow rate of 7.6 l/s was acquired as an estimate. Nominal flow rate of the CBHE design used in simulations is 2.3 l/s. Also, based on a quick investigation using EED (Earth Energy Designer), a tool commonly used for dimensioning boreholes and borehole fields, it seemed that given load profile would

require 2-3 BHEs for sustainable operation in the perspective of ground response. Therefore 3 BHE's was decided as a starting point for simulations described in section 8.

5.6 Heat pump model

Heat pumps act as a link between the demand profile and the BHE's, and therefore their operation needed to be modelled somehow. In this thesis a simplistic approach was taken: using a polynomial function with variables for evaporator inlet and condenser exit temperatures. The polynomial function was fit to product data of a commercial inverter heat pump (Nibe F1355-43) using least squares method. The data points used were (Nibe, p.14):

Table 7. Heat pump data for COP fit.

$T_{c,out}$	$T_{c,out}$ - $T_{e,in}$	COP
35	35	4.55
35	25	5.6
45	45	3.59
45	35	4.4

The resulting polynomial fit is:

$$COP = -0.0149 \cdot T_{\mathrm{c,out}} - 0.092 \cdot \left(T_{\mathrm{c,out}} - T_{\mathrm{e,in}}\right) + 8.39, \quad (27)$$

Using the equation, COP for the heat pump can be calculated for each time step when T_e and T_c are known. In reality the heat pump condenser is not directly connected to the heating circulation, but instead heat storage tanks are used as coupling in between. In this thesis a simple approach of neglecting the buffer tanks (except the DHW correction shown before) is taken; the COP is instead calculated separately for each load, using condenser temperature levels correspond to the temperatures of each of the heating system (SH, AHU, DHW). A weighted average of the three COP's is then used to estimate the total COP of the heat pump, and to calculate the ground heat load at each moment. The effect of partial load on the efficiency is also ignored.

The heat pump model was implemented in Apros as a user module, to be coupled with the borehole & ground model. The model takes as inputs the borehole outlet temperature, heat carrier flow rate, building heating loads and heating system temperatures for each timestep. The previously presented polynomial function (27), implemented in an SCL script is used to

calculate COP, and set the temperature of the heat carrier fluid exiting heat pump evaporator. The SCL script of the heat pump model is presented in appendix 3.

Cooling system calculation

In the SCL script, the cooling heat exchanger is implemented in the model as a load after the heat pump; heat carrier exiting the heat pump would, during periods of cooling demand, receive heating corresponding to the cooling load. A free cooling validity check was implemented: if the temperature of the heat carrier exiting heat pump evaporator exceeds a specific level (9 °C was used), the cooling load will be instead calculated assuming a refrigerator with EER of 4.

6 BHE MODEL & VALIDATION

This section will introduce the BHE & ground modelling tools used, then describe the validation and configuration of the model, and finally the model input data concerning ground & BHE properties will be shown.

6.1 Model description

Apros

The CBHE model is implemented in Apros. Apros is a dynamic process simulation tool developed by VTT and Fortum. The main applications for it are design, training and safety analysis simulations for nuclear power plants, but its thermal hydraulics model is suitable for use for various kind of dynamic processes. The flow models in Apros are one-dimensional, and finite difference method is used for discretization. The solver uses implicit method. Three-equation and six-equation flow models are available, with conservation equations for mass, momentum and energy, for one or two phases. Convection heat transfer is calculated by experimental correlations. (Apros Datasheet).

CBHE model

The model is discretized into axial sections, each containing a cylindrical heat structure representing the ground. The radial heat structures are linked to each other only through fluid flow in the collector tubes; in other words there is no axial heat transfer between ground nodes. Figure 19 displays Apros configuration view with the CBHE model (cylinders on the left) connected to the HP module and a regeneration heat exchanger module (which will be introduced in the next section).

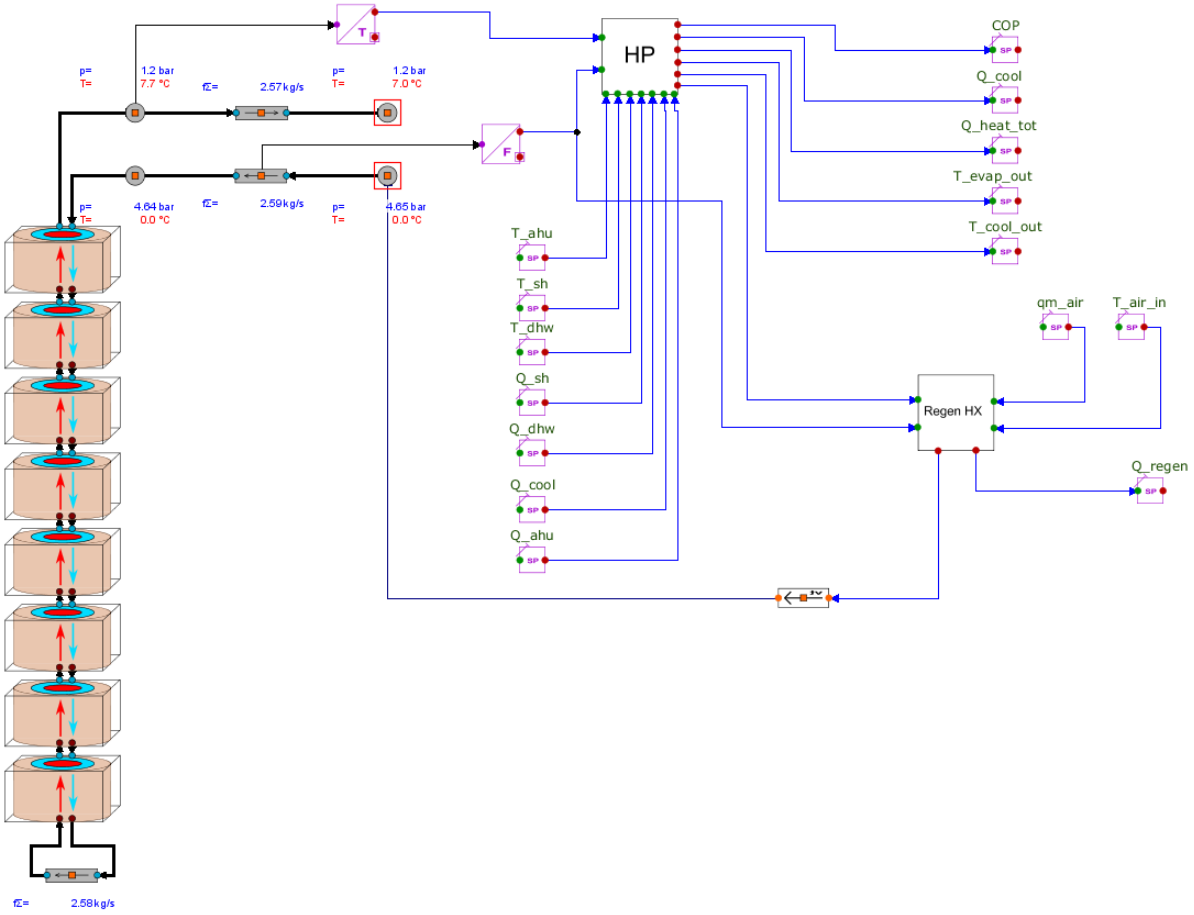

Figure 18. Screenshot of the Apros configuration window, with the HP module connected to the BHE model.

Model simplifications

Axial heat transfer in the ground is ignored, as mentioned previously. In addition, the grid is axially extended only as far as the BHE tubes reach; ground at lower levels is not modelled. Effectively this means that upward heat flux from lower levels is ignored. In undisturbed ground this heat flux (geothermal heat flux) is low, but after long periods of operation ignoring it might cause more error, due to increasing temperature gradients. Similarly the heat flux from ground surface to ambient air and vice versa is ignored. Therefore the top level of ground also doesn't experience seasonal variation (shown in figure 5), but instead starts at the assumed annual average ground temperature, and only loses and gains heat from radial heat transfer at that level.

In radial direction the tube wall of the tube-and-shell heat exchanger module is directly connected to ground, meaning that no contact resistances, groundwater or grout layer are modelled. This introduces some error in the case that the resistance caused by this layer is considerable.

Flow disturbances due to prompt turns in top and bottom parts of the BHE are not modelled. In reality some effect to heat transfer and especially pressure drop is to be expected.

6.2 Model validation

The CBHE model was recently developed, and not yet validated against measurement data, so a brief validation study is included in this work. Two reference cases were used. One was a reference measurement of a DTRT conducted to a 188 m long coaxial BHE, as reported in (Beier et al, 2013). In addition long-term heat carrier temperature evolution with constant heat load was compared to the results from EED (demo version).

6.2.1 Validation against DTRT measurement data

In the DTRT a constant heat flow of 6380 W was applied to the heat carrier between BHE outlet and inlet. In Apros this was simulated by setting the temperature difference between the outlet and inlet to constant 2.63 °C, resulting from

$$\Delta T = \frac{q}{q_{\mathrm{m}} \cdot c_{\mathrm{p}}} = \frac{6380\ \mathrm{W}}{0.58 \frac{\mathrm{kg}}{\mathrm{s}} \cdot 4190 \frac{\mathrm{J}}{\mathrm{kgC}}} = 2.63\ ^{\circ}\mathrm{C} \tag{28}$$

The model was set up with the parameters given in the study. The parameters used are listed in the appendix.

Contact resistance correction

As mentioned previously, the model does not directly account for the resistance between outer tube wall and ground. In (Gimenez, 2020, p. 47), in which the same measurement case is used for validating an analytical model, borehole resistance of the geometry was solved by an iterative method, and reported to be 0.00609 mK/W. To include the effect of the additional resistance between the outer wall and the borehole, outer wall *k* was decreased to reach the same value for the total resistance from annulus flow to ground.

The simulation was ran for 64 hours, with temperature outputs written every one hour. The resulting BHE inlet/outlet temperature evolution, in linear and log10 scale is presented in figures 20 and 21.

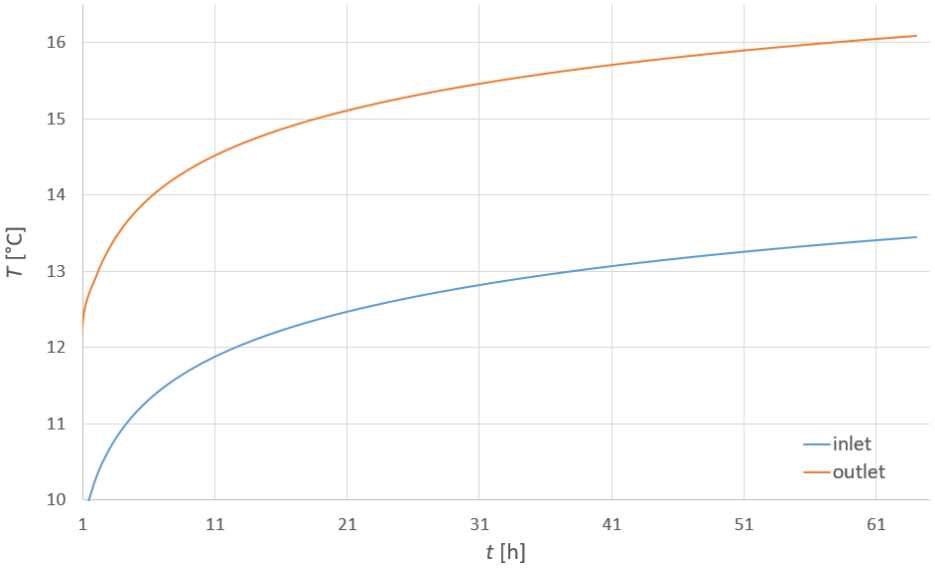

Figure 19. Inlet and outlet temperature evolution from t = 1 to t = 64 h, linear scale.

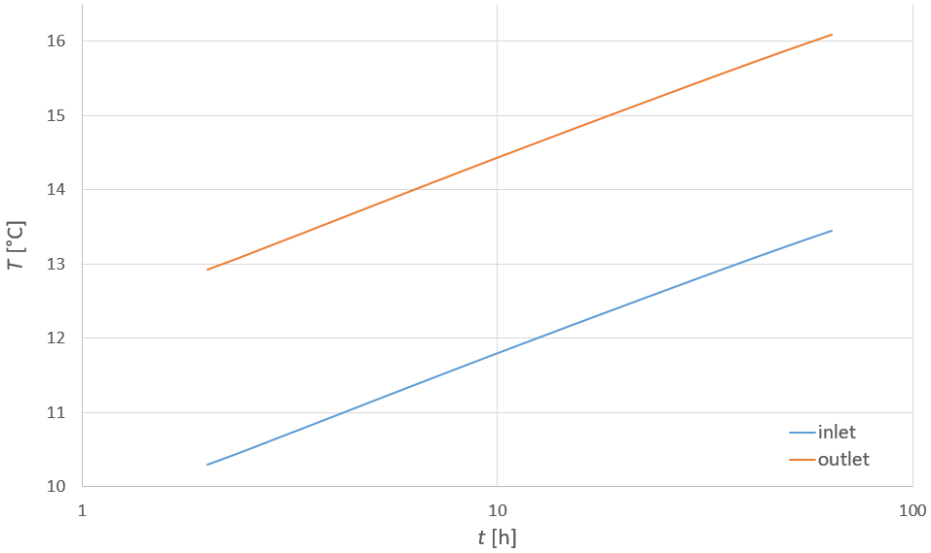

Figure 20. Inlet and outlet temperature evolution from t = 1 to t = 64 h, logarithmic scale.

Evolution of the simulated temperatures is seen to behave as is typical for heat injection TRT's, with linear behavior in log10 time scale. (Gimenez, 2020, p. 48).

In figure 22 the vertical fluid temperature profile given by the Apros model at t = 63 h is compared to DTRT measurement data presented in in (Beier et al, 2013).

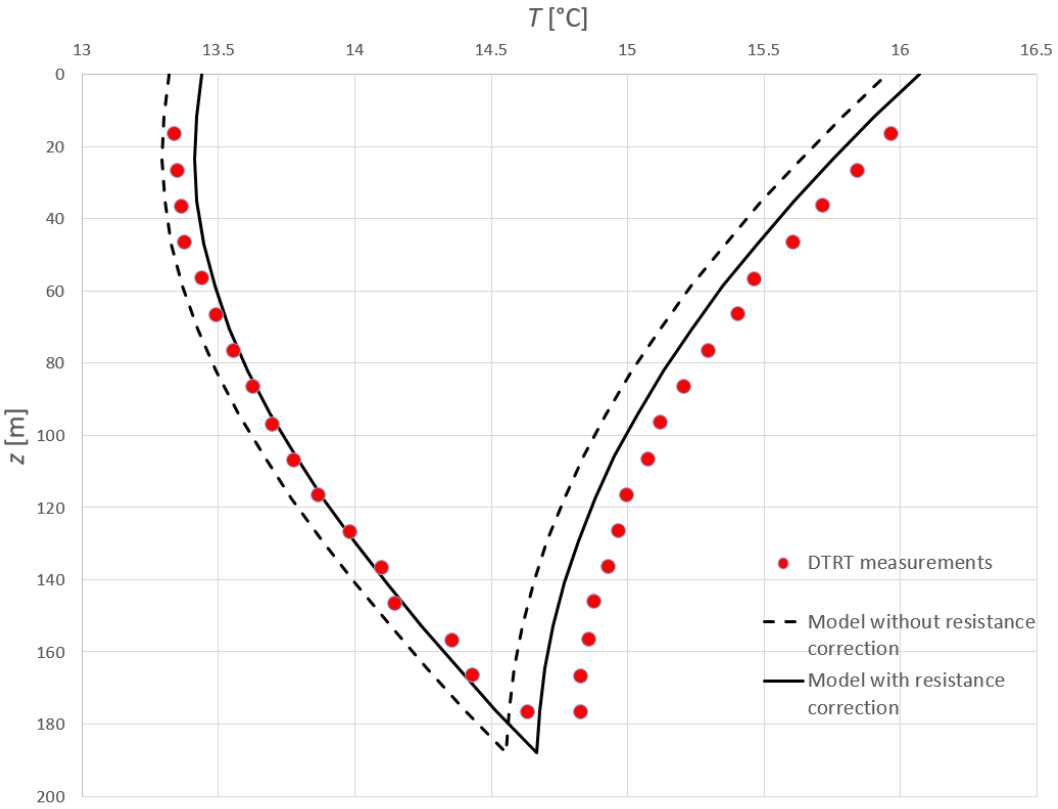

Figure 21. Heat carrier temperature profile at t = 63 h, measurements and model output.

The temperature profile predicted by the model is in good agreement with the measurement data. The resistance correction resulted in an offset of around 0.2 °C in the temperature profile, for the most part reducing the difference between the measurements and the model output.

On the other hand, flow pressure loss predicted by the model is 29-30 kPa, which is higher than in (Gimenez, 2020), in which a pressure drop of around 22 kPa was predicted by the same case by two different models.

6.2.2 Validation against EED simulation results

The Apros model was also validated against simulations results from EED. It should be noted that EED also makes simplifications: for example constant heat flux along BHE length is assumed (Sliwa et al, 2016, p. 32). Acknowledging this, it can still be used to confirm that the CBHE model produces plausible results also in long-term simulations of several decades.

Borehole depth of 800 m was used, and constant heat extraction rate was set to 22.83 kW. More detailed parameters of the run are listed in the appendix.

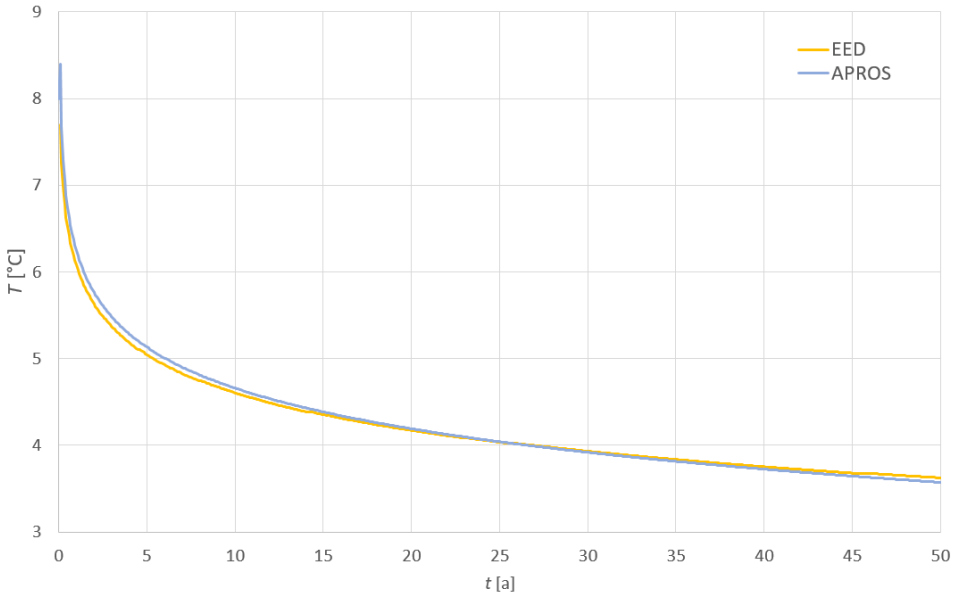

Figure 22. Mean fluid temperature (MFT) for 50 years, calculated with the Apros model and EED.

The results were found to be in good agreement for the 50 year period of constant heat flux. There remains some uncertainty about the exact definition of mean fluid temperature in EED which might introduce offset in the results (Apros MFT was defined as the average of inlet and outlet temperatures). However, the long-term behavior of the ground heat response model is considered validated for the purposes of this thesis.

In the process of validation, useful information about setting up the Apros model was also obtained, regarding radial and axial discretization, as well as simulation time step.

6.3 Model configuration

Radial discretization

As mentioned previously, the model is discretized in both axial and radial directions. By default the calculation grid reached radially to 40 m, with denser grid near the borehole wall. Grid length of only 40 m was found to warp the results during the EED validation case, due to an implicit adiabatic boundary at the end of the grid; therefore additional calculation nodes were added to extend the grid to 120 m in 5 m intervals. The number and intervals of the calculation nodes of the modified grid are presented in table 8.

Table 8. Radial discretization.

5 x 0.01 m	5 x 0.05 m	7 x 0.1 m	9 x 1 m	22 x 5 m

Short-term simulations, such as the DTRT test, do not obviously require the radial grid to extend very far from the borehole, since the ground thermal response will be limited to a much

smaller radius. In principle the length of the grid should then be optimized to each simulation, although in the author's experience the change in grid length had negligible effect on simulation speed.

Time step verification/validation

During the validation, time step was found to be the most important factor determining simulation speed. Other factors, such as calculation grid discretization, inputs/outputs and additional calculations in the heat pump module were also found to have an effect, but to much lesser degree.

Generally in numerical simulations time step in conjunction with grid discretization density dictates the accuracy of the solution. In explicit numerical schemes, in which the solution is calculated directly from previous time steps, there exists a strict maximum limit for the time step. The maximum time step can be calculated from the definition of Courant number, which for 1D case is expressed as:

$$\mathrm{C} = \frac{w\Delta t}{\Delta x}, \tag{29}$$

where w is characteristic speed [m/s],
Δt is time step [s],
Δx is grid spacing length scale [m].

The characteristic speed refers to the speed that information travels through the system. In fluid flow simulations it is typically defined by flow velocity, and in heat conduction simulations by material thermal diffusivity.

For explicit methods the maximum value of C is 1. In implicit schemes such unconditional upper limit for the time step does not exist, since the solution is calculated from an equation involving both current and future state of the system. However, the time step should be short enough to capture simulated phenomenon, or solution accuracy will be compromised. What then exactly constitutes a suitable time step depends on the nature of the simulated phenomenon and the desired accuracy.

For the CBHE model it was discovered during the EED validation case that the long-term simulation with constant heat flow is very insensitive to changes in time step, and accurate (with respect to EED) results were obtained with time step as large as 50 000 s, at which point

a simulation of 50 years took only several seconds. This can be attributed to the relatively steady state and small temperature and velocity gradients present in BHE's.

To test the effect of time step length to result accuracy during transient states, short-term simulations were made using fluctuating data. Figure 24 displays the simulated mean temperature during one week of the case building's load data, with time steps of different length. Axial discretization of 16 cylinders and inner tube flow velocity of 1.92 m/s.

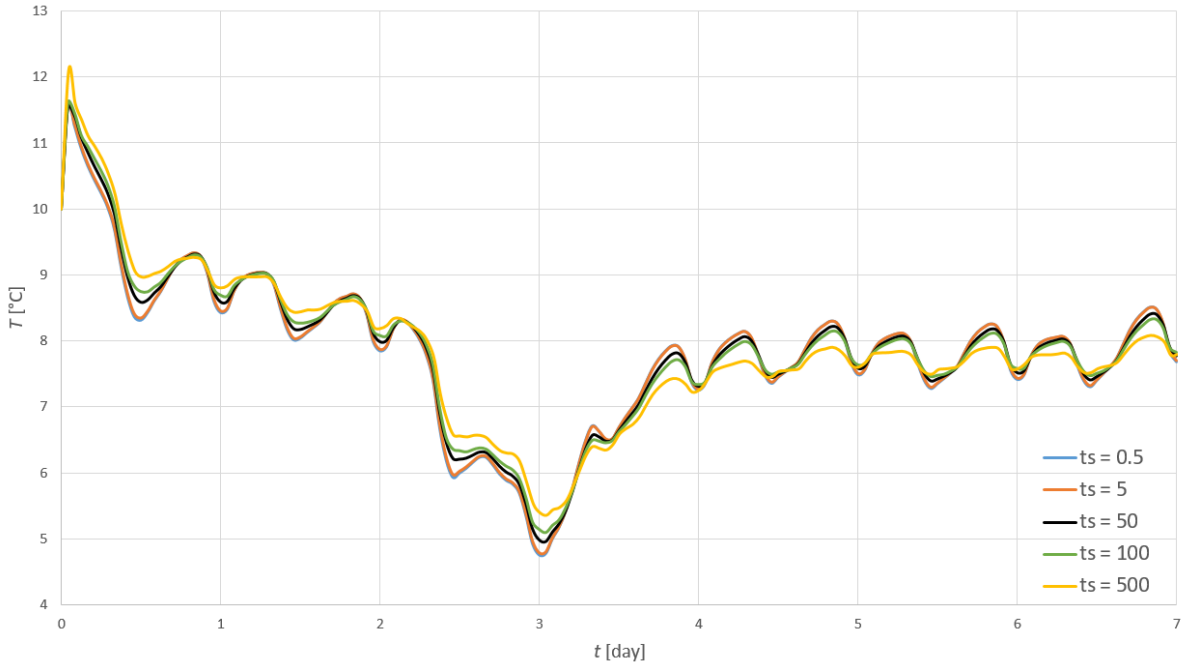

Figure 23. Time step verification with fluctuating heat flux, with 16 axial cylinders.

As seen in the figure, at higher time steps the predicted MFT doesn't accurately follow the load peaks. When choosing a suitable time step, flow velocity and axial discretization also need to be taken into account (recall eq. 29). For the purposes of this thesis, using a less dense axial discretization of 8 cylinders, time step of 100 was deemed to be a suitable compromise between computational time and accuracy. Simulation of 50 years of the BHE operation then took roughly 4 hours each time.

7 SIMULATION STUDY METHODOLOGY

This section describes the simulations conducted in accordance to the objectives stated in the beginning of the thesis. CBHE model inputs and each of the separate simulation scenarios is described.

7.1 Objectives

To reiterate, the first objective was concerned with the minimum amount of BHE's to sustain the geothermal system for 50 years.

For the sustainable temperature level there are different recommendations. In (Blocon, 2015, p. 37) it is recommended that during base load mean fluid temperature (MFT) should not stay below 0 °C for several weeks, and during peak heat load MFT should not drop below -5 °C. For the purposes of this thesis we define MFT as:

$$\mathrm{MFT} = \frac{T_{\mathrm{BHE,in}} + T_{\mathrm{BHE,out}}}{2} \tag{30}$$

Initially a temperature limit of 0 °C is chosen for the MFT. This choice will be scrutinized based on the exact temperature profiles.

A second point of interest is the viability of a free cooling system; which will be assessed by the temperature of the fluid entering cooling heat exchanger during the first year of operation.

Finally, the potential of ground regeneration utilizing excess heat of ventilation outlet air during summer is to be assessed.

A fourth relevant object of study was also discovered, regarding uncertainty caused by unknown factors of borehole resistance. This will be described in the next subsection.

7.1.1 Borehole resistance

The borehole diameter is known to range from 152 mm (at the top) to 140 mm (at the bottom) due to practicalities related to drilling, but the exact profile is unknown. In addition the effect of groundwater natural convection (described in section 4) is uncertain, since the CBHE model does not include a description of the phenomena. These factors present uncertainty to the contribution of the groundwater layer to BHE thermal resistance.

Natural convection

In Holmberg (2016) it is stated that the after calculating Nu using correlation (20), Nu can be used as a factor for borehole resistance (recall that Nusselt number is effectively the ratio between conductive and convective resistance). Holmberg used the following equation for calculating total borehole resistance:

$$R_{\mathrm{b}} = R_{\mathrm{gw}} + R_{\mathrm{collector}} \tag{31}$$

$$R_{\mathrm{gw}} = \frac{R_{\mathrm{gw,conductance}}}{\mathrm{Nu}} \tag{32}$$

The results part of the article states that $R_{\mathrm{b,collector}}$ equals constant 0.026 mK/W, and that R_{b} without natural convection equals 0.185 mK/W. Groundwater resistance with no natural convection (only conduction) is then $R_{\mathrm{gw,cond}}$ = 0.185 - 0.026 = 0.159 mK/W. It is also said that R_{b} with natural convection varies locally (from bottom to top) between 0.054 mK/W and 0.1 mK/W. Subtracting $R_{\mathrm{collector}}$, R_{gw} varies between 0.028 mK/W and 0.074 mK/W. Values for Nu of natural convection values can then be calculated using equation (32):

$$\mathrm{Nu} \in \left[\frac{0.159}{0.074}, \frac{0.159}{0.028}\right] = [2.15, 5.68] \tag{33}$$

The vertical average of R_{b} is stated to be 0.068 W/mK, leading through the same calculation steps to vertical average of Nu = 3.8.

In practice this means that natural convection decreased groundwater thermal resistance with a ratio of 2.15 (at the top) to 5.68 (at the bottom), with a (weighted) average of 3.8, compared to conductive heat transfer. The local value of Nu depends mostly on groundwater temperature, which in turn depends on the depth coordinate, as explained earlier in section 4. These simulation results presented were for a heat extraction case, with a u-tube collector.

The effect of natural convection can be roughly estimated by an equivalent value of heat conductivity k. Recalling eq.(11), $R_{\mathrm{gw,cond}}$ is inversely proportional to k, and as such an equivalent value of k can be acquired simply by multiplying it with Nu: for example with Nu = 2, $R_{\mathrm{gw}} = R_{\mathrm{gw,cond}} / 2$ and $k_{\mathrm{eq}} = \mathrm{Nu} \cdot k$. Assuming groundwater conductivity 1 W/mK, the Nu values presented earlier would then results in an equivalent average k_{eq} of 3.8 W/mK. For some perspective, this can be compared with solid grouting materials, the conductivity of which according to (Erol, Francois 2014, p.1) usually ranges from 1 W/mK to 2.4 W/mK.

In this study the actual local Nu value expected from the CBHE installation cannot be calculated since the model does not yet include a description of natural convection; instead we

opt to study the practical effect of improved k_{eq} by comparing value 2.4 W/mK to water conductivity 1 W/mK; the improved value can be interpreted either as representing a high-end grout material, or a conservative approximation for the effect of natural convection, if we accept the assumption that the effect of natural convection for the CBHE is roughly comparable to the effect on u-tube BHE's.

Borehole diameter

The borehole diameter (thickness of the groundwater layer) also affects R_{gw}, but it cannot be as simply reduced to the value of k_{eq}, since it also affects the heat transfer area with the surrounding ground. The CBHE model could be modified to allow for changing diameter along the depth, but within the scope of this thesis the effect of borehole diameter to the MFT will be assessed by conducting separate simulations with 140 mm and 152 mm boreholes.

7.2 Scenarios

This subsection describes the performed simulations in more detail.

7.2.1 Minimum number of BHE's

In the default scenario the MFT evolution over the time span of 50 years is studied, with alternatively 3 and 4 BHE's. Vertical fluid temperature profiles at times of minimum and maximum peak MFT's are presented.

7.2.2 Diameter & conductivity analysis

The heat transfer coefficient of the grouting material introduces some uncertainty, since natural convection modelling is yet unimplemented. To investigate the effect of grout conductivity, the value will also be altered. In addition, the borehole diameter in the real installation is expected to change from 152 mm (at the top) to 140 mm (at the bottom) along the length of the borehole. Currently the BHE model only allows for constant borehole diameter, so separate simulations were conducted for both diameters.

7.2.3 Free cooling analysis

The possibility of implementing free cooling is assessed by the temperature level after heat pump. The temperature level which allows for free cooling depends on the heat exchanger type between heat carrier and the cooling system (the required temperature difference), as well as cooling system supply temperature (which depends on the type of the local cooling units). In (Uponor, 2013, p. 18), which is focused on free cooling with radiant emitter cooling systems,

a dimensioning example with a u-tube BHE suggests 10 °C / 13 °C as supply and return temperatures for heat carrier fluid used for free cooling.

Since the exact limit for the free cooling maximum temperature limit is not known, the running hours of free cooling will be compared with different temperature limits imposed, ranging from 9 °C to 12 °C. Notably each temperature limit needs to be studied in a separate simulation, since the use of refrigerator (which depends on the set temperature limit) increases the heat load by its electricity consumption, which is q / EER. Therefore the use of refrigerator further undermines the possibility to use free cooling at later moments of time.

7.2.4 Regeneration analysis

In this section the technical potential of regenerating the ground with heat from ventilation outlet air during summer is studied. During summer the ventilation outlet air is at room temperature, and is typically not used for heat recovery. Figure 25 shows annual temperature levels for the outlet air and heat carrier after the heat pump. The temperature of ventilation outle air is obtained from IDA-ICE case building simulation.

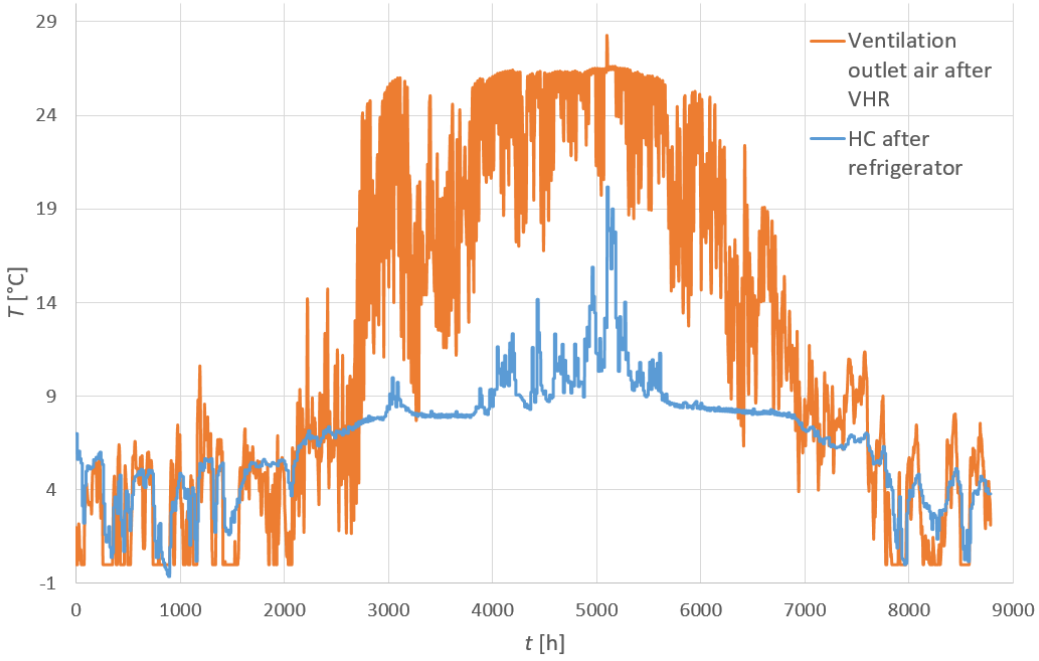

Figure 24. First year heat carrier temperature after refrigerator and VHR outlet temperature.

Ventilation outlet air temperature after VHR is near zero in the winter, since during that time most of the available heat is recovered into inlet air. During summer no heat recovery takes place, and from figure 24 it can be seen that there exists a large temperature difference between outlet air and heat carrier fluid entering the borehole; by the use of a heat exchanger some of

the waste heat can be captured to reduce ground cooling in the long-term. In the short term the regenerative heat increases the COP of DHW heating, which is required also during summer. As an adverse effect the EER of cooling is on the contrary decreased. In this thesis the focus is only on the amount of regenerative heat utilizable, and its effect on heat carrier & ground temperatures. Detailed techno-economic assessments are left for further studies.

Regeneration heat exchanger can be placed before or after the heat pump/refrigerator in the circuit. Figure 26 shows the latter configuration.

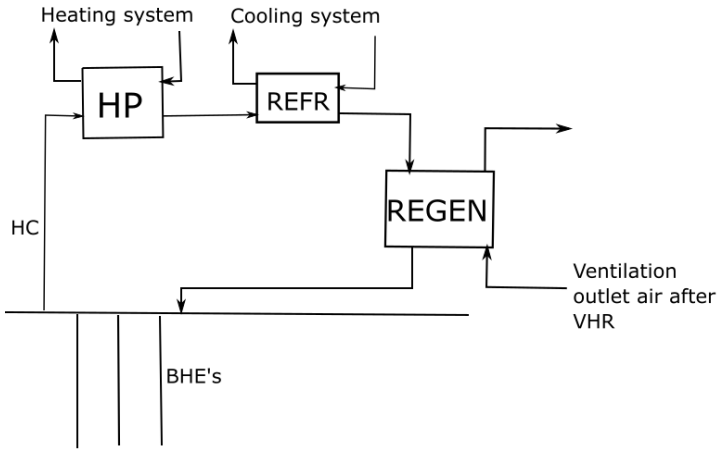

Figure 25. Illustration of the regeneration heat exchanger's position in the system.

Theoretically regenerative heat exchange can take place when $T_{air} > T_{hc}$, but in reality the heat exchanger requires a finite temperature difference, and in this case two heat exchangers might be needed. Semi-arbitrarily a minimum temperature difference of 6 °C between the inlet temperatures (similarly to the free cooling system) is in this case assumed for any heat transfer to take place. Figure 27 demonstrates the heat transfer from ventilation outlet air to heat carrier fluid.

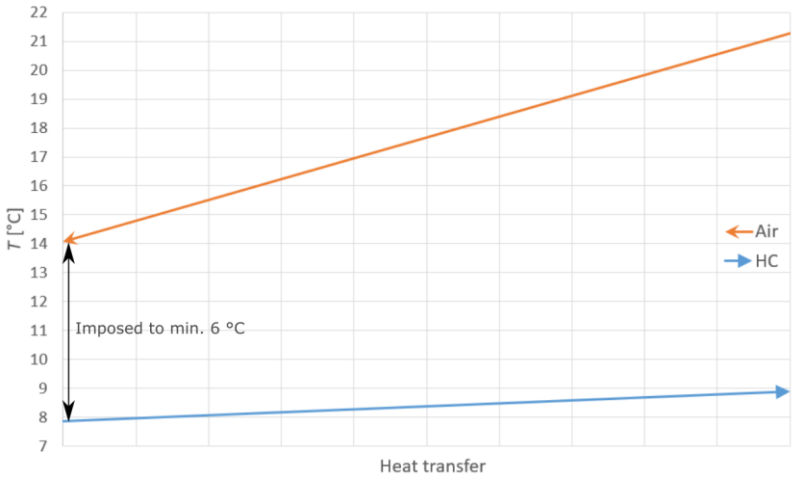

Figure 26. Regeneration heat transfer diagram, at an arbitrary time.

Heat flow available from ventilation outlet air is calculated with

$$q = q_{\mathrm{m,hot}} c_{\mathrm{p,hot}} (T_{\mathrm{hot,in}} - T_{\mathrm{hot,out}}) \quad (34)$$

All the other values are known, and $T_{\mathrm{hot,out}}$ is set to the temperature value of heat carrier fluid exiting the cooling HX plus 6 °C. After q is known, the exit temperature of the cold side is than calculated from:

$$T_{\mathrm{cold,out}} = T_{\mathrm{cold,in}} + \frac{q}{q_{\mathrm{m,cold}} \cdot c_{\mathrm{p,cold}}} \quad (35)$$

Heat capacity rate of the cold side is at all times much higher than for the hot side; therefore the physically impossible situation where $T_{\mathrm{cold,out}} > T_{\mathrm{hot,in}}$ is avoided.

The regeneration exhibits dynamic behavior: heat carrier fluid flows in a closed circulation, and therefore regenerative heat transfer increasing heat carrier temperature reduces the temperature difference between air and fluid at later times, reducing the potential for further regeneration. Thereby static calculations utilizing separately calculated temperature profiles of the heat source and carrier fluid (such as in fig. 24) tend to overestimate the utilizable heat.

7.3 Model inputs

Ground properties

A geological study of the Helsinki region, for geothermal energy purposes, was conducted in 2019 by Geological Survey of Finland, with the objective of assessing the geothermal potential of the area. Ground properties (density, heat conduction coefficient and heat capacity) were determined by laboratory experiments conducted to a total of 51 specimens, collected based on an existing map of the ground composition in the area. Maps of the mentioned properties were then made based on the measurements and the existing ground composition map. In addition maps of ground temperature, geothermal gradient and soil thickness are provided. (GTK, 2019).

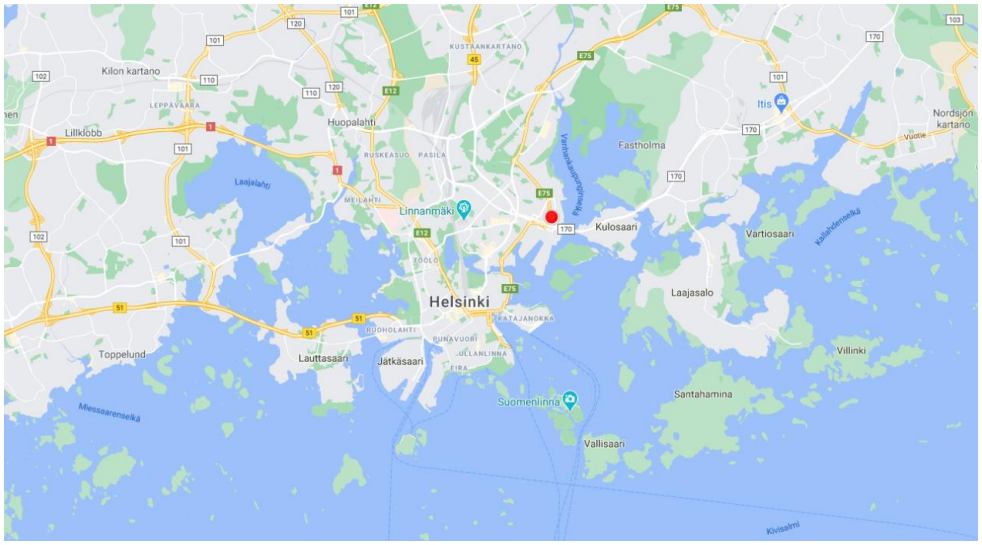

Figure 27. Building site location.

Table 9. Relevant ground properties at the building site.

Thermal conductivity [W/mK]	3.17
Specific heat capacity [J/kgK]	721
Density [kg/m^3]	2640
Geothermal gradient [K/hm]	1.3
Surface temperature [°C]	7

Simulation configuration

Simulations were run for 1 year or 50 years, depending on the output of interest. The settings used are presented in table 10.

Table 10. Simulation parameters.

Simulation period	1 - 50 years
Simulation time step	100 seconds
Result log interval	1 hour
Load profile resolution	1 hour
Axial resolution	8

BHE parameters

The BHE parameters used will be based on an actual design by a company, not disclosed in this thesis. Altering geometrical & material properties of the BHE will not be included in the study, since in the design practical aspects of durability and installation have been taken into account, in addition to aspects of thermal performance.

Table 1. BHE parameters.

Heat carrier fluid	EA20 %
Borehole diameter	140-152 mm
Flow rate	2.3 l/s
Grout conductivity	1 - 2.4 W/mK
Number of boreholes	3-4

8 RESULTS

This section contains simulation results for the scenarios presented in the previous section.

8.1 Minimum number of BHE's

The shape of the annual MFT profile is presented in figure 29.

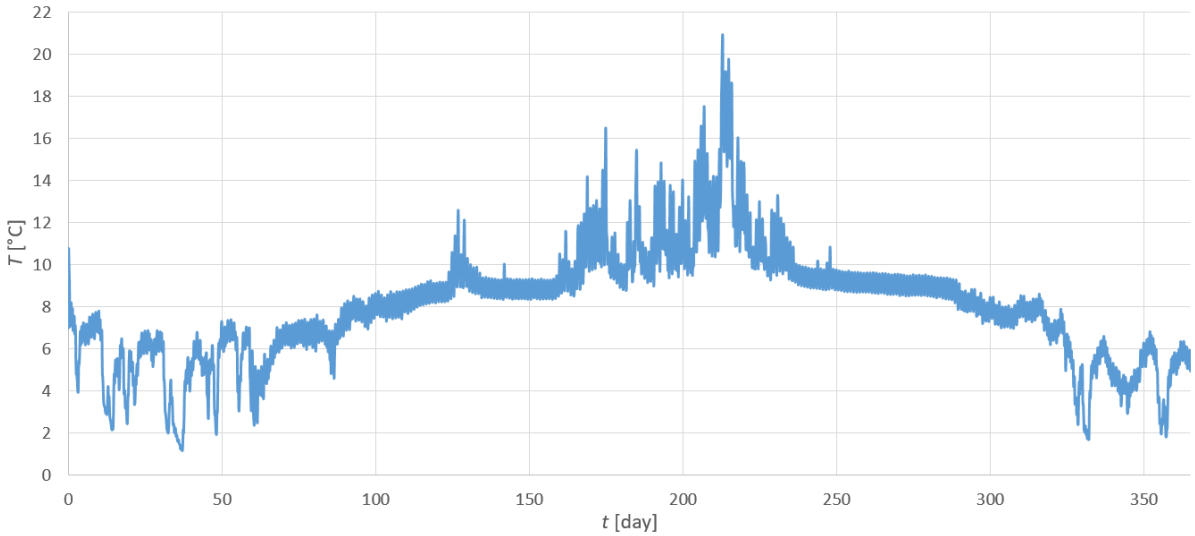

Figure 28. First year MFT profile (3 BHE's), 1 hour log interval.

Minimum temperature peak is seen to occur during mid-February, and maximum temperature peak during July. Duration of the minimum peak is around 50 hours (the time MFT is below 2 °C during the lowest peak in fig 28). Maximum temperature peaks are more transient; e.g. the peak exceeding 20 °C in fig 28 only lasts for 12 hours.

For further results in this section displaying a 50-year period, only the annual minimum and maximum of MFT (referred to as Tmin and Tmax) will be plotted to maintain clarity of the figures. Figure 30 displays these quantities for alternative scenarios of 3 and 4 BHE's with d = 152 mm and k = 1 W/mK.

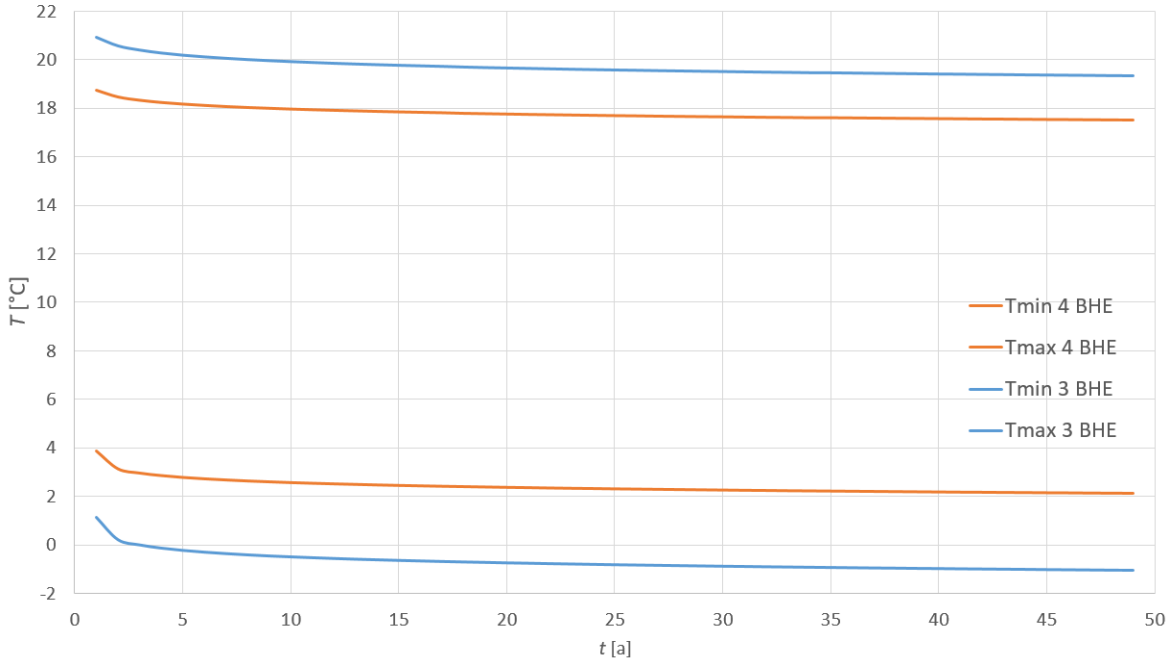

Figure 29. 50 year annual minimum and maximum of mean fluid temperatures, 3 BHE's vs. 4 BHE's.

Minimum and maximum of MFT for both scenarios display a slightly decreasing trend, due to ground response. 4 BHE's seems enough to keep Tmin above 0 °C for the 50 year time period. Dividing the heating & cooling loads to 4 BHE's instead of 3 BHE's affects minimum peak temperatures more than maximum peak temperatures. This is because the absolute heating demand is higher than cooling demand, and therefore by dividing the loads by a constant the absolute change in heating demand is also higher. Notably the MFT curves' slopes are similar to both cases; the curves differ only by an offset.

Table 12. Key values of BHE 1st year operation.

	3 BHE	**4 BHE**
Peak specific heat flow [W/m]	35	28
Extracted energy [kWh/m]	140	106
SPF	3.69	3.79

Vertical temperature profiles for the 3 BHE scenario during peak minimum temperature are presented in figure 31, to give more insight about fluid temperature within the BHE:

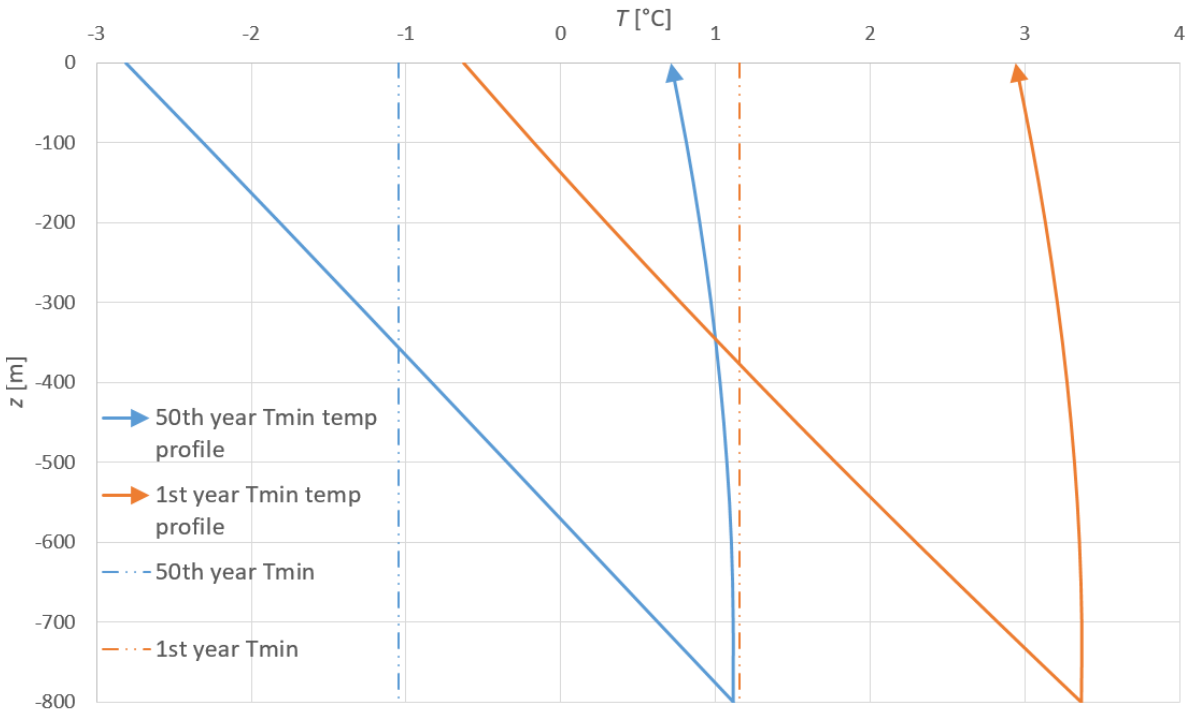

Figure 30. 1st year and 50th year vertical temperature profile during peak minimum temperature.

Annulus fluid temperature increases almost linearly with depth. Inner tube fluid temperature decrease is relatively small (0.5 °C vs. 4 °C increase in the annulus), indicating that shunt heat transfer is minimal compared to heat transfer with ground.

Other CBHE studies (e.g. Holmberg et al, 2016, p. 74) have pointed out that in deep boreholes most of heat extraction takes place in the lower sections of the borehole. Linear temperature profile in the annulus would not seem to suggest that, until we note that shunt heat transfer is relatively higher in the top part of the CBHE.

The figure also shows the relation between the simple arithmetic MFT and actual fluid temperature. For the first year Tmin peak the MFT is well above 0 °C (1.15 °C), yet in the top 150 m annulus tube heat carrier temperature is below 0 °C.

The shape of the temperature profiles does not seem to change during 50 years of heat extraction, instead an increasing offset is introduced.

For comparison, figure 32 shows the vertical temperature profile during heat injection. Notably during heat injection the same flow direction was imposed as during extraction: inlet in annulus tube.

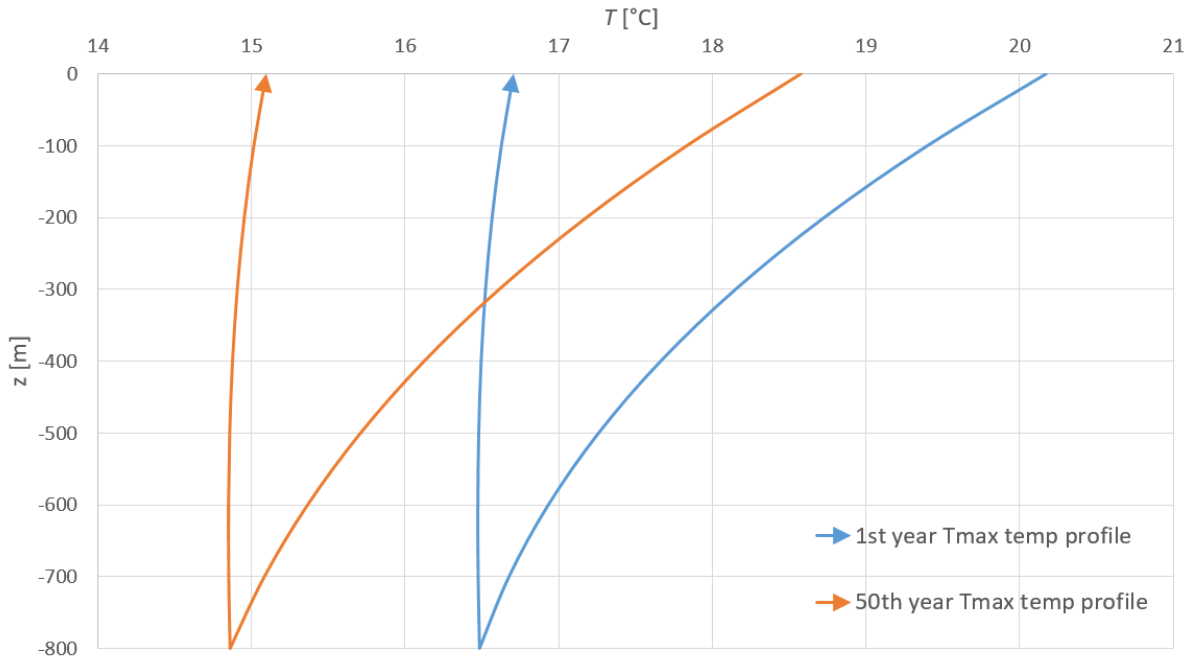

Figure 31. 1st year and 50th year vertical temperature profile during peak maximum temperature.

8.2 Diameter & conductivity

The results in this section display the effect of borehole resistance uncertainty. The simulations were run only for the 3 BHE case.

Borehole diameter

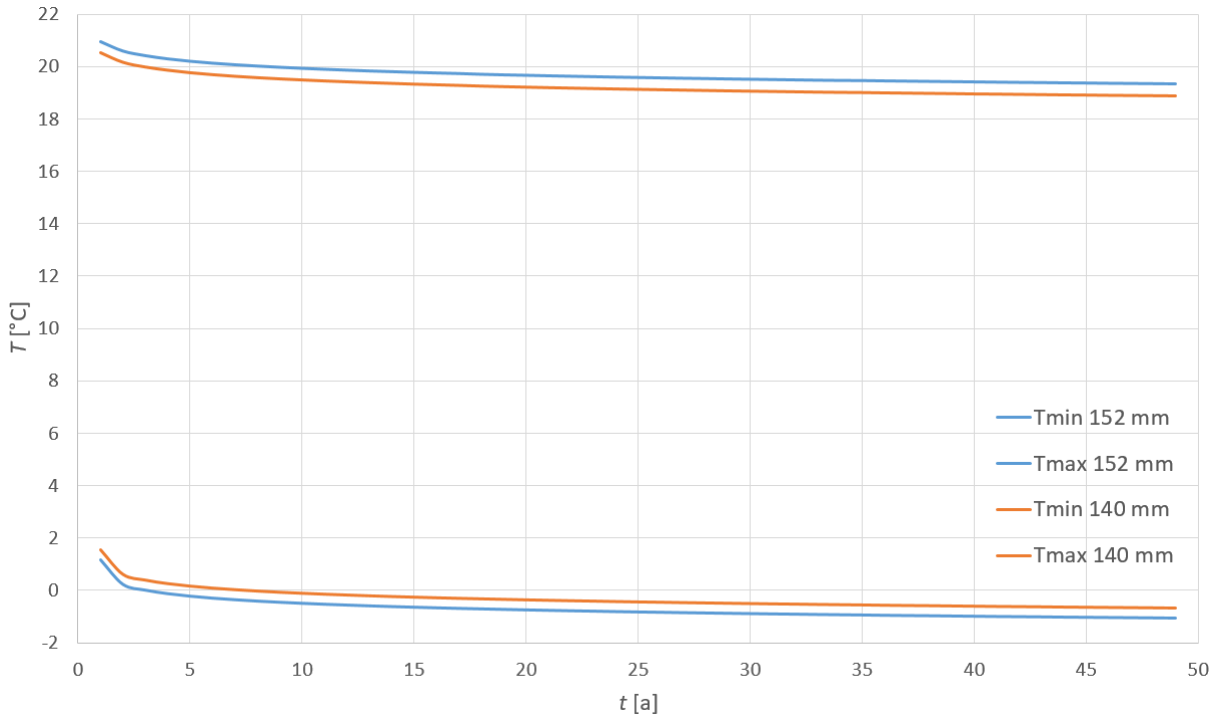

Figure 32. The effect of borehole diameter on the min/max mean fluid temperatures, 3 BHE's.

Change in borehole diameter introduces a slight, constant effect of around 0.4 °C on the minimum and 0.3 °C on the maximum temperatures. Minimum temperatures are increased and maximum temperatures are decreased, since at lower values of borehole resistance fluid temperature will tend to be closer to ground temperature.

Figure 34 presents fluid temperature evolution with k = 2.4 W/mK.

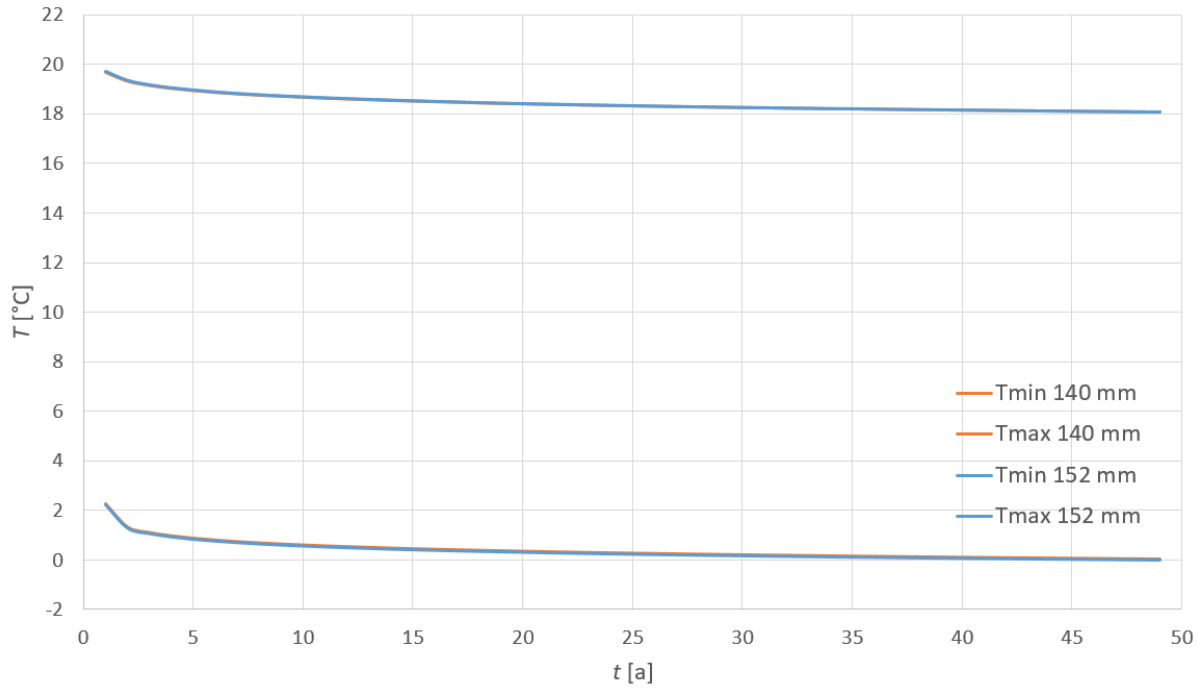

Figure 33. The effect of borehole diameter on the min/max mean fluid temperatures with improved grout k.

MFT with both diameters sees an improvement with k increased to 2.4 W/mK; for 152 mm Tmin increases by around 1 °C, and for 140 mm by around 0.7 °C. Another observation is that there is barely any difference between MFT's for the different diameters at k = 2.4 W/mK, the temperature difference being around constant 0.04 °C for both heating and cooling.

8.3 Utilization of free cooling

The first year temperature level of heat carrier fluid exiting the heat pump is shown in the figure below. The simulation was done with the 4 BHE scenario, since that configuration was deemed sufficient in the heating point of view. Free cooling temperature limit of 9 °C was used for the profile shown in figure 35.

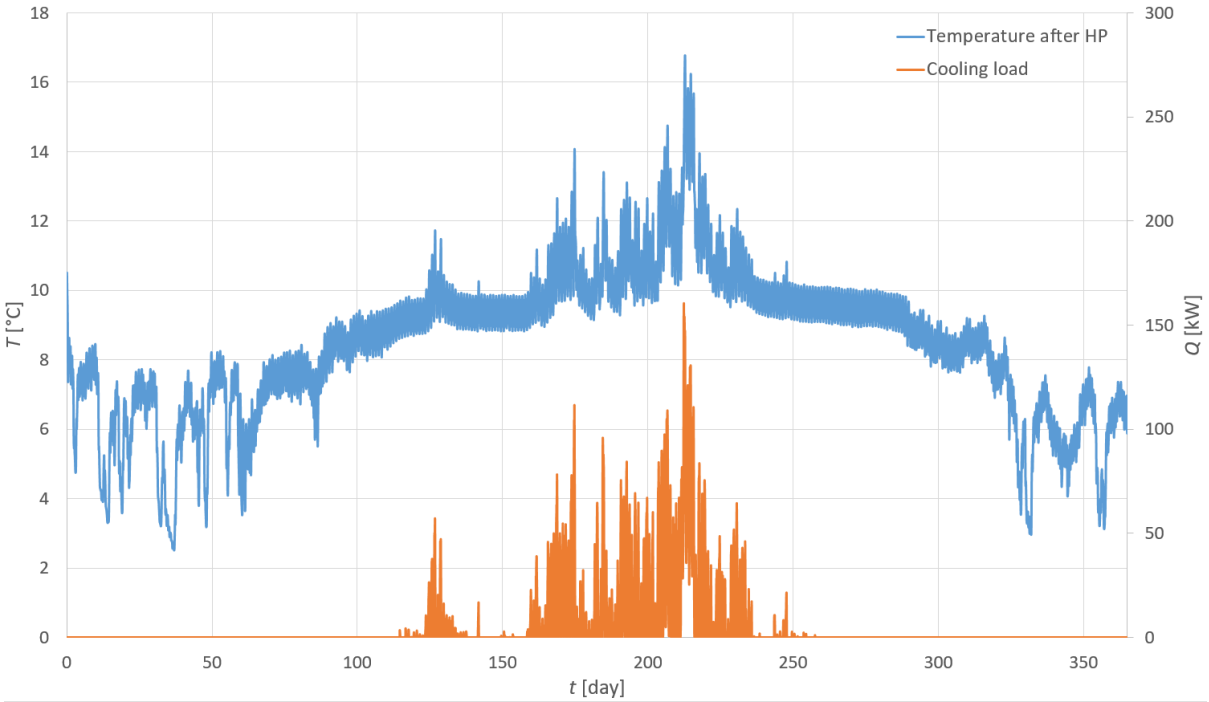

Figure 34. 1st year heat carrier temperature after HP displayed along the annual cooling load profile.

Temperature profile of heat carrier after HP is of similar shape as annual MFT displayed in figure 28, but with different temperature levels during cooling season.

Table 13 displays the operating hours for FC with different upper temperature limits.

Table 13. 1st year running hours of FC and refrigerator with different temperature limits.

	FC limit 9 °C	**FC limit 10 °C**	**FC limit 11 °C**	**FC limit 12 °C**
FC operating time [h]	42	572	1136	1438
Refrigerator operating time [h]	1626	1095	530	228
FC operating time coverage [%]	3	34	68	86
Refrigerator electricity consumption [MWh]	8.5	7.2	5.3	3.2
Peak specific injection load [W/m]	50	50	50	50
Injected energy [kWh/m]	13.2	12.9	12.3	11.6

Potential can be seen for a substantial increase in FC operating hours by increasing the temperature limit by only a couple degrees. However, it should be noted that refrigerator electricity consumption does not decrease in proportion to the operating hours, since the cooling load is not evenly distributed to the annual operating hours.

8.4 Regeneration

Regeneration calculations were conducted using the method presented in the previous section. The simulations were performed for the 3 BHE configuration, to see whether regeneration could make the configuration more feasible. Annual utilizable regenerative heat during a 50-year period is displayed in figure 36. The results for regeneration before and after the heat pump & cooling system are shown separately.

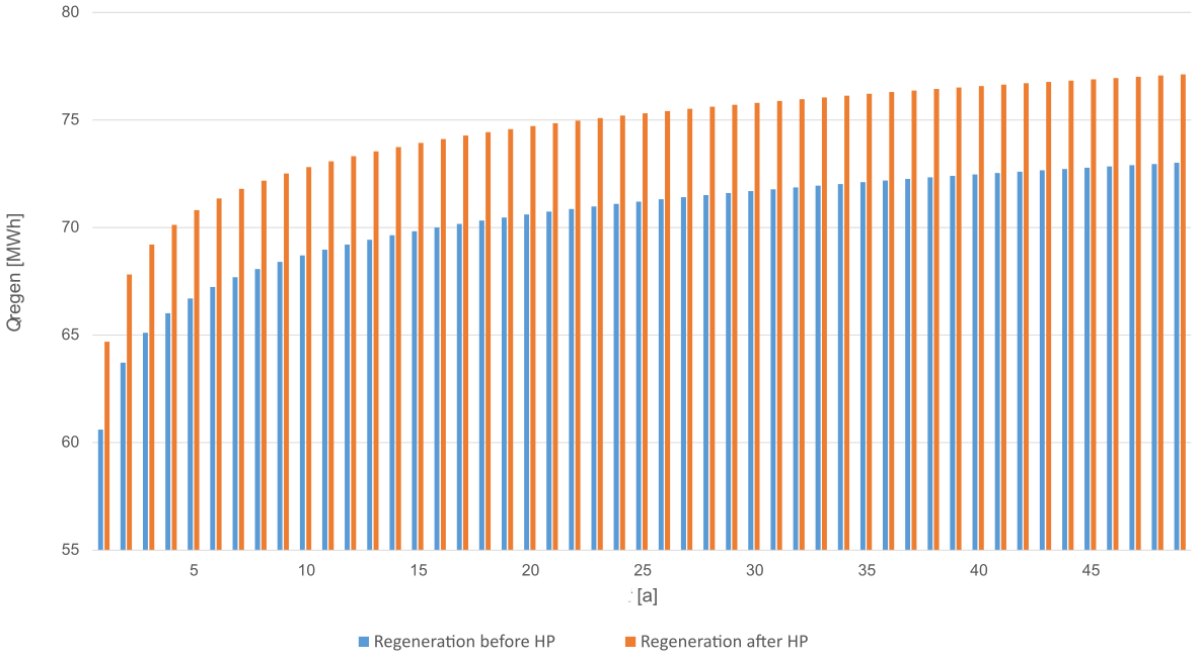

Figure 35. Annual available regenerative heat, heat exchanger before HP vs. after HP.

Utilizable regenerative heat is seen to increase with time for both configurations; this is because the decreasing trend of MFT leads to higher temperature difference between heat source (ventilation outlet air) and the heat carrier fluid. Positioning the HX after the heat pump & refrigerator allows for slightly higher amount of utilizable heat, since in this configuration heat carrier temperature at regen HX inlet is lower.

Table 14 shows the amount of annual regenerative heat relative to heat extraction.

Table 14. Injection/extraction ratio with and without regeneration.

	1st year no regen	**50th year no regen**	**1st year regen after HP**	**50th year regen after HP**	**1st year regen before HP**	**50th year regen before HP**
Qextract [MWh]	337	331	339	335	340	336
SPF	3.69	3.52	3.76	3.65	3.78	3.66

Qinject [MWh]	42	39	107	119	103	115
Inject/extract ratio	0.12	0.12	0.32	0.35	0.30	0.34

Although in this scenario introducing regeneration almost triples the annual heat injection for both cases, the effect on SPF is small. Positioning the regen HX before HP results in a slightly higher SPF, since in this case the heat carrier enters the HP in a higher temperature.

Figure 37 presents the effect of regenerative heat on 50-year Tmin.

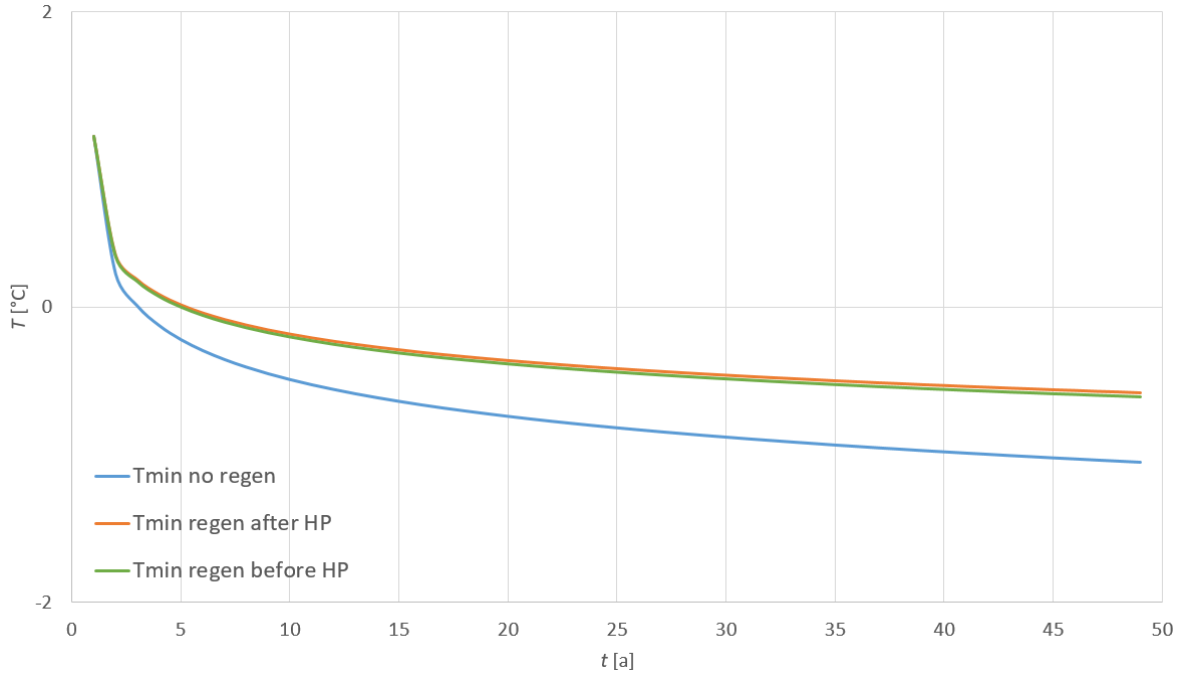

Figure 36. The effect of regeneration before or after HP to long-term MFT.

Introducing regenerative heat seems to have a limited but noticeable effect on Tmin; the difference between the default and non-regenerated case increases over time, leading to a value of around 0.5 °C after 50 years. Regarding Tmin the position of the regen HX seems to be of no practical consequence.

The effect of regeneration on ground response

Figures 38 and 39 display the ground thermal response in the form of temperature change contours, the first without regeneration and the second with regeneration. The borehole is situated on the vertical axis (left side of figure).

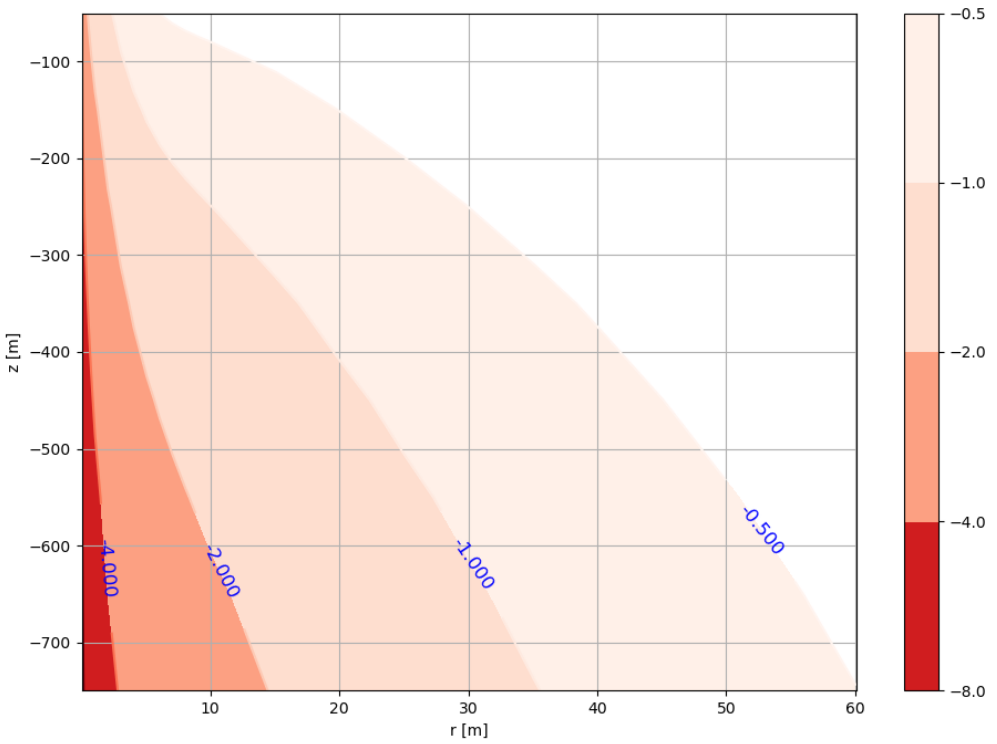

Figure 37. Ground temperature change contour after 50 years of operation, without regen.

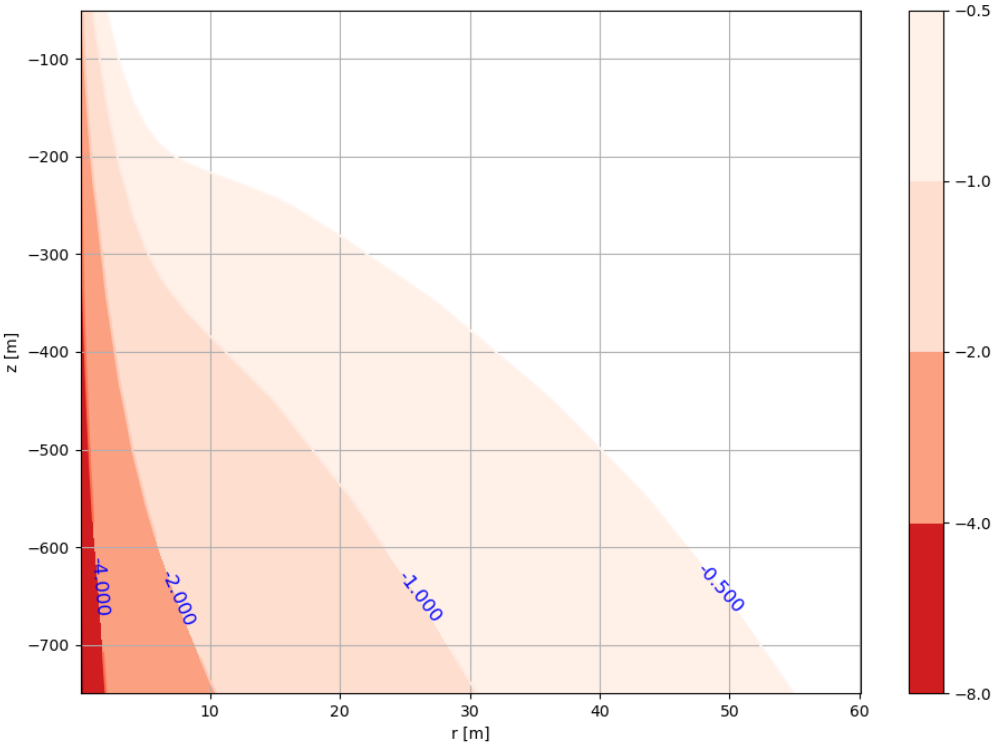

Figure 38. Ground temperature change contour after 50 years of operation, with regen.

In both figures ground temperature change extends much father in radial direction in the deeper parts. This suggests that the heat extraction flux is the highest in the low parts of the BHE.

At the bottom part of the figures, which shows the average temperature of the last cylinder (700 m - 800 m), temperature change of -0.5 °C extends to 60 m in the case without regeneration. Introducing regeneration reduces the range of ground response at all depths, but most noticeably the contour shape is changed in the upper ~200 m, suggesting that heat injection heat flux is instead highest in the top part. This seems reasonable, given that for heat injection the temperature difference between the fluid and ground is largest in the top part. Flow direction was not reversed at any point, meaning that the annulus was used as flow inlet also during heat injection.

9 DISCUSSION

This section contains discussion about the consequences of the presented results. Improvements and objects of further study are pointed out.

9.1 Minimum number of BHE's

The default scenario (3 boreholes, k = 1 W/mK, etc.) is clearly not sustainable, since the MFT falls below 0 already within the first years of operation. Further, the duration of the minimum temperature peak is seen to be relatively long (50 hours). Shorter low temperature peaks of a couple of hours might be more acceptable. Four boreholes seem enough to keep the MFT well above zero even with the pessimistic borehole resistance.

Neither of the cases seems to suffer from excessive ground cooling, given that the MFT curve slopes are not very steep after the first couple years. Instead of long-term ground cooling, the lower MFT of the 3 BHE case is more likely due to excessive peak heat rate per meter of BHE; in practice the limited ground conductivity causes high temperature gradients in the vicinity of the BHE during peak demand (recall heat conduction equation (23)), and this then causes low heat carrier fluid temperatures. This is supported by the fact that the MFT curve slopes are similar for both cases.

Average (per meter) specific heat rates during first year peak heat demand for the two cases are 35 W/m for 3 BHE's and 28 W/m for 4 BHE's. Changing the heat pump coverage factor to higher values will have negligibly small effect on extracted energy, but it would increase the specific heat rates, likely requiring increased BHE length.

For shallow borehole heat exchangers a specific heat load of value around 30 - 45 W/m is often cited as a typical dimensioning value (Uponor, p. 7), (Sweco, 2020, p. 49), (FCG, 2017, p. 7). In (Holmberg et al, 2016, p. 75) a parametric study is conducted to find out the sustainable heat load of a CBHE at different values of borehole depth, geothermal gradient and borehole diameter. It is observed that the sustainable specific heat load (W/m) increases with borehole depth; for example with geothermal gradient of 1.5 °C/100 m the sustainable heat load is 25 W/m for a 300 m borehole, compared to 50 W/m for an 800 m borehole. The article consequentally concludes that deep CBHE's offer potentially much higher heating load per meter than conventional installations, due to higher temperature levels deeper in the ground.

Compared to these numbers the estimated sustainable peak specific heat rate of 32 W/m of the installation studied in this thesis seems low. However, there are many differences in the used parameters between (Holmberg et al, 2016) and the installation in this thesis, suggesting that a lower sustainable specific heat load is to be expected. Firstly the geothermal gradient used in this thesis (1.26 °C/100 m) is lower than even the lowest value used in the article. Secondly the CBHE design used in the article exhibits lower thermal resistance than the design used in this thesis. Thirdly, the constant flow rate used in the article was set to enforce an average temperature difference of 3 °C in the borehole. Specifically, it is mentioned that for the 800 m case a flow rate of 4 l/s was used, which is considerably higher than the flow rate of 2.3 l/s used in this thesis. Higher flow rates have the effect of further decreasing BHE thermal resistance due to improved convection heat transfer, as well as enabling higher heat flow with the same temperature difference between inlet and outlet. While the geometrical & material properties of the CBHE used in this thesis were taken as granted, the dimensioning flow rate might have possibilities of optimization. Further studies should certainly be made regarding the flow rate in this particular installation, to determine whether it would be within technical and economical limits to increase the heat carrier flow rate.

Sustainable heat load indicator

Integral to studying the sustainability of the heat load is the limit indicator used. Using MFT as an indicator is perhaps ill-fitting, in case the indicator is to reflect the possibility of groundwater freezing. In u-tubes the groundwater temperature is affected by the temperature of both tubes: even in the case that the downward travelling fluid is well below 0, the groundwater will also be in contact with the tube containing the upward travelling fluid, which is (likely) at above 0 °C. In CBHE's, however, only the annulus fluid is contact with the groundwater; possibly subjecting the top levels in more risk of freezing if the fluid is at subzero temperatures. Perhaps fluid inlet temperature, combined with a time parameter (peak duration), could provide a practical freezing indicator. In case a separate grout layer is implemented in the model, the temperature of the groundwater itself can be used as an indicator, instead of heat carrier temperature.

In case groundwater freezing is not the main concern (e.g. when utilizing a solid grouting instead), the lower limit is instead likely dictated by heat pump COP and economical concerns. Economically the limit of profitability comes down to the fluid temperature's effect on heat pump's COP. In the configurations studied in this thesis the decrease of MFT was quite modest,

only around 2 °C in the span of 50 years, and the resulting decrease of COP is negligible compared to other economic uncertainties concerning a similar time span.

It is necessary to recall that perhaps as a the single most important delimitation in this study, the thermal interaction between the boreholes was not modelled. Given the small size of the parcel (fig. 13), it is not feasible in reality to avoid the thermal interactions altogether, although the radius of temperature change surrounding each borehole can be affected by ground regeneration, as will be seen further below. There is also uncertainty regarding the parcel area available for drilling; for example drilling below the building can help in maximizing the distance between boreholes. In practice including the thermal interactions between boreholes will have the effect of introducing higher downward slope to the MFT figure (fig. 29), depending on the distance between boreholes and annual extracted energy.

9.2 Borehole diameter and grout conductivity

With the default *k* of 1 W/mK, changing borehole diameter causes a slight difference on Tmin and Tmax. However, the difference will be lower than that for a borehole with changing diameter, depending on the exact diameter profile along the depth. Notably the diameter at the lower end is somewhat more critical since more heat transfer takes place in that part.

With the *k* value of 2.4 W/mK, meant to represent an equivalent conductivity for conservative estimation of natural convection, or alternatively a high conductivity solid grout, varying borehole diameter at least between the studied values seems to have a negligible effect. The results are supported by the analytical equation of the radial conductive resistance:

$$R = \frac{\ln(\frac{r_2}{r_1})}{2\pi k} \tag{36}$$

$$\frac{dR}{dr_2} = \frac{d\left(\ln\left(\frac{r_2}{r_1}\right)\right)}{dr_2} \cdot \frac{1}{2\pi k} = \frac{1}{2\pi k r_2} \tag{37}$$

In (37) it can be seen that the derivative of the resistance with respect to r_2 tends to decrease at higher values of *k*, which is what was observed. Compared to the case with 1 W/mK, grout conductivity of 2.4 W/mK increases the sustainable specific heat rate to 35 W/mK, as the 3 BHE scenario is observed to remain above 0 in figure 34.

As for practical implications; if solid grouting were to be used, the space between borehole could possibly be left a bit wider to ease the installation of the CBHE, without much detriment to heat transfer. This would lead to higher required amount of grouting material, however.

The actual effect of natural convection with the CBHE geometry should be investigated in further studies.

9.3 Free cooling

With the FC limit temperature range studied here (9 °C - 12 °C), covering the entire cooling demand by free cooling was even theoretically impossible, since during the highest demand peaks heat carrier temperature was higher than the cooling system supply temperature assumed in the building simulation (15 °C). Further studies could be conducted on cold water storage tanks' effect to cooling load peaks; possibly by spreading the peak loads to a longer duration FC coverage could be increased. Furthermore, for defining an exact limit temperature for FC in the studied case, the exact implementation of the building cooling system needs to be known, and the system model should utilize a more detailed heat exchanger model for the cooling.

In the case that full FC coverage is unfeasible, FC could still be utilized during the times when fluid temperatures allow for it, as was done in the simulations. Partial free cooling could also be implemented: in this kind of system free cooling heat exchanger and a refrigerator can operate simultaneously to minimize refrigerator electricity consumption.

As an additional note, in the case that ground regeneration during summer is implemented, the resulting increase in summertime fluid temperatures will further undermine the possibility of utilizing free cooling.

9.4 Regeneration

The available regenerative heat using the assumed dT = 6 results in around three times more annual heat injection compared to the default case without regeneration. The effect of regeneration is noticeable both for MFT and ground thermal response.

Annual regeneration of 65 - 80 MWh, which corresponds to 27 - 33 kWh/m, decreases the radius of ground temperature change around 5 m, when looking at the -1 °C contour at the depth of 750 m. However, it seems that with flow inlet in annulus the effect of regeneration might be emphasized at the top part. It should be further studied whether reverting the flow during specific times or the whole summer could change the focus of the regeneration into the lower parts of the borehole, which are more critical for heat extraction.

Looking at the contour figures 37 and 38, the implicit assumption of an adiabatic boundary in the ground at BHE bottom level seems questionable, since the thermal response is concentrated at the lower parts and the resulting axial temperature gradients may cause considerable heat

conduction also in vertical direction. It is also possible that including axial heat transfer within the ground could even out the ground temperature profiles along the length of the BHE, resulting in smaller radius of temperature change than predicted in this study. For further studies of ground regeneration it is recommended to include axial conduction in the model, also from the ground mass below the borehole.

Also, while ventilation outlet air is most of the time at higher temperature than ambient air, its flow rate is also limited compared to ambient air which can theoretically be utilized at infinite flow rate. Which option is more profitable will then likely depend on the desired heat flow rate of the regeneration heat exchanger.

9.5 Further study

This section presents other possibilities and requirements for further study. The first subsection consists of technical improvements within the CBHE model, and the second subsection proposes further studies of relevance.

9.5.1 Technical model improvements

CBHE model

During use the model was found to have potential for both long-term and short-term simulations, since simulation computation time can be highly affected by adjusting time step; for long-term simulations large time step can be used, in case detailed variations do not need to be modelled.

Another benefit of the model is the capability of dynamic coupling with other system components, as demonstrated with the modules used in this thesis. Yet, more work should be done to validate and to improve the flexibility of the model.

Further validation

The model was validated by DTRT measurement data from a relatively short CBHE. Validation against measurements from a deep CBHE should also be done. At the latest measurements from the case building's system can be used once it is in operation. Pressure loss calculation of the model should also be validated; in this thesis the model was found to predict higher pressure loss than expected, also compared to an analytical CBHE dimensioning tool developed in-house at VTT. The model should be accurate in different flow situations, for accurate flow rate optimization studies etc.

Model improvements

Inclusion of axial heat transfer in the model, as discussed in the regeneration subsection, might have the effect of increasing the fluid temperature levels compared to current predictions.

Inclusion of an explicitly defined grout layer, with the option for modelling groundwater natural convection, would improve the applicability of the CBHE for different collector geometries and provide more accurate results compared to using equivalent conductivities. Also, by a separate option to set up the model for varying borehole diameter, the model would be better suited for deep boreholes which often have varying diameter along the depth.

In case the model is to be used for modelling & design of BHE fields instead of optimization of individual BHE's, modelling the thermal interaction between neighboring boreholes is obviously necessary.

It should also be recalled that this thesis utilized a simplistic heat pump model. For more detailed studies the used heat pump model should also include a fit for partial load efficiency. Refrigerator operation also requires a proper model. In addition dynamic thermal storages should be included, e.g. within the Apros model.

9.5.2 Further studies of relevance

This thesis only studied undisturbed performance of the CBHE's. A further study needs to be conducted using an appropriate modelling tool allowing for studies of BHE thermal interaction and different borehole configurations.

Flow rate/pumping power studies were not included in this thesis. The optimization of heat transfer and pumping power is a relevant topic of study. Flow rate affects temperature levels, which in turn dictate what kind of technical solutions are possible/necessary in the system, as seen in the results of this thesis.

The effect of building side load manipulation options should be studied, as the behavior and requirements from the GSHP and ground loop are highly dependent on the peak loads present on the building side. The studies could include e.g. variable heat storage volumes.

In this study the effect of only one regeneration source was studied. Possible other sources should be investigated, not only at the building but also at district level. As one example, the ground floor of the building will house a restaurant and another commercial space. In the case that the commercial spaces utilize refrigerators of considerable capacity, excess heat can be

utilized by the heat pumps. Regeneration sources would be more useful during winter, but during that time excess heat can be utilized directly for heating. At any rate the end objective is the same; reduce the net ground load so that long-term heat carrier temperatures remain at higher level.

10 CONCLUSIONS

This thesis studied the applicability of deep CBHE for the case building. The objectives were concerned with the required number of boreholes for sustainable operation of 50 years, viability of free cooling, and the potential of using heat from ventilation outlet air for ground regeneration during summer.

Building load profiles, representing the case building with energy-efficient building technology, were calculated with IDA-ICE. Based on the load profiles, heat pump coverage factor of 66 % was decided for heat pump simulations. The load profiles were later used as inputs for the simulation studies of the GSHP system.

A previous dynamic CBHE model implemented in Apros was coupled with a simple heat pump model calculating COP as a function of evaporator inlet temperature (calculated in the CBHE model) and condenser outlet temperature (heating system temperature level) to represent the GSHP system. The CBHE model was validated using measurement data and results from another simulation model EED. The thermal performance predicted by the model was found to agree with both sets of comparison data, but more validation using measurements from actual deep CBHE's should be done in the future. The model predicted higher pressure losses compared to two different models in literature, therefore the flow calculations should be checked.

Four different simulation scenarios were conducted in accordance to the three objectives specified in the beginning, and in addition to study the effect of uncertainty from grout/groundwater layer thickness and conductivity.

Sustainability of operation during a 50-year time period was studied from the evolution of annual minimum of mean fluid temperature. 4 undisturbed CBHE's were found to be an adequate number for the given coverage factor of 66 %. In this case specific heat load [W/m] was inferred to be a more limiting factor to minimum MFT than long-term ground response, due to the shapes of the MFT curves. Average specific heat load of around 32 W/m was found to be the limit for sustainable operation, in case of pessimistic grout specifications (152 mm borehole diameter, 1 W/mK conductivity) and no regeneration. Long-term ground cooling will likely have more effect on the results if thermal interaction between the boreholes will be included the model; this should be done in further studies.

A good indicator for the sustainable long-term heat extraction was discussed. It was noted that mean fluid temperature, as an average of heat carrier inlet and outlet temperatures, does not correspond well to the actual risk of groundwater freezing. Groundwater temperature itself would be the most accurate indicator for groundwater freezing, but this requires a more detailed model for the borehole.

The effect of borehole diameter and grout conductivity on MFT was studied. It was found that at a lower value (1 W/mK) varying borehole diameter between 140 and 152 mm introduces an offset of around 0.4 °C to minimum and 0.3 °C to annual maximum MFT, but at a higher value (2.4 W/mK) of grout conductivity varying borehole diameter between the same values has practically no effect. This can be taken into account when planning the required borehole diameter and optimal grouting material for a CBHE installation.

Using the heat carrier for cooling the apartment without refrigerator (free cooling) during summer requires relatively low temperature levels, since it is assumed that the building cooling water needs to be cooled down to 15 °C. Based on the first year temperature profile of the heat carrier after the heat pump, free cooling is unfeasible during most of cooling season due to excessive heat carrier temperatures. Further studies could include the effect of cold storage tanks, as well as different building side cooling system options.

Ventilation outlet air during summer is typically at room temperature, since it is only used for heat recovery during the heating season. The excess heat available could potentially be transferred to the heat carrier, to regenerate the ground and improve long-term fluid & ground temperatures. The potentially available regenerative was calculated by assuming a simple heat exchanger. It was found that the available regenerative heat increases as time goes on, since long-term heat carrier cooling increases the temperature difference between regeneration source and heat sink (the heat carrier). For regeneration heat exchanger situated after the heat pump, during a 50-year period the available annual regenerative energy increased from 65 to 80 MWh, which corresponds to 27 - 33 kWh/m.

The effect of regenerative heat on long-term heat carrier fluid temperatures and ground thermal response was studied. Regeneration decreased the slope of minimum MFT, resulting in around 0.6 °C higher fluid temperature after 50 years. As for the effect on ground response, regeneration was seen to increase ground temperatures more at the top levels (depth of around 0-200 m), which is suboptimal since the lower levels are subject to higher heat extraction flux from the CBHE's. Possibility of inverting the flow during summer for more

benefit from regeneration should be studied. Regeneration is likely to have a higher effect on fluid temperatures when including borehole thermal interaction in the model, since local ground cooling from heat extraction will be higher.

Finally, improvements for the CBHE model were suggested, regarding modelling of the grout layer, variable borehole diameter and axial heat transfer from below borehole bottom level. Further system level studies were also suggested, including flow rate/pumping power optimization, the effect buffer tank size on required BHE dimensions, and the use of other heat sources for regeneration.

REFERENCES

Acuna Jose, 2013. Distributed thermal response tests - New insights on U-pipe and Coaxial heat exchangers in groundwater-filled boreholes. Doctoral thesis [online]. Available at: urn:nbn:se:kth:diva-117746 (accessed 19.11.2020). KTH.

Airaksinen Miimu, Vainio Terttu, Vesanen Teemu, Ala-Kotila Paula, 2015. Rakennusten jäähdytysmarkkinat. Available at: https://energia.fi/files/399/Rakennusten_jaahdytysmarkkinat_18-12-2015.pdf (accessed 19.11.2020). Espoo: VTT.

Apros datasheet, (no date). Thermal Hydraulics Modelling. Available at: http://www.apros.fi/filebank/209-Apros_Datasheet_Thermal_Hydraulics_Modelling.pdf (accessed 19.11.2020)

Aresti Lazaros, Christodoulides Paul, Florides Georgios, 2018. A review of the design aspects of ground heat exchangers. Renewable and sustainable energy reviews, vol 92 [online]. Available at: https://doi.org/10.1016/j.rser.2018.04.053 (accessed 19.11.2020). Amsterdam: Elsevier.

Arvola Ville, 2017. Lämmöntalteenotto harmaasta jätevedestä. Bachelor's thesis [online]. Available at: https://www.theseus.fi/bitstream/handle/10024/124037/Arvola_Ville.pdf?sequence=1 (accessed 19.11.2020). Oulu University of Applied Science.

Beier Richard A., Acuna Jose, Mogensen Palne, Palm Björn, 2013. Borehole resistance and vertical temperature profiles in coaxial borehole heat exchangers. Applied Energy, vol. 102 [online]. Available at: https://doi.org/10.1016/j.apenergy.2012.08.007 (accessed 19.11.2020). Amsterdam: Elsevier.

Bergman Theodore L., Lavine Adrienne S, 2017. Fundamentals of heat and mass transfer. 8th edition. Hoboken: John Wily & Sons, Inc. ISBN 9781119337676.

Blocon, 2015. EED 3 manual [online]. Available at: https://www.buildingphysics.com/manuals/EED3.pdf (accessed 19.11.2020)

Carbonell D., Cadafalch J., Pärisch P., Consul R., 2012. Numerical analysis of heat pump models. Comparative study bertween equation -fit and refrigerant cycle based models. Conference paper [online]. Available at : https://www.researchgate.net/publication/266266373_NUMERICAL_ANALYSIS_OF_HEAT_PUMP_MODELS_COMPARATIVE_STUDY_BETWEEN_EQUATION-FIT_AND_REFRIGERANT_CYCLE_BASED_MODELS (accessed 19.11.2020)

Equa Simulation AB, 2020. Dialog for glass construction (IDA-ICE help).

Equa Simulation AB, 2020. IDA Indoor Climate and Energy. Available at: https://www.equa.se/en/ida-ice (accessed 19.11.2020)

Erol Selcuk, Francois Bertrand, 2014. Efficiency of various grouting materials for borehole heat exchangers. Applied Thermal Engineering, vol. 70 [online]. Available at: https://doi.org/10.1016/j.applthermaleng.2014.05.034 (accessed 19.11. 2020). Amsterdam: Elsevier.

FCG, 2017. Pohjois-Savon kohdennettu geoenergiapotentiaaliselvitys [online]. Available at: https://www.pohjois-savo.fi/media/liitetiedostot/aluesuunnittelu/maakuntakaava-2040/kaavaselvitykset/pohjois-savon_geoenergiapotentiaaliselvitys_raportti_fcg_2017.pdf (accessed 20.11.2020). Pohjois-Savon Liitto.

Fisher Daniel E., Rees Simon J., 2005. Modeling ground source heat pump systems in a building energy simulation program (energyplus). Conference paper [online]. Available at: https://www.researchgate.net/publication/252174885_Modeling_ground_source_heat_pump_systems_in_a_building_energy_simulation_program_energyplus (accessed 19.11.2020).

Gehlin, S.E.A., J.D. Spitler, G. Hellström. 2016. Deep Boreholes for Ground Source Heat Pump Systems - Scandinavian Experience and Future Prospects. Conference paper [online]. Available at: https://hvac.okstate.edu/sites/default/files/pubs/papers/2016/Gehlin_Spitler_Hellstr%C3%B6m_2016_Deep_BH.pdf (accessed 19.11.2020).

GTK, 2019. Helsingin geoenergiapotentiaali [online]. Available at: https://www.hel.fi/static/liitteet/kaupunkiymparisto/julkaisut/julkaisut/Helsingin_geoenergiapotentiaali_luonnos.pdf (accessed 19.11.2020).

Helen Oy, 2020. Helen is creating a new heat production model for households with a new pilot project – Ground-source heat to be part of the company's carbon-neutral range of energy solutions. Available at: https://www.helen.fi/en/news/2020/geothermal-heat (accessed 19.11.2020)

Hellström Göran, 1991. Thermal Analyses of Duct Storage Systems. I. Theory. Department of Mathematical Physics, University of Lund, Sweden.

Helsingin maalämpötyöryhmä, 2019. Available at: https://www.hel.fi/static/liitteet/kaupunkiymparisto/julkaisut/julkaisut//Maalampotyoryhman_raportti_keskustelua-varten.pdf (accessed 19.11.2020)

Holmberg Henrik, Acuna Jose, Näss Erling, Sönju Otto K., 2016. Thermal evaluation of coaxial deep borehole heat exchangers. Renewable Energy, vol. 97 [online]. Amsterdam: Elsevier. Available at: https://doi.org/10.1016/j.renene.2016.05.048 (accessed 19.11.2020).

IEA, 2020. Tracking Buildings 2020 [online]. Available at: https://www.iea.org/reports/tracking-buildings-2020 (accessed 19.11.2020).

Javed S., Fahlen P., Claesson J, 2009. Vertical ground heat exchangers: a review of heat flow models. Conference paper [online]. Available at: https://research.chalmers.se/en/publication/107909 (accessed 19.11. 2020). Chalmers University of Technology.

JH-Lämpö, (no date). Lämpökaivo. Available at: http://www.jh-lampo.fi/lampokaivo/ (accessed 19.11.2020).

Johansson Eric, 2019. Parametric study of a wastewater heat recovery system for buildings. Master's Thesis [online]. Available at: https://www.diva-portal.org/smash/get/diva2:1327330/FULLTEXT01.pdf (accessed 19.11.2020) Umeå University.

Lauttamäki Ville, 2018. Geoenergia kiinteistöjen lämmitysratkaisujen markkinoilla Suomessa energiakriisien ajoista 2030-luvulle. Doctoral thesis [online]. Available at: http://urn.fi/URN:ISBN:978-951-29-7234-0 (accessed 19.11.2020). University of Turku.

Lehtinen Lauri, 2020. Kaukolämpö etsii uusia energianlähteitä. Suomen Kuvalehti 30/2020 [online]. Available at: https://suomenkuvalehti.fi/jutut/kotimaa/hakkeesta-tulee-pula-turvetta-

ajetaan-alas-kaukolampoon-tarvitaan-kipeasti-uusia-energialahteita/ (accessed 19.11.2020). Helsinki: Otavamedia.

Lund Andreas, 2019. Analysis of deep-heat energy wells for heat pump systems. Master's thesis [online]. Available at: http://urn.fi/URN:NBN:fi:aalto-201912226623 (accessed 19.11.2020). Aalto University.

Mazzotti Willem, Acuna Jose, Lazzarotto Alberto, Palm Björn, 2018. Deep Boreholes for Ground-Source Heat Pump [online]. Available at: http://www.diva-portal.org/smash/get/diva2:1269108/FULLTEXT01.pdf (accessed 19.11.2020).

Mechanical Engineering and Metals Industry Standardization in Finland, 2018. SFS-EN 14511-2:2018. Standard.

Meggers Forrest, Leibundgur Hansjurg, 2011. The potential of wastewater heat and exergy: Decentralized high-temperature recovery with a heat pump. Energy and Buildings, vol. 43 [online]. Available at: https://doi.org/10.1016/j.enbuild.2010.12.008 (accessed 19.11.2020). Amsterdarm: Elsevier.

Mendrinos Dimitrios, Katsantonis Spyridon, Karytsas Constantine, 2016. Pipe materials for borehole heat exchanger. Conference paper [online]. Available at: https://www.researchgate.net/publication/328232447_Pipe_materials_for_borehole_heat_exchangers (accessed 19.11.2020).

Morchio Stefano, Fossa Marco, 2019. Thermal modeling of deep borehole heat exchangers for geothermal applications in densely populated urban areas. Thermal Science and Engineering Progress, vol. 13 [online]. Available at: https://doi.org/10.1016/j.tsep.2019.100363 (accessed 19.11.2020). Amsterdam: Elsevier.

Nibe, (no date). F1355-43 product data (online) Available at : https://www.nibe.eu/assets/documents/28028/M12254-3.pdf (accessed 7.12.2020)

Official Statistics of Finland (OSF), 2018. Energy consumption in households [online]. Available at: http://www.stat.fi/til/asen/2018/asen_2018_2019-11-21_tie_001_en.html (accessed 19.11.2020).

Pan Sheng, Kong Yanlong, Chen Chaofan, Pang Zhonghe, Wang Jiyang, 2020. Optimization of the utilization of deep borehole heat exchangers. Geothermal Energy vol. 8 [online].

Available at: https://doi.org/10.1186/s40517-020-0161-4 (accessed 19.11.2020). Berlin: Springer.

Polo Emilio Gimenez, 2020. Coaxial Borehole Heat Exchanger: modelling, hydronic and thermal analysis. Master's thesis [online], Available at: http://oa.upm.es/62825/ (accessed 19.11.2020). Linköping University.

Ranta-Korpi Matias, 2018. Aurinko- ja ilmalämmön hyödyntäminen maalämpöjärjestelmän energiatehokkuuden parantamisessa. Master's thesis [online]. Available at: http://urn.fi/URN:NBN:fi:aalto-201809034861 (accessed 19.11.2020). Aalto University.

Reda Francesco, Fatima Zarrin, 2019. Northern European nearly zero energy building concepts for apartment buildings using integrated solar technologies and dynamic occupancy profile: Focus on Finland and other Northern European countries. Applied Energy, vol. 237 [online]. Available at: https://doi.org/10.1016/j.apenergy.2019.01.029 (accessed 19.11.2020). Amsterdam: Elsevier.

Rouhiainen Virve, 2018. Uusiutuva energia valtaa alaa pientalojen lämmityksessä [online]. Available at: https://www.stat.fi/tietotrendit/artikkelit/2018/uusiutuva-energia-valtaa-alaa-pientalojen-lammityksessa/ (accessed 19.11.2020)

Schild Peter G., 2004. Air-to-air heat recovery in ventilation systems. Ventilation Information Paper 6 [online]. Available at: https://www.aivc.org/sites/default/files/members_area/medias/pdf/VIP/VIP06_Heat_Recovery.pdf (accessed 19.11.2020). Air Infiltration and Ventilation Centre.

Sliwa T., Nowosiad T., Vytyaz O., Sapinska-Sliwa A., 2016. Study on the efficiency of deep borehole heat exchangers. SPCAR Proceedings No.2 [online]. Available at: https://www.researchgate.net/publication/306208661_Study_on_the_efficiency_of_deep_borehole_heat_exchangers (accessed 19.11.2020).

Seppänen Olli, Seppänen Matti, 1996. Rakennusten sisäilmasto ja LVI-tekniikka. 2nd Edition. Sisäilmayhdistys ry. ISBN 951-97186-5-6.

Sweco Oy, 2020. Maankäytön suunnittelu ja maalämpö [online]. Available at: https://www.hel.fi/hel2/ksv/liitteet/2020_kaava/5066_9_Maalamposelvitys_Sweco_2019.pdf (accessed 20.11.2020). City of Helsinki.

Smart Otaniemi, 2020. Available at: https://smartotaniemi.fi/ (accessed 19.11.2020)

The European Parliament and the Council of the European Union, 2010. Directive 2010/31/EU on the energy performance of buildings. Directive [online]. Available at: https://eur-lex.europa.eu/legal-content/EN/TXT/PDF/?uri=CELEX:32010L0031&from=EN (accessed 19.11.2020)

Tommerup H., Svendsen S., 2005. Energy savings in Danish residential building stock. Energy and Buildings, vol. 38 [online]. Available at: https://doi.org/10.1016/j.enbuild.2005.08.017 (accessed 19.11.2020). Amsterdam: Elsevier.

Uponor, 2013. Free cooling guide. Available at: https://issuu.com/uponor/docs/free-cooling-guide (accessed 20.11.2020).

Uponor, (no date). Uponor G12- lämmönkeruuputki [online]. Available at: https://www.uponor.fi/UponorInternet/DirectDownload?did=DF791764475442E3BDA9A486640065CD (accessed 20.11.2020).

Vihola Jaakko, Sorri Jaakko, Heljo Juhani, Kero Paavo, 2015. Heat loss rate of the Finnish building stock. Procedia, vol. 21 [online]. Available at: https://doi.org/10.1016/S2212-5671(15)00218-X (accessed 19.11.2020). Elsevier.

Ympäristöministeriö, 2017. Ympäristöministeriön asetus uuden rakennuksen energiatehokkuudesta (1010/2017). Available at: https://www.finlex.fi/fi/laki/alkup/2017/20171010 (accessed 19.11.2020)

Yrjölä Jukka, Laaksonen Eetu, 2015. Domestic Hot Water Production with Ground Source Heat Pump in Apartment Buildings. Energies 2015, issue 8 [online]. Available at: https://doi.org/10.3390/en8088447 (accessed 19.11.2020). Basel: MDPI.

APPENDIX

Appendix 1. Parameters used in the TRT validation study.

Borehole depth	188 m
Borehole diameter	115.075 mm
Outer tube outer diameter	115.075 mm
Outer tube wall thickness	0.9375
Inner tube outer diameter	40 mm
Inner tube wall thickness	2.4 mm
Inner & outer tube conductivity	0.4 W/mK
Heat carrier	Water
Flow rate	0.58 l/s
Constant heat injection load	6380 W
Ground conductivity	3.15 W/mK
Ground heat capacity	2.24 MJ/m^3K
Ground surface temperature	8.9 °C
Geothermal gradient	T(z) = (-6e-9·z^4+2e-6·z^3-5e-5·z^2-0.0189·z+9.2037) ° C

Appendix 2. Parameters used in the EED validation study.

Borehole depth	800 m
Borehole diameter	110 mm
Outer tube outer diameter	110 mm
Outer tube thickness	4 mm
Inner tube outer diameter	50 mm
Outer tube conductivity	0.4 W/mK
Inner tube conductivity	0.22 W/mK
Inner tube wall thickness	4.6 mm
Heat carrier	Water
Flow rate	1.5 l/s
Constant heat extraction load	22.83 kW
Ground conductivity	3.5 W/mK
Ground heat capacity	2.16 MJ/m^3K
Ground surface temperature	8 °C
Geothermal gradient	0.0171 K/m

Appendix 3. SCL script for the Apros heat pump module.

```
//parameters of the cop polynomial fit
a = -0.014991
b = -0.09301114
c = 8.39002993

//constants for calculation
boreholeCount = 4 //used only to divide the total loads from an input file
eer = 4 //refrigerator eer
q_max = 133000 / boreholeCount //hp max capacity (dictated by the coverage factor)
cp_fluid = 4400 //circulating fluid cp, for temperature change calculation
fc_limit = 10 //temperature limit for free cooling

//temperature and heat demand values
//t_evap and qm are from the simulation, others from an input file
qm = SP34.SP_VALUE
t_dhw = SP03.SP_VALUE
t_sh = SP09.SP_VALUE
t_ahu = SP10.SP_VALUE
t_evap = SP05.SP_VALUE
q_dhw = SP08.SP_VALUE / boreholeCount
q_sh = SP06.SP_VALUE / boreholeCount
q_ahu = SP07.SP_VALUE / boreholeCount
q_cool = SP11.SP_VALUE / boreholeCount

//limit total heat pump output power
limitCheck q_dhw q_sh q_ahu
    | q_tot < q_max = q_tot
    | otherwise = q_max
    where q_tot = q_dhw + q_sh + q_ahu
q_tot = limitCheck q_dhw q_sh q_ahu

//COP's
cop_dhw = a * t_dhw + b * (t_dhw - t_evap) + c
cop_sh = a * t_sh + b * (t_sh - t_evap) + c
cop_ahu = a * t_ahu + b * (t_ahu - t_evap) + c

//weighted mean for the COP
cop_mean = (cop_dhw * q_dhw + cop_sh * q_sh + cop_ahu * q_ahu) / q_tot

//ground load from heating
q_ground = q_tot - (q_tot) / cop_mean

//evaporator exit temperature
dT_evap = q_ground / (cp_fluid * qm)
t_evap_out = t_evap - dT_evap

//check if free cooling is used
fc_check t_evap_out
    | t_evap_out > fc_limit = (q_cool + q_cool / eer, 0)
    | otherwise = (q_cool, 1)
q_cool = fc_check t_evap_out

//calculate temperature change from cooling
dT_cool = (fst q_cool) / (cp_fluid * qm)
t_out = t_evap_out + dT_cool

//set outputs
set.SP04.SP_VALUE t_evap_out
set.SP18.SP_VALUE t_out
set.SP26.SP_VALUE t_out
set.SP21.SP_VALUE q_tot
set.SP20.SP_VALUE (fst q_cool)
set.SP37.SP_VALUE (snd q_cool)
set.SP19.SP_VALUE cop_mean
```

Appendix 4. SCL script for the regeneration heat exchanger module.

```
boreholeCount = 3

t_fluid_in = SP27.SP_VALUE
qm_fluid = SP31.SP_VALUE
t_air_in = SP29.SP_VALUE
qm_air = SP28.SP_VALUE

cp_air = 1000 //J/kgK
cp_fluid = 4400 //J/kgK

temperatureCheck t_fluid_in t_air_in qm_air cp_air
    | t_air_in > (t_fluid_in + 6) = qm_air * cp_air * (t_air_in - (t_fluid_in + 6))
    | otherwise = 0
q = (temperatureCheck t_fluid_in t_air_in qm_air cp_air) / boreholeCount

t_fluid_out = t_fluid_in + q / (qm_fluid * cp_fluid)

set.SP35.SP_VALUE q
set.SP30.SP_VALUE t_fluid_out
```